STRUCTURAL BASIS OF VPS4 FUNCTION AND REGULATION IN THE MULTIVESICULAR BODY PATHWAY

by

Junyu Xiao

A dissertation submitted in partial fulfillment
of the requirements for the degree of
Doctor of Philosophy
(Biological Chemistry)
in The University of Michigan
2009

Doctoral Committee:

Associate Professor Zhaohui Xu, Chair
Professor Robert S. Fuller
Professor Daniel J. Klionsky
Professor Janet L. Smith
Associate Professor John J.G. Tesmer

To my parents
Xiuying Wang and Qinghuai Xiao

Acknowledgements

I am deeply indebted to the many people who have helped me with my graduate career especially my mentor, Dr. Zhaohui Xu. As said by Han Yu (Chinese writer, Tang Dynasty), “it takes a teacher to transmit the Way, impart knowledge and resolve doubts (translated by Shih Shun Liu)”. Zhaohui opened the door of science and crystallography to me, taught me things from experimental techniques to critical thinking and scientific writing and presentation, gave me intellectual freedom, and provided guidance all along. I cannot have asked for a better mentor for my graduate study. I also owe many thanks to my thesis committee members: Drs. Robert Fuller, Janet Smith, John Tesmer, and Daniel Klionsky, for their scientific insights, patience and encouragements. I sincerely appreciate that they took the time to critically read my manuscripts and give me advice on my future career development.

I am also indebted to former and current members of the Xu lab for their help and friendship. Dr. Jiahai Zhou taught me many things when I just started in the lab. Since then, Jiahai has been a constant source of help and advices both scientifically and personally. Dr. Hengchuan Xia and I have had a fruitful collaboration on the work presented in Chapter 3, in which Hengchuan produced the Vta1CTD crystal and characterized the interaction between Vta1CTD and Vps4. Kae Yoshino-Koh and Dr. Anthony Ludlam have been very good friends to me and helped develop my projects in

the early stage. I would also like to thank other Xu lab members including Dr. Brian Moore and Ulla Lilienthal for providing an enjoyable environment to work in.

I owe particular thanks to Dr. Xiao-Wei Chen and his wife Dr. Qian Wang. Our friendship dates back to the college time in China, and their help made my life transition in this country much easier. Xiao-Wei is also such a superb scientist, and I sincerely appreciate his help on my research and his willingness to collaborate on the mammalian cell biology study regarding to the project presented in Chapter 4.

I would also like to extend special thanks to Dr. Ming Lei and his group members: Dr. Yuting Yang, Dr. Yong Chen, and Feng Wang. I enjoyed our many synchrotron trips together and appreciate their help with data collection. Dr. Ming Lei and Dr. Yuting Yang also taught me many tricks about crystal heavy atom soaking. I really appreciate their help and friendship.

This work cannot be completed without the help from my scientific collaborators. In particular, I would like to thank Dr. David Katzmann and his lab members, including Ishara Azmi and Dr. Brian Davies in the Mayo Clinic College of Medicine. I appreciate their generosity in sharing information with us, and I have benefited tremendously from their yeast cell biology studies.

I would also like to acknowledge staffs of the Center for Structural Biology at the University of Michigan for maintaining the X-ray facility and staffs at the Advanced Photon Source beam lines 21-ID and 23-ID of Argonne National Laboratory for access and help with data collection. I owe thanks to Dr. Ursula Jakob and Dr. Marianne Amenta-Ilbert in the Jakob lab for access and help with CD spectral analysis. I am also

sincerely grateful to Drs. Rowena Matthews and Lois Weisman for their critical reading of my manuscripts.

Finally, I would like to express my gratitude to my family and friends. I am especially grateful to my parents. Although they are thousands of miles away on the other side of the earth, their love and inspiration are always with me. I am proud of being their son, and I will always do my best to make them proud.

Preface

This thesis is composed of three related manuscripts, each representing a chapter (Chapter 2-4). Chapter 2 and Chapter 3 have been published (Chapter 2: Journal of Molecular Biology, 2007. 374(3): p. 655-70; Chapter 3: Developmental Cell, 2008. 14(1): p. 37-49). Work in Chapter 4 is in progress and will also be published as research article in a peer reviewed journal. Chapter 1 introduces background information, progress during the past ten years and unresolved questions in the field. Chapter 5 summarizes the work presented in this thesis and proposes directions for future studies.

Figure 3.1D, 3.2E, 3.5, and 4.6 were prepared by members of the Katzmann lab: Ishara Azmi, Dr. Brian Davies, and Dr. David Katzmann in Mayo Clinic College of Medicine. Figure 4.7 was prepared by Dr. Xiao-Wei Chen in the University of Michigan.

Table of Contents

Dedication ii

Acknowledgements iii

Preface vi

List of Figures xi

List of Tables xiii

Abstract xiv

CHAPTER 1: INTRODUCTION 1

MVB, CLASS E VPS PROTEINS AND THE ESCRT MACHINERY 3

DELINEATING THE MOLECULAR MECHANISM OF THE MVB PATHWAY 10

Cargo recognition by the upstream components of the ESCRT machinery 10

ESCRT-III, membrane deformation, and ESCRT-III associated regulators 17

Vps4 catalyzed ESCRT disassembly 23

Regulation of Vps4 activity by Vta1 29

Regulation of Vps4 activity by Ist1 31

ESCRT FUNCTIONS IN ENVELOPE VIRUS BUDDING, CYTOKINESIS, AND AUTOPHAGY-ASSOCIATED NEURODEGENERATION 33

SUMMARY 36

REFERENCES 38

CHAPTER 2: STRUCTURAL CHARACTERIZATION OF THE ATPASE REACTION CYCLE OF ENDOSOMAL AAA-PROTEIN VPS4 55

ABSTRACT 55

INTRODUCTION 56

RESULTS 58

Structure determination 58

Overall structure 58

Comparison to human VPS4B structure 63

The quaternary structure of Vps4 in its nucleotide-free form 63

The quaternary structure of Vps4 in its ADP-bound form 66

ADP binding 68

Structural flexibility within Vps4 71

Structural basis of ATP-dependent ESCRT-III binding 74

DISCUSSION 78

METHODS 81

REFERENCES 87

CHAPTER 3: STRUCTURAL BASIS OF VTA1 FUNCTION IN THE MULTIVESICULAR BODY SORTING PATHWAY 90

ABSTRACT 90

INTRODUCTION 90

RESULTS....93
Structure determination....93
The crystal structure of Vta1NTD....95
Vta1NTD consists of two MIT motifs....95
Potential Vps60 and Did2 binding surface on Vta1NTD....98
The crystal structure of Vta1CTD....102
Oligomerization state of Vta1....102
Vps4 binding surface on Vta1CTD....106
The dimer structure of Vta1 is required for Vps4 interaction....109
The structure of intact Vta1....110
DISCUSSION....114
METHODS....118
REFERENCES....125

CHAPTER 4: STRUCTURAL BASIS OF IST1 FUNCTION AND IST1-DID2 INTERACTION IN THE ESCRT PATHWAY....128
ABSTRACT....128
INTRODUCTION....128
RESULTS....131
The N-terminal domain of Ist1 specifically interacts with the MIM1 sequence of Did2....132
The crystal structure of Ist1NTD....135
The crystal structure of Ist1NTD in complex with Did2-MIM1....140
Did2-MIM1 displays a novel mode of binding....146

Ist1-Did2 interaction is important for MVB sorting 147

Conserved Ist1-Did2 interaction is important for efficient cytokinesis and abscission 149

DISCUSSION 154

METHODS 162

REFERENCES 171

CHAPTER 5: CONCLUSIONS AND PERSPECTIVES 175

REFERENCES 181

List of Figures

CHAPTER 1

Figure 1.1 The MVB pathway functions in membrane fission processes.....2

Figure 1.2 Receptor down-regulation by the MVB pathway 4

Figure 1.3 Molecular mechanism of the MVB pathway.....6

Figure 1.4 Known structures of proteins and protein complexes functioning in the MVB pathway 12

CHAPTER 2

Figure 2.1 Crystal structure of yeast Vps4 and sequence alignment of Vps4 proteins.....62

Figure 2.2 Yeast Vps4 exists as a monomer in the absence of ATP 65

Figure 2.3 Crystal packing within the lattice of the ADP-bound Vps4 structure.....67

Figure 2.4 ADP binding causes conformational changes in Vps4 70

Figure 2.5 Structural flexibility within Vps4 73

Figure 2.6 Nucleotide binding induces conformational change within the N-terminal region of Vps4.....76

Figure 2.7 Conserved surface patches on Vps4.....80

CHAPTER 3

Figure 3.1 The crystal structure of Vta1NTD.....97

Figure 3.2 Potential Vps60 binding sites on Vta1NTD 101

Figure 3.3 The crystal structure of Vta1CTD..... 104

Figure 3.4 Vps4 binding sites on Vta1CTD..... 108

Figure 3.5 Residues involved in dimerization and Vps4 binding are required for cargo sorting in the MVB pathway..... 111

Figure 3.6 The structure of intact Vta1 113

Figure 3.7 A model of Vps4-Vta1 complex..... 116

CHAPTER 4

Figure 4.1 The N-terminal Domain of Ist1 specifically interacts with the MIM1 motif of Did2..... 134

Figure 4.2 The crystal structure of Ist1NTD 138

Figure 4.3 Crystal packing in Ist1NTD and Ist1NTD/Did2-MIM1 complex structures reveal Ist1NTD can potentially form polymers/oligomers..... 141

Figure 4.4 Ist1NTD interacts with Did2-MIM1 using a novel binding mechanism..... 144

Figure 4.5 Did2 binding induces conformational change at the C-terminal region of Ist1..... 148

Figure 4.6 Residues involved in Did2 binding are required for cargo sorting in the MVB pathway 150

Figure 4.7 hIst1-CHMP1 interaction is important for cytokinesis 153

Figure 4.8 Did2 uses a similar surface to bind to Ist1NTD and Vps4-MIT..... 157

Figure 4.9 Structure based sequence alignment of the ESCRT-III protein CHMP3/Vps24..... 159

Figure 4.10 A model for the functional cycle of the ESCRT-III proteins 160

List of Tables

CHAPTER 1

Table 1.1 Proteins function in the MVB pathway 8

CHAPTER 2

Table 2.1 Crystallographic Data Statistics 59

CHAPTER 3

Table 3.1 Data collection and refinement statistics 94

CHAPTER 4

Table 4.1 Crystallographic Data and Refinement Statistics 137

Abstract

The multivesicular body (MVB) pathway is an important biological process that functions in a number of different physiological and pathological settings in the eukaryotic cells, including down-regulation of cell surface receptor signaling, enveloped virus budding and abscission during cytokinesis. The AAA ATPase Vps4 plays a pivotal role in this pathway by catalyzing structural remodeling of the membrane-associated Endosomal Sorting Complexes Required for Transport (ESCRT) machinery. This activity leads to the recycling of the ESCRT machinery and may also be linked to membrane fission.

The active form of Vps4 is a double-ring dodecameric structure in the presence of ATP. The crystal structure of *S. cerevisiae* Vps4 shows the protein contains a canonical AAA domain fold and undergoes conformational change upon nucleotide binding, providing a possible mechanism of oligomerization. Positive regulators Vta1, Vps60 and Did2 and negative regulator Ist1 further modulate the activity of Vps4 in the cell. Structural and biochemical analyses of these proteins and their interactions with Vps4 provide further insights into their mechanisms of action. Vta1 is organized into two well-folded domains connected by a flexible linker region. The dimeric C-terminal domain is responsible for Vps4 binding. It stimulates the ATPase activity of Vps4 by stabilizing the double-ring structure. The N-terminal domain contains two tandem MIT domains previously seen in the N-terminal ESCRT-III-binding domain of Vps4. The second MIT

domain contains Vps60 and Did2 binding activity, and these interactions further stimulate the Vps4 activity in a Vta1-dependent manner. Ist1 contains a well-folded N-terminal domain and a C-terminal MIT-interacting motif. The crystal structure of the N-terminal domain of Ist1 reveals it resembles the fold of an ESCRT-III protein, suggesting that Ist1 might inhibit Vps4 activity by acting as a substrate mimic. Ist1 also interacts with Did2 via a novel binding mechanism and this interaction is important for both yeast vacuolar sorting and mammalian cytokinesis. Taken together, these results enable us to better understand the molecular mechanism of Vps4 function and its regulation in the MVB pathway.

CHAPTER 1

INTRODUCTION

Biological membranes are selectively permeable barriers that separate the cell from the exterior environment and contents of organelles from the cytosol. They are also highly dynamic in nature and constantly undergo structural changes that accompany specific cellular processes. Remarkably, topologically equivalent membrane-fission events have been shown to occur in several physiological and pathological conditions. These include maturation of enveloped viruses such as HIV (human immunodeficiency virus), separation of the two daughter cells during cell division (the abscission step in cytokinesis), and formation of the internal vesicles at the multivesicular body (MVB) in eukaryotic cells (Figure 1.1). The commonality in these activities lies in their membranes budding away from the cytoplasm. Furthermore, a common cellular pathway has been implicated in all three processes. This pathway was originally characterized during the study of MVB biogenesis in the yeast cell; as a result, it is known as the MVB pathway. Because of its essential function in regulating cell growth and proliferation, abnormality of this pathway is often related to cancer where the balance of regulation is often subverted. Moreover, owing to its close tie with viral infection, it has also ignited enormous interest in this regard. Therefore, the past ten years have seen an explosion of research in this field. The proteins involved in this pathway have been identified by

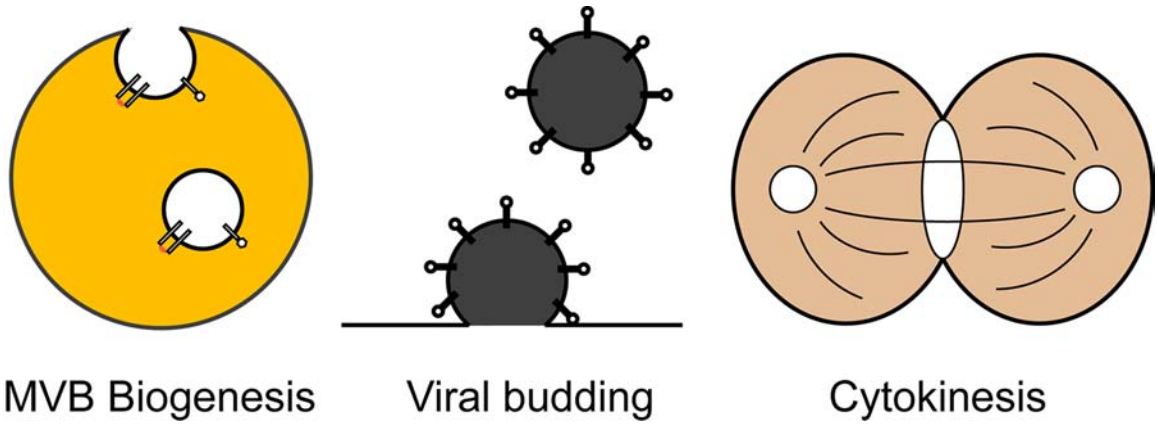

Figure 1.1 The MVB pathway functions in membrane fission processes.
The MVB pathway functions in formation of the internal vesicles at the multivesicular body (MVB), envelope virus budding, and cytokinesis. The common feature of these activities lies in that their membranes bud away from the cytoplasm.

genetic and cell biology studies, and the mechanism of their actions elucidated biochemically and structurally (reviewed in [1-4]).

MVB, CLASS E VPS PROTEINS AND THE ESCRT MACHINERY

The MVBs are special compartments in the eukaryotic cells and are defined based on their unique morphology revealed by the electron microscope. The characteristic feature of an MVB is the presence of many internal vesicles, all known as intralumenal vesicles (ILVs) (reviewed in [5, 6]). The link between the MVBs and the endosome system is established by monitoring the proteins that undergo constitutive internalization. For example, the epidermal growth factor receptor (EGFR) is the cell-surface receptor for the EGF-family extracellular growth factors. When engaged with EGF, EGFR switches on its protein-tyrosine kinase activity, which in turn activates intracellular signaling pathways to promote cell growth, proliferation, and differentiation [7, 8]. To avoid overgrowth, the cells will regulate the signaling duration by subsequently conveying the EGF-EGFR complexes to the lysosome for degradation. This process is often known as receptor down-regulation, which mediates the degradation of not only EGFR but also many other transmembrane proteins (Figure 1.2) [9-12]. To achieve this, these receptor complexes are first displaced from the plasma membrane and delivered to the early endosome through a process known as endocytosis [9, 13]. Protein sorting then takes place: reusable materials will be recycled back to the plasma membrane, while molecules doomed for destruction will be directed into the invaginating ILVs [10, 14]. As a result of this vesiculation process, the resulting endosome displays a multi-vesicular appearance

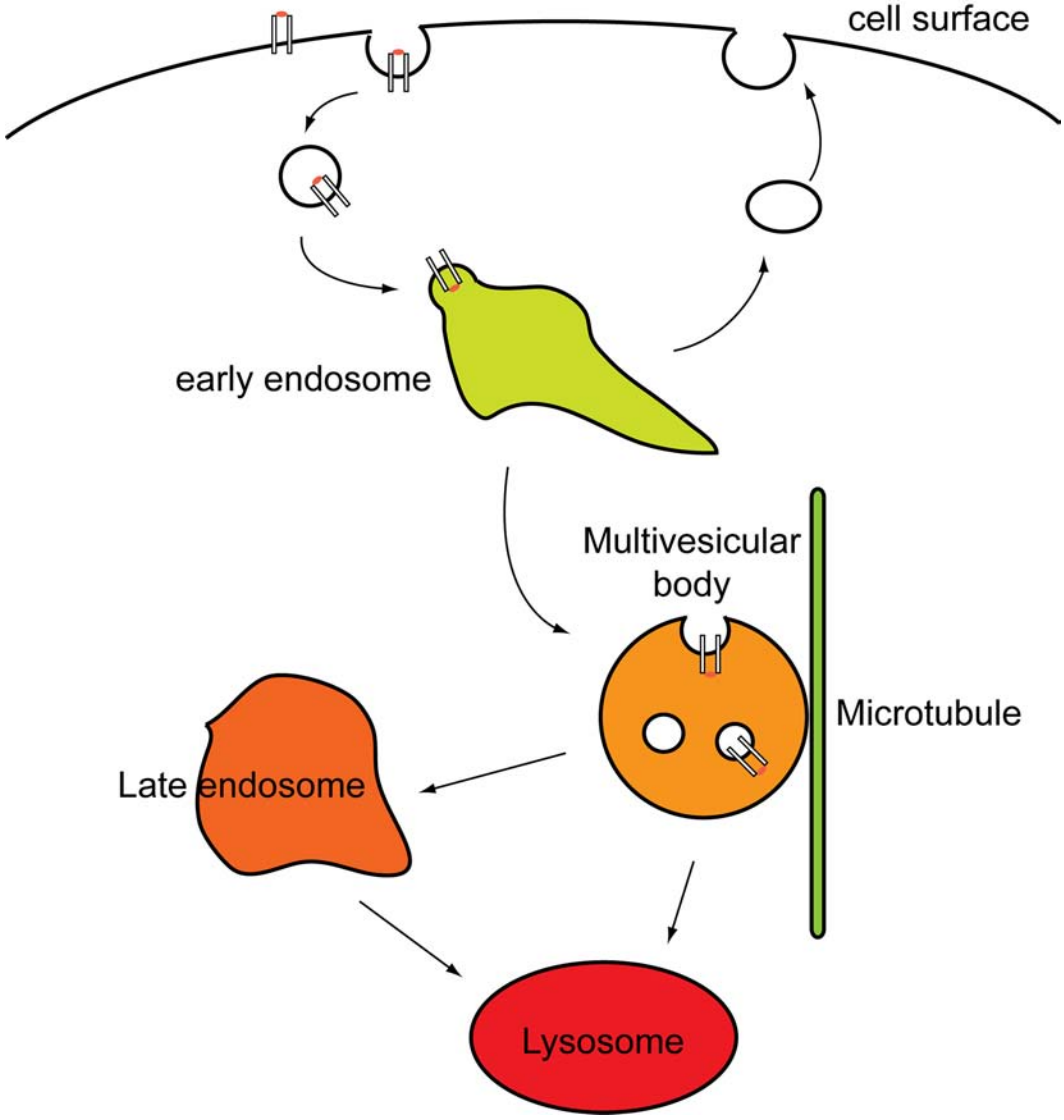

Figure 1.2 Receptor down-regulation by the MVB pathway.
During the receptor down-regulation process, cell-surface receptors and transmembrane proteins are internalized and transported to the early endosome. They are further sorted into the forming ILVs. The MVB is generated when many of such ILVs are present within an endosome. MVBs move along the microtubules until they finally fuse with the lysosomes, resulting in the degradation of their internal materials.

and becomes an MVB. Meanwhile, MVBs move along the microtubules toward the cell interior and eventually fuse with the lysosome. This will deliver the molecules residing in the ILVs into the lumen of the lysosome, where they will be digested [15, 16]. Hence, MVBs are specialized forms of mature endosomes that serve a lysosomal transport function. The purpose of forming the ILVs and sorting the cargo into them is to expose transmembrane cargo molecules to the digestive enzymes within the lysosome (Figure 1.2).

MVB biogenesis can be functionally dissected into three related steps: cargo sorting and concentrating, endosomal membrane deformation, and ILV formation and fission (Figure 1.3). These steps are achieved by the interplay between membrane lipids and cellular proteins. For example, at least four types of lipids have been implicated in these processes to date: phosphoinositides, cholesterol, the unconventional lipid lysobisphosphatidic acid (LBPA; also called BMP, for bis(monoacylglycero)phosphate), and the sphingolipid ceramide. Specifically, phosphatidylinositol-3-phosphate (PI_3P) is enriched on the cytosolic side of early endosomes and has a well-established role in recruiting cellular proteins [17, 18]. The PI_3P 5-kinase activity is required for the MVB function, suggesting phosphatidylinositol-3, 5-bisphosphate ($PI_{3,5}P_2$) might play important roles as well [19]. Both LBPA and ceramide can induce ILV formation under some circumstances [20, 21]. It is believed that their unique shapes may play a role that affects the local membrane curvature. The role of cholesterol remains undefined. However, blocking of the MVB pathway results in the accumulation of cholesterol in the endosomes, suggesting that cholesterol sorting is associated with MVB function [22-24]. Indeed, many aspects of lipid involvement await further characterization, particularly

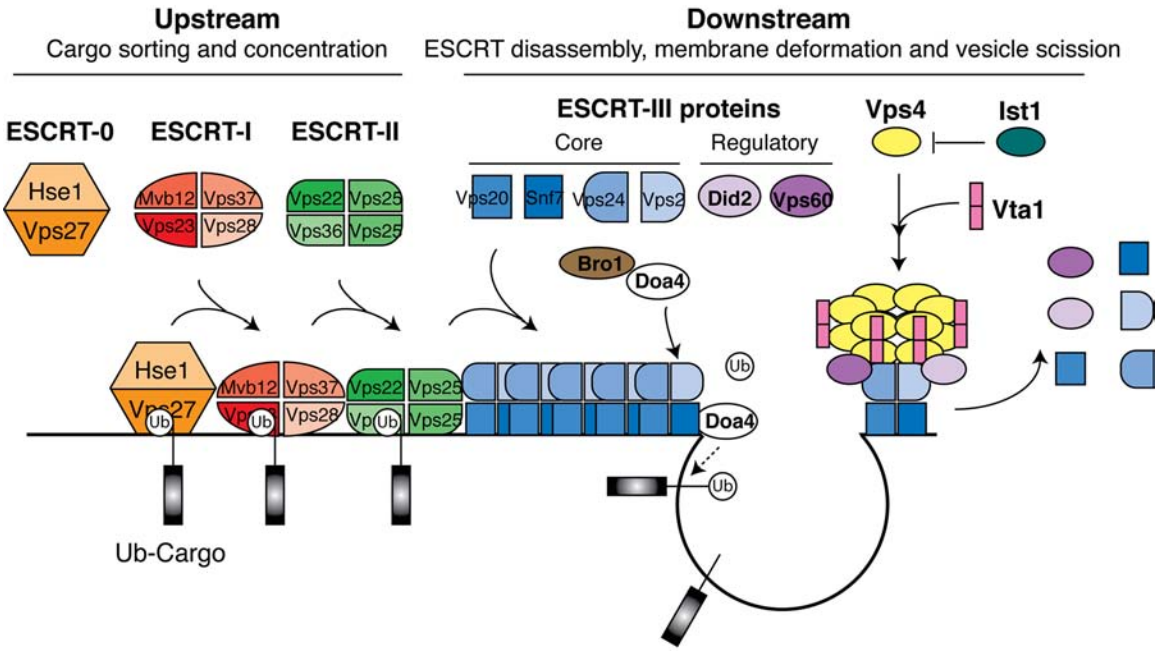

Figure 1.3 Molecular mechanism of the MVB pathway.
Function of the MVB pathway depends on the action of several protein complexes called Endosomal Sorting Complexes Required for Transport (ESCRT-I, -II, and -III). The Vps27-Hse1 complex, ESCRT-I, and ESCRT–II bind to ubiquitinated cargo and cluster multiple cargo molecules on the membrane. ESCRT-III recruits other regulators such as the deubiquitinating enzymes and may also be responsible for membrane deformation. Vps4 catalyzes the disassembly of ESCRT-III for sustained functional cycle of the MVB pathway; and this disassembly process is likely to be mechanistically coupled to the vesicle scission process as well. Several proteins, including Vta1 and Ist1, regulate the function of Vps4, suggesting Vps4 carries out a critical step in the MVB pathway.

with regard to ILV formation and detaching, where the participation of lipids is clearly critical.

In contrast, the molecular details of cellular proteins involved in this pathway have been extensively studied and a clear picture has emerged (Figure 1.3). Both cargo sorting and ILV formation depends on the functions of a group of proteins called class E Vacuolar protein sorting (Vps) proteins, first identified in the yeast *Saccharomyces cerevisiae* by the Tom Stevens lab in the early 90s [25]. Deletion of many of these proteins results in not only loss of MVB formation, but also mislocalization of MVB cargo to a distinctive abnormal subcellular structure called class E compartment. Clearly, these proteins are required for the normal MVB function. Subsequently, Scott Emr and colleagues further demonstrated a majority of the class E Vps proteins function in the form of three protein complexes: ESCRT-I, -II and –III, where "ESCRT" is an abbreviation for "Endosomal Sorting Complex Required for Transport" [26-28]. ESCRT-I and –II are constitutive complexes and are recruited to the endosome in their fully assembled forms. In contrast, the ESCRT-III proteins are monomers in the cytoplasm and assemble into the ESCRT-III complex only at the endosome membrane. Besides ESCRT-I, -II, and -III, major components of the MVB pathway also include the Vps27-Hse1 complex (sometimes also referred as ESCRT-0 in the literature) [29-31], the ATPase Vps4 [32, 33] and other ESCRT associated regulators [34] (Table 1.1). By the concerted function of these proteins and protein complexes, the cargo molecules are "escorted" into the ILVs of the MVB in order to be primed for their eventual degradation.

The signal that designates a protein molecule as an MVB cargo has also been elucidated. Like its function in targeting proteins to the proteasome system,

Table 1.1 Proteins function in the MVB pathway

MVB machinery	Yeast	Interactions	Mammal homologs
ESCRT-0			
	Vps27	Cargo, membrane, Vps23	Hrs
	Hse1	Cargo, ubiquitin ligase and deubiquitinating enzymes	STAM1, STAM2
ESCRT-I			
	Vps23	Vps27, cargo	Tsg101
	Vps28	Vps20, Vps36	Vps28
	Vps37		Vps37A-D
	Mvb12		Mvb12A-B
ESCRT-II			
	Vps22		EAP30
	Vps25	Vps20	EAP20
	Vps36	Cargo, membrane, Vps28	EAP45
ESCRT-III proteins			
	Vps2	Vps4	CHMP2A-B
	Vps20	Vps4, Vps28, Vps25	CHMP6
	Vps24	Vps4	CHMP3
	Snf7	Vps4, Bro1	CHMP4A-C
	Did2	Vps4, Vta1, Ist1	CHMP1A-B
	Vps60	Vta1	CHMP5
Disassembly			
	Vps4	ESCRT-III, Vta1, Ist1	Vps4A, Vps4B (SKD1)
	Vta1	Vps4, Vps60, Did2	SBP1/Lip5
Others			
	Bro1	Snf7, deubiquitinating enzyme Doa4	Alix/AIP1
	Ist1	Vps4, Did2	KIAA0174

ubiquitination serves as the destruction signal in this pathway. However, instead of forming long poly-ubiquitination chains linked through Lys-48 in the proteasome pathway [35, 36], a mono-ubiquitin conjugation appears to be sufficient to direct a protein molecule into the MVB pathway in most cases [37]; though Lys-63 linked poly-ubiquitin chains have also been observed [38, 39]. The ubiquitination modifications are recognized by the Vps27-Hse1 complex, ESCRT-I complex, and ESCRT-II complex (Figure 1.3). Following their action, the ESCRT-III complex is formed on the endosomal membrane. ESCRT-III recruits regulatory proteins including the deubiquitinating enzymes to remove the ubiquitin tag from the cargo. More importantly, the ESCRT-III complex may also be responsible for deforming the membrane to generate the ILVs. Finally, the ATPase Vps4 catalyzes the recycling of the ESCRT complexes by dissociating them from the membrane, and this disassembly process is likely to be mechanistically coupled to vesicle scission. The activity of Vps4 is closely regulated by a group of positive and negative regulators, including Vta1 and Ist1, suggesting Vps4 carries out a critical step in the MVB pathway.

The ESCRT system and all the associating regulatory factors are highly conserved in the eukaryotic cells [40, 41]. Many proteins in this pathway have multiple isoforms in higher-level species, suggesting an evolved functional complexity (Table 1.1). Not surprisingly, improper function of this pathway is often linked to human diseases. For example, dysfunctions of several genes in the ESCRT complex have been connected to cancer related cell overgrowth, and some will be discussed in more detail in the following sections. Interestingly, proteins in the ESCRT machinery are employed in viral budding and cytokinesis, which mirror the MVB vesicle-generation process in their nature of

membranes curving and budding away from the cytoplasm [42-44]. Furthermore, recent research has revealed that the ESCRTs are also involved in autophagy-associated neurodegeneration [45, 46]. As such, understanding the molecular mechanism of the ESCRT machinery is critical for promoting the discovery of novel therapeutics against diseases including cancer, viral infection and neurodegeneration.

DELINEATING THE MOLECULAR MECHANISM OF THE MVB PATHWAY

Cargo recognition by the upstream components of the ESCRT machinery

As mentioned above, the protein machinery involved in cargo sorting and concentration are the three upstream protein complexes: Vps27-Hse1, ESCRT-I, and ESCRT-II. Efforts by several groups have clarified the overall structural organization for each (Figure 1.4A-C). A common structural feature of these complexes is that they all contain phospholipid-binding domains for membrane targeting, ubiquitin-binding domains for interacting with cargo molecules, and protein-protein interaction motifs for interacting with each other and recruiting other proteins.

The Vps27-Hse1 complex is recruited to the endosome through its interaction with the endosomal lipid PI_3P. The Fab1-YGL023-Vps27-EEA1 (FYVE) domain in Vps27 mediates this interaction [47-49]. Both Vps27 and Hse1 harbor ubiquitin-interacting motif (UIM) domains, which bind to ubiquitinated cargo [50-53]. Interestingly, the Vps27-Hse1 complex is also associated with both ubiquitin ligase and deubiquitinating enzymes [54-56]. The counter-actions of these activities are hypothesized to be important for performing the final check on the cargo before they

Figure 1.4 Known structures of proteins and protein complexes functioning in the MVB pathway.
(A) Vps27-Hse1 complex. Pieced together from the VHS-FYVE tandem domain of Hrs (PDB ID: 1DVP), the tandem UIM domains of Vps27 (PDB ID: 1Q0V), the VHS domain of human STAM2 (PDB ID: 1X5B), the Vps27 UIM1 domain (PDB ID: 1O06), the STAM2 SH3 domain (PDB ID: 1UJ0), and the Vps27/Hse1 complex core (PDB ID: 2PJW) according to [63].
(B) ESCRT-I. Pieced together from the Vps23 UEV domain (PDB ID: 1UZX), the Vps28 C-terminal domain (PDB ID: 2J9V), and the ESCRT-I core (PDB ID: 2P22) according to [64].
(C) ESCRT-II. Pieced together from the human ESCRT-II complex (PDB ID: 3CUQ) and the Vps36 Glue domain (PDB ID: 2HTH) according to [102].
(D) The open conformation of the ESCRT-III subunit CHMP3 (PDB ID: 2GD5).
(E) The Bro1-V tandem domains of human Alix (PDB ID: 2R05).
(F) Vps4. Pieced together from the yeast Vps4 MIT domain (PDB ID: 2V6X) and AAA ATPase domain (PDB ID: 2QPA).
(G) Vta1. Pieced together from the yeast Vta1-NTD (PDB ID: 2RKK) and Vta1-CTD (PDB ID: 2RKL) according to [178].
(H) The N-terminal domain of Ist1.

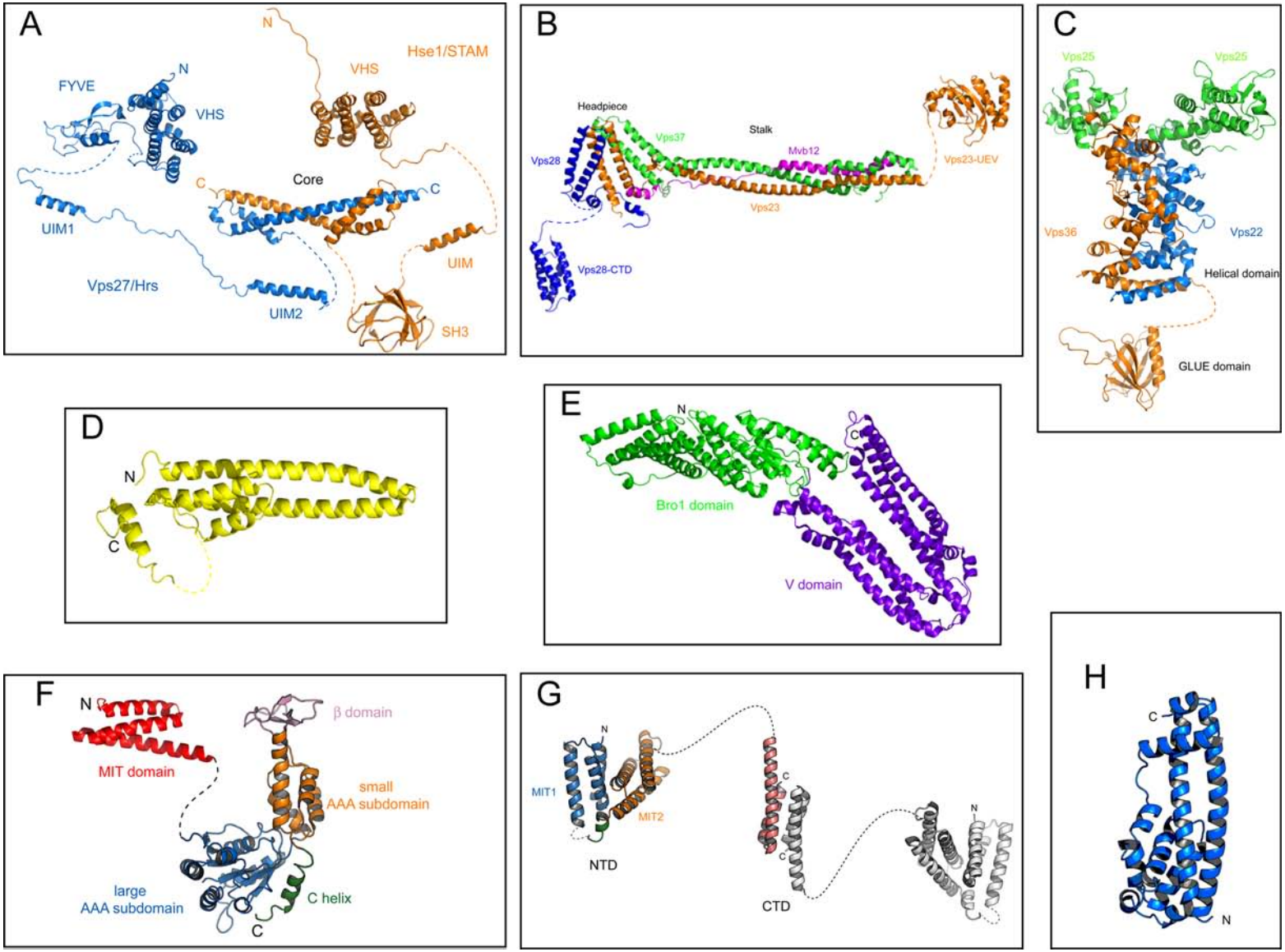
A
N
Hse1/STAM
VHS
N
FYVE
VHS
Core
C
C
UIM1
UIM
Vps27/Hrs
UIM2
SH3
B
Headpiece
Vps37
Stalk
Mvb12
Vps28
Vps23-UEV
Vps23
Vps28-CTD
C
Vps25
Vps25
Vps36
Vps22
Helical domain
GLUE domain
D
N
C
E
N
C
Bro1 domain
V domain
F
N
β domain
MIT domain
small
AAA subdomain
large
AAA subdomain
C helix
C
G
N
MIT1
MIT2
NTD
C
C
CTD
N
H
C
N

enter the MVB pathway. Human Vps27 is known as Hrs (Hepatocyte growth factor-regulated tyrosine kinase substrate), and Hse1 has two human orthologs, STAM1 and STAM2 (signal transducing adaptor molecule). Hrs recruits clathrin, which forms a planar lattice on the endosome [57, 58]. In contrast to its well-established role in coating the endocytic vesicles on the cell surface [59], the function of this flat clathrin lattice appears to be defining a special domain on the endosomal membrane to concentrate cargo and organize the sorting machinery. Vps27/Hrs also serves as a docking site for ESCRT-I (see below).

Structures of many isolated fragments of the Vps27-Hse1 complex have been determined, including the FYVE domain [47], UIM1 in complex with ubiquitin [51], and UIM1-UIM2 tandem domains of Vps27 [51]; double-sided ubiquitin binding UIM domain [60] and the VHS (Vps27, Hrs, STAM)-FYVE tandem domains of Hrs [61]; the SH3 (Src homology 3) domain of human STAM2 in complex with a fragment of the deubiquitinating enzyme UBPY (ubiquitin isopeptidase Y) [62]; as well as the core domain responsible for the Vps27-Hse1 complex assembly [63]. As a result, a nearly complete model of the entire Vps27-Hse1 complex can be pieced together (Figure 1.4A). The entire Vps27-Hse1 complex appears to be an open and dynamic assembly, where many distinct activities can be coordinated [63].

The ESCRT-I complex is a heterotetramer, containing one copy each of Vps23, Vps28, Vps37 and Mvb12 [26, 64]. ESCRT-I is recruited to the endosome by the Vps27-Hse1 complex through the interaction between Vps27 and Vps23. Specifically, the P-T/S-x-P motif within the C-terminal region of Vps27 interacts with the UEV (ubiquitin E2 variant) domain of Vps23 [65-67]. (P-T/S-x-P refers to the tetrapeptide Proline-

Threonine/Serine-any amino acid-Proline. Similar one-letter codes for amino acids are also used in the following text.) The UEV domain of Vps23 can also bind to the ubiquitin using a different binding surface [68, 69]. Therefore, Vps27-binding and ubiquitin-binding can be independent of each other. Tsg101, the mammalian homolog of Vps23 has been a great interest of study even before the discovery of ESCRT-I. Tsg101 was identified as a tumor susceptibility gene in a genetic screen (thus the name: tumor susceptibility gene 101), as either functionally knocking-out or over-expression of Tsg101 resulted in transformation of NIH3T3 fibroblast cells [70, 71]. Mutation in *erupted*, the *Drosophila* ortholog of Tsg101 also causes tissue overgrowth [72]. This is consistent with the role of the MVB pathway in regulating growth factor signaling and cell division. On the other hand, it was observed that HIV p6 protein could recruit Tsg101 through the same P-T/S-x-P motif [73-77]. Therefore, it appears that HIV can mimic the action of Hrs and take over the MVB pathway for its own purpose.

ESCRT-I activates ESCRT-II through direct interaction between the C-terminal domain of Vps28 and ESCRT-II [78]. Based on this sequential activation scenario between Vps27-Hse1, ESCRT-I, and ESCRT-II, it was originally proposed that a cargo molecule is passed from Vps27-Hse1 through ESCRT-I to ESCRT-II (reviewed in [4] and [79]). However, there appears to be no reason for a cargo to travel through all three complexes in order to enter the ILVs. On the other hand, although all the ubiquitin-binding motifs in Vps27-Hse1, ESCRT-I, and ESCRT-II essentially interact with the same surface on ubiquitin [5], a direct hand-off reaction between them has not been observed so far. Notably, a recent structure study on ESCRT-I suggests that direct cargo passing between ESCRT-I and ESCRT-II is physically difficult [64].

The overall structure of the ESCRT-I core can be best described as a fan-shaped "headpiece" connected to a 13 nm rigid "stalk" (Figure 1.4B) [64]. The headpiece is mainly composed of three anti-parallel two-helix hairpins. Vps23, Vps28, and Vps37 each contribute one of the hairpins [78, 80]. The stalk consists of four long helices, two from Vps23 and one each from Vps37 and Mvb12 [64]. It is worth noting that the structure of the ESCRT-I core could only be determined after the discovery of Mvb12, which is an integral component of ESCRT-I and stabilizes the overall structure of the complex [81-85]. This structure organization of ESCRT-I projects the Vps23 UEV domain (cargo binding) and the Vps28 C-terminal domain (ESCRT-II binding) to the opposite ends of this exceptionally elongated assembly (Figure 1.4B) [64]. This observation does not seem to support a model of direct transfer between ESCRT-I and ESCRT–II. Therefore, it appears that Vps27-Hse1, ESCRT-I and ESCRT-II function in a cooperative rather than competitive manner to tether multiple cargo molecules at the same time [1]. This cooperative model is also consistent with several previous observations. For example, over-expression of ESCRT-II can suppress the effect of loss of ESCRT-I in yeast [27], while mammalian ESCRT-II is dispensable for sorting of some cargo molecules [86].

In addition to the core of ESCRT-I, the structures of the Vps23/Tsg101 UEV domain in complex with either ubiquitin or the P-T-A-P motif of the HIV-1 p6 protein have also been reported [68, 69, 87], as well as the C-terminal domain of Vps28 that mediates the interaction with ESCRT-II [88] (Figure 1.4B). ESCRT-I binds to the endosomal membrane via the basic N-terminal region of Vps37 with modest affinity [64]; however, membrane targeting appears to rely more on the simultaneous and reinforcing

interactions with cargo, Vps27-Hse1 and ESCRT-II. Both Vps37 and Mvb12 have multiple isoforms in mammals (Vps37A-D and Mvb12A-B) [83, 89], and their functional differences have not been fully explored.

The ESCRT-II complex consists of one molecule each of Vps22 and Vps36, and two molecules of Vps25 [27]. Their homologs in mammals are also referred as EAP30, EAP45, and EAP20, respectively [90]. In *Drosophila*, the ESCRT-II subunit Vps25 acts as a tumor suppressor. Mutation of Vps25 triggers tumor-like overgrowth [91-93]. This is reminiscent of the effect of Tsg101 mutation. Vps25 interacts with Vps20 in the ESCRT-III complex. Therefore, ESCRT-II may play a critical role in initiating the assembly of ESCRT-III [94, 95]. Meanwhile, Vps22 interacts with RILP (Rab7-interacting lysosomal protein), which in turn binds to the dynein-dynactin motor complex [96-98]. This might be important for moving the MVBs along the microtubules.

Mammalian Vps36 contains a PH (Pleckstrin homology) domain variant called the “GLUE (Gram-like ubiquitin binding domain in EAP45)” domain. This domain binds to both phosphoinositides and ubiquitin [78, 99-101]. Besides the GLUE domain, there is also a second lipid-binding site in ESCRT-II, which lies in the extreme N-terminal helix of Vps22 [102]. This suggests a combinatorial mechanism for high-affinity membrane targeting. A region immediately C-terminal to the GLUE domain mediates the interaction with Vps28 in ESCRT-I [102]. Therefore, ESCRT-I binds to a region very close to the membrane-binding site in ESCRT-II, and the binding might trigger a conformational change to activate ESCRT-II. In yeast, Vps36 contains two NZF (Npl4 zinc finger) domains, NZF1 and NZF2, inserted in the GLUE domain. NZF1 mediates interaction with Vps28, while NZF2 binds to ubiquitin [103, 104]. Notably, although the detailed

mechanisms of binding to both ESCRT-I and cargo have altered, the binding events *per se* have been conserved through evolution. This highlights the functional importance of these interactions.

Structures have been determined for both the yeast ESCRT-II core and a more intact human ESCRT-II (Figure 1.4C) [94, 102, 105]. The core of the ESCRT-II resembles the letter "Y", with one Vps25 subunit forming the stalk, and the other Vps25 and the Vps22-Vps36 subcomplex forming the two branches. Although the three subunits do not have primary sequence homology to each other, each subunit consists of two repeats of winged helix (WH) domains. An additional helical domain is seen in the human ESCRT-II structure, which is conserved in the yeast complex as well. The helical domain is contributed by both Vps22 and Vps36 and extends further along the Vps22-Vps36 branch of the Y shape. Compared with the rest of the structure, this domain has a more dynamic nature. Hydrodynamic analysis suggests the N-terminal GLUE domain of Vps36 might sit on this domain in its inactivated state (Figure 1.4C). However, membrane targeting of the GLUE domain could potentially trigger a conformational change in the rest of the complex through this domain [102].

ESCRT-III, membrane deformation, and ESCRT-III associated regulators

The ESCRT-III proteins are a family of small, bi-polar molecules, including Vps2, Vps20, Vps24, Snf7, Did2 and Vps60. They have related sequences and perhaps evolve from a common origin [28]. All ESCRT-III proteins have a basic N-terminal half and an acidic C-terminal half. In a working model, the ESCRT-III proteins exist in a monomeric, auto-inhibited form in the cytosol due to interaction between the N- and C-

halves. Upon stimulatory signals, they hetero-oligomerize to assemble into a large protein lattice on the endosomal membrane with an undefined stoichiometry. This assembly is collectively called the ESCRT-III complex [3]. The nature of the stimulatory signal is not entirely clear; and both protein-protein and protein-lipid interactions could be involved. For example, the ESCRT-III subunit Vps20 can directly interact with both Vps28 in ESCRT-I and Vps25 in ESCRT-II [88, 94, 95, 106], while both Vps24 and Snf7 in ESCRT-III are able to bind to phospholipids [107, 108]. In addition, Vps20 is myristoylated at its N-terminal region, which also contributes to its membrane localization [28, 106].

In contrast to ESCRT-I and ESCRT-II whose subunit compositions are well defined, the structural organization of the ESCRT-III complex is only vaguely understood. In yeast, it is generally believed that Vps2, Vps20, Vps24 and Snf7 form the core of the ESCRT-III complex while Did2 and Vps60 play regulatory roles in the assembly and disassembly process of the complex [28, 109]. More importantly, it appears that the core subunits are placed onto the endosome in a well-established order [110]. Specifically, Vps20 is recruited first, probably through its interactions with Vps28 and Vps25 and its myristoylation modification. Vps20 subsequently nucleates the oligomerization of Snf7, which seems to be the major building block of the ESCRT-III complex. The Vps20-Snf7 subcomplex further recruits Vps24-Vps2 to terminate Snf7 oligomer expansion and initiate Vps4-dependent dissociation.

The mammalian ESCRT-III proteins are also known as CHMPs (charged multivesicular body proteins). CHMP proteins function in a much more complicated manner compared with their yeast counterparts. In yeast, deletion of only the core

ESCRT-III subunits gives rise to the class E morphology, while deletion of Did2 or Vps60 only generates a weak phenotype [28]. In mammals, however, all CHMPs seem to be indispensable. For example, disruption of the normal function of CHMP3/Vps24 and CHMP6/Vps20 in mammals leads to the accumulation of EGFR in endosomes [106, 111]. CHMP5/Vps60 is essential for receptor down-regulation during mouse embryogenesis, and deletion of CHMP5 in mice results in early embryonic lethality [112]. CHMP1A/Did2 has recently been characterized as a novel tumor suppressor gene, especially in the pancreas [113]. Moreover, many CHMP proteins have multiple isoforms (CHMP1A-B, CHMP2A-B, CHMP4A-C) in mammals, and these isoforms sometimes function differentially [114]. Finally, a mammal specific CHMP7 protein has no yeast ortholog [115]. Notably, dominant-negative versions of many CHMP proteins are potent inhibitors of HIV and other enveloped viruses, which provide a significant clinical interest [116-118].

CHMP3/Vps24 is the only ESCRT-III subunit whose structure has been determined to atomic resolution (Figure 1.4D) [119]. This structure has served as a model for all ESCRT-III protein. The core of CHMP3 consists of an asymmetrical antiparallel four-helix bundle, with the first two helices forming a 70 Å long helical hairpin. This hairpin mediates two types of interactions with neighboring molecules in the crystal lattice, and these interaction sites are hypothesized to constitute binding surfaces for other ESCRT-III proteins *in vivo*. Moreover, arrangement of molecules in the crystal displays a contiguous basic surface, which could potentially represent a membrane-binding interface. The CHMP3 fragment used in the structure determination contains a deletion in its most C-terminal predicted helix. This C-terminal helix together with the nearby helix

(helix α5 in the structure) are important for auto-inhibiting ESCRT-III proteins to retain them in their monomeric states [116, 120]. As a result of the deletion, the auto-inhibition has been relieved therefore the determined structure represents an open state of the molecule. In Chapter 4, I will describe the structure of a protein called Ist1. Strikingly, it has an ESCRT-III like fold with its N-terminal region highly resembling the CHMP3 core. More importantly, the structure organization in Ist1 might reflect a closed conformation for the proteins containing the ESCRT-III fold.

Because the ESCRT-III subunits function in the late stage of the MVB pathway and can form polymer structures on the membrane, they have been the prime candidates for the membrane scission machine that makes and detaches the ILVs. The main evidence to support this comes from an Snf7 over-expression study performed by Phyllis Hanson and colleagues [121]. When hSnf7-1 (CHMP4A) or hSnf7-2 (CHMP4B) is over-expressed in cultured cells, they form curved filaments on the cytoplasmic face of the plasma membrane. Furthermore, these filaments can deform membranes into buds and tubules that project away from the cytosol in the presence of Vps4. This experiment suggests the Snf7 proteins can promote membrane curvature in the direction required for ILV formation. Interestingly, other ESCRT-III proteins are also capable of forming helical or tubular structures, and these assemblies can affect the shape of membrane *in vitro* [122, 123]. Taken together, these observations support a direct role for the ESCRT-III subunits in the mechanics of ILV invagination. Remarkably, the unusual long helical hairpin motif in the CHMP3 structure and the ability of the ESCRT-III proteins to form helical assemblies are both reminiscent of the BAR-domain containing proteins, which function along with dynamin to deform plasma membrane during endocytosis [124-127].

In this regard, it is tempting to speculate the ESCRT-III proteins function in a related mechanism, but bend membrane into the opposite direction.

Certainly, many questions remain to be addressed. For example, CHMP3 depleted mammalian cells can still form ILVs, as can mammalian cells depleted of CHMP5 and yeast cells depleted of Did2 [109, 111, 112]. Given the recent study suggesting Snf7 is the most abundant components in the ESCRT-III complex [110], one possible explanation for these observations is that Snf7 oligomer is the major driving force for ILV formation, while other ESCRT-III proteins can be dispensable for this purpose. However, this also highlights the complicated nature of the ILV formation process. In reality, membrane deformation in MVB biogenesis is likely an event contributed by many factors. Membrane lipids are expected to play a key role as well. Several different or overlapping mechanisms have been proposed in animal cells regarding the role of lipid in ILV formation. For example, the ESCRT-III interacting proteins, Alix (see below), can bind to the mammal-specific lipid LBPA/BMP [20]. LBPA has an inverted cone shape and can drive the formation of membrane invaginations in acidic liposomes *in vitro*, and Alix can regulate this process. Moreover, Alix controls the organization of LBPA-containing endosomes *in vivo* [20, 128]. Another protein, SNX3 (sorting nexin 3), which binds to PI_3P and functions downstream of Hrs, has also recently been implicated in ILV formation [129]. Furthermore, ESCRT-independent mechanism appears to exist as well, and one such mechanism depends on sphingolipid ceramide [21]. Therefore, we are still in an early stage of understanding how the ILVs are actually formed. Interconnection between these different mechanisms need to be considered and further explored.

In addition to its likely role in mediating membrane deformation, the ESCRT-III complex recruits a myriad of important adaptor proteins and regulatory enzymes to the endosomal membrane, often using their C-terminal amphipathic auto-inhibitory helices. Membrane-bound ESCRT-III subunits expose their C-terminal regions, making them available to recruit their specific binding partners. Reciprocally, binding of other proteins to the C-terminal helices within the ESCRT-III proteins can potentially lead to or stabilize their open conformation, therefore regulating their membrane localization and oligomerization. For example, the ubiquitin tags on the cargo molecules need to be removed before they are sorted into the ILVs. Targeting of the deubiquitinating enzymes (DUBs) to the endosomal membrane depends on the assembly of the ESCRT-III lattice. In yeast, Snf7 recruits Bro1, which in turn recruits the DUB Doa4 [130, 131]. A Doa4-like DUB has yet to be identified in animal cells; however, two other DUBs, AMSH and UBPY, have been implicated in this process. Both AMSH and UBPY interact directly with the ESCRT-III proteins, providing a unified theme for the ESCRT-III coordinated deubiquitinating event [54, 132-134].

Alix or AIP1, the mammalian homolog of Bro1, has attracted much attention in its own right, due to its interesting cellular activities. It was first identified as an interacting partner for ALG-2, a protein implicated in apoptosis (therefore the name, ALG-2-interacting protein X or ALG-2 interacting protein 1) [135, 136]. Besides its role in the endosomal sorting pathway, it has well-defined functions in processes such as retrovirus budding and cytokinesis [137-140]. However, it appears that its interaction with Snf7/CHMP4 is key in each case. Alix has three distinct regions: an N-terminal Bro1 domain, a central V domain, and a C-terminal proline-rich region. The structure of

the Bro1-V tandem domains of Alix is shown in Figure 1.4E. The banana-shaped Bro1 domain specifically interacts with the C-terminal helix of Snf7/CHMP4 [141-144]. The V domain is composed of two extended helical arms that fold in the shape of the letter V, and is the target of many retroviruses including HIV [145-147]. The C-terminal proline-rich domain contains binding epitopes for many cellular proteins, including Tsg101 [117, 148]. Therefore, Alix can also potentially mediate the communication between ESCRT-I and ESCRT-III.

For sustained protein trafficking through the MVB pathway, the ESCRT-III lattice needs to be disassembled from the endosomal membrane and recycled. This membrane-dissociation event is crucial for forming the ILVs. Vps4, which catalyzes this disassembly and dissociation process, is targeted to the endosomal membrane via its interaction with the ESCRT-III complex as well.

Vps4 catalyzed ESCRT disassembly

Vps4 is an indispensable component and a master regulator of the ESCRT machinery. Inhibition of Vps4 function affects almost all biological processes that the ESCRT machinery is known to participate in. For example, deletion of the Vps4 gene in yeast leads to a pronounced class E phenotype displaying severe defects in cargo sorting and ILV formation [33]. In mammalian cells, inhibiting Vps4 results in swollen endosomes, impaired EGFR degradation, arrested cytokinesis and blockade of retrovirus budding [22, 114, 118, 140, 149]. In both yeast and mammals, the common phenotype of interfering with the normal function of Vps4 is the massive accumulation of the ESCRT components on endosomal membranes; therefore the entire MVB pathway is

handicapped. Vps4 is highly conserved throughout evolution. The two isoforms of human Vps4, Vps4A and Vps4B (also know as SKD1), are 80% identical; and both display a high degree of sequence identity to the yeast Vps4 protein (59% and 60%, respectively) [150]. Furthermore, human Vps4B can functionally replace yeast Vps4 in yeast cell [150, 151], highlighting the functional conservation of Vps4 during the evolution of eukaryotic lineage.

Vps4 belongs to a protein family called AAA (ATPase Associated with various cellular Activities) ATPase, the signature feature of which is the existence of one or multiple 200-250 amino acid AAA domains in their sequences [152-154]. The AAA domain is an ATP binding cassette that contains many conserved sequence motifs, such as the Walker A (with the consensus sequence G-x-x-x-x-G-K-T/S, where x is any amino acid) and Walker B (with the consensus sequence h-h-h-h-D-E, where h represents a hydrophobic residue) motifs, both are important for ATP binding and hydrolysis. In addition, there are regions called Sensor 1 and Sensor 2 that are important for communicating changes in the adenosine nucleotide status to other parts of the structure. Finally, a region called second region of homology (SRH) provides a highly conserved arginine residue that serves as an “arginine finger” to stabilize the transition state during ATP hydrolysis [155]. As the name suggested, the AAA proteins perform many different functions and are involved in many aspects of cellular life [156]. The general theme of their function is to convert the energy from ATP binding and hydrolysis into mechanical forces to remodel protein or protein complexes [155, 157]. Therefore, the ESCRT disassembly process by Vps4 is analogous to the activities of many other AAA ATPases in their disassembly of protein networks; such as spastin or katanin mediated microtubule

disassembly or NSF (N-ethylmaleimide sensitive fusion protein) catalyzed SNARE (soluble NSF attachment receptor) complex dissociation [158-160].

The crystal structure of the monomeric Vps4 AAA domain has been determined by several groups including ours (Figure 1.4F) [161-165]. I will describe the structure of yeast Vps4 in more detail in Chapter 2 and discuss its ATPase reaction cycle. Briefly, the crystal structure of Vps4 shows that the protein contains a single AAA domain fold with several unique structural features. The AAA domain in Vps4 is structurally analogous to the AAA domains in other proteins, and can be further divided into a large AAA subdomain and a small AAA subdomain. The large subdomain has a Rossmann fold, and the small subdomain has a four-helix bundle structure. The unique structural features of Vps4 include a middle insertion in the small AAA subdomain and a C-terminal helical region. The middle insertion domain contains three beta strands and therefore named the beta domain. This domain mediates the interaction between Vps4 and its regulator Vta1 [161]. The C-terminal region folds into a single helix that packs onto the large subdomain. Interestingly, similar C-terminal helices also exist in other AAA ATPase members that do not form stable oligomers and undergo quaternary structure change upon ATP binding and hydrolysis, such as spastin or the D2 domain of p97 [166, 167]. Whether this is simply a coincidence or has more important functional implications remains to be understood.

Like other AAA family member proteins, the active form of Vps4 is an oligomer. An important structural feature of the AAA ATPases is that they form ring-shaped structures upon ATP binding, usually with six-fold symmetry [155, 168]. Many AAA proteins contain two tandem AAA domains in their sequences. One domain undergoes

large conformational change with respect to ATP binding/hydrolysis and provides the "remodeling" activity of the protein, while the other is mainly responsible for hexamerization. This "divided-responsibility" mechanism represents a major functional theme for the AAA proteins, and there is a long list of proteins belonging to this group, such as p97 and NSF [169]. For these AAA proteins, the ring structures are maintained during their respective ATPase reaction cycles. However, others including Vps4 contain only one AAA domain, which is responsible for both oligomerization and energy conversion. As a result, ATP binding and hydrolysis induces not only conformational change in the tertiary structure of the protein, but also the quaternary structure.

The active form of Vps4 can be trapped using an ATPase deficient mutant, and is confirmed as a high molecular-weight oligomer by gel filtration analysis and cross-linking [33, 161]. These experiments further suggested that the oligomer contains 10-12 subunits. Interestingly, this seems to indicate that the active form of Vps4 contains a double-ring structure. Indeed, the double-ring shaped assembly of Vps4 has been recently observed by cryo-EM studies [163, 170]. Assuming that the oligomer of Vps4 obeys the six-fold symmetry seen in other AAA proteins, these results suggest that the biologically active form of Vps4 is most likely a double-ring dodecameric structure in the presence of ATP. Moreover, this double-ring assembly of Vps4 is stabilized by its co-factor Vta1 *in vivo*, which I will discuss more in detail in Chapter 3.

Although most of the ESCRT proteins are held captive on the endosomal membrane in the absence of Vps4 function, the direct substrates of Vps4 appear to be the ESCRT-III proteins [95, 118]. Other ESCRTs are also trapped because of their association with the ESCRT-III lattice. Of the six ESCRT-III proteins in yeast, Vps4

directly interacts with five of them, with Vps60 as the only exception [109, 162]. Similar interaction patterns have also been found in mammals [118]. More importantly, binding between Vps4 and the ESCRT-III proteins either requires ATP or is strongly enhanced by ATP [162]. Therefore, the ATP status in Vps4 is directly coordinated with substrate binding and release, which is consistent with the function of Vps4.

How Vps4 interacts with the ESCRT-III proteins has also been extensively studied. The substrate-binding domain of Vps4 is called the MIT (microtubule interacting and transport) domain, located in the N-terminal region of the molecule and named after its sequence homology to the microtubule binding motifs in a number of proteins [171]. Structurally, the MIT domain folds into an asymmetric three-helix bundle, resembling part of a TPR (tetratricopeptide repeat) motif (Figure 1.4F) [172, 173]. More interestingly, it can interact with the substrates in two different ways. Some proteins bind to the Vps4 MIT domain using their most C-terminal amphipathic helices, which have been named as “MIM (MIT interacting motif)”; while others use a “MIM2” motif, which is a proline-rich strand that is located in the interior of the ESCRT-III proteins [174-176]. The former include Vps2/CHMP2, Did2/CHMP1 and a regulator of Vps4 called Ist1; and the latter include Vps20/CHMP6 and Snf7/CHMP4. MIM1 has a core consensus sequence of (D/E)-x-x-L-x-x-R-L-x-x-L-(K/R) and binds to a surface groove formed by helices 2 and 3 on MIT, while MIM2 has a core consensus sequence of (L/V)-P-x-(V/L)-P and binds between helices 1 and 3. Furthermore, a single MIT domain seems to be able to engage with both MIM1 and MIM2 elements simultaneously, since neither binding induces significant conformational change in the MIT domain and the binding surfaces are not overlapping [176]. Therefore, it appears that in a fully assembled oligomer

structure of Vps4, there would be 12 MIT domains from 12 subunits thus 24 substrate-binding surfaces to engage with the ESCRT-III network at the same time. Strikingly, the Vps4 regulator Vta1 also contains two structurally similar MIT domains and interacts with a subgroup of the ESCRT-III proteins, including Vps60 and Did2 [177-179]. As a result, Vta1 increases the valence of binding between Vps4 and the ESCRT-III complex. Apparently, the multivalent-binding capability of Vps4-Vta1 complex is crucial for its function to remodel and disassemble the ESCRT-III polymer. Reciprocally, a need for a multivalent-binding disassembly machine in turn suggests that the ESCRT-III proteins form a complicated structure on the membrane.

After substrate recognition, how Vps4 remodels the ESCRT-III proteins and releases them from the membrane is still a mystery. Based on a model built based on perceived structural homology to p97, it was suggested that there is a pore at the center of the Vps4 dodecamer. Similar pores or channels are essential for the function of AAA proteins in numerous cases [180-184]. In an analogy to the mechanism of these proteins, it is speculated that the ESCRT-III proteins are “fed” into the pore by the MIT domains of both Vps4 and Vta1, and then “pulled” through by conformational changes induced by ATP binding and/or hydrolysis [4]. During this process, the substrates are remodeled and converted to their monomeric state and thus dissociated from the membrane. Vps4 essentially acts as a chaperone-like “unfoldase” in this working model. Mutations on loops located in the pore of Vps4 inhibit HIV-1 release, indicating the activity of Vps4 is impaired [161]. However, direct observation that substrates are threaded through the pore is still lacking.

There is also speculation that ESCRT binding and disassembly by Vps4 may directly contribute to membrane bending and/or constriction. In the Snf7 over-expression experiment mentioned above, buds and tubules that protrude from the cell surface are only formed when a mutant form of Vps4 ($hVps4B^{E235Q}$) is co-expressed in cultured cells [121]. The mutant Vps4 is unable to hydrolyze ATP thus is associated with the substrate proteins permanently. Therefore, it seems that Vps4 binding to the ESCRT-III complex might be important for membrane deformation. Furthermore, a recent cryo-EM study reveals Vps4 can bind on the inside of the tubular structure formed by the ESCRT-III proteins [122]. These results lead to the hypothesis that similar tubular structures could form within the neck of an inwardly budding vesicle. When Vps4 hydrolyzes ATP, it will apply a pulling force on the ESCRT-III proteins from within, leading to the eventual vesicle fission. This theory is reminiscent of the action of dynamins, GTPases that form spiral collars around the neck of an endocytosed vesicle and constrict through GTP hydrolysis, resulting in vesicle scission [185, 186]. Although this aspect of Vps4 function remains largely speculative, these experimental results suggest it is possible that the action of Vps4 is mechanistically coupled to ILV formation. In fact, it is tempting to think the mechanism of ESCRT-III and Vps4 system could be a process of déjà vu, resembling the functions of BAR domain-containing proteins and dynamin in a broad context.

Regulation of Vps4 activity by Vta1

The reaction catalyzed by Vps4 provides the only energy input to the MVB pathway. As a result, the function of Vps4 is tightly regulated in the cell. Both positive

and negative regulators have been identified. ESCRT-III and Vta1 can directly enhance the ATPase activity of Vps4, while Ist1 inhibits its activity [177, 187-189]. In addition, both Vta1 and Ist1 interact with specific ESCRT-III proteins, which may present a higher level of regulation *in vivo*.

Vta1 and its mammalian homolog SBP1 were both originally identified in yeast two-hybrid analysis as Vps4-binding proteins [190, 191]. Subsequently, the plant ortholog, Lip5 was also demonstrated to interact with Vps4 [192]. Furthermore, they all interact with Vps4 through a highly conserved C-terminal sequence region called VSL (Vta1/SBP1/Lip5) [187]. Deletion of Vta1 in yeast generates a milder phenotype compared with that of Vps4 [187, 193], which is consistent with its regulatory function. Similarly, depletion of Vta1 in mammalian cells does not alter the morphology of the endosomes but does reduce the level of EGFR degradation. Importantly, depletion of Vta1 significantly decreases HIV-1 budding in cultured cells [194]. Biochemically, Vta1 stimulates the ATPase activity of Vps4 by promoting the assembly of Vps4 into its active oligomeric form [187]. In addition, Vta1 also interacts with other proteins acting in the late stage of the MVB pathway, including the ESCRT-III proteins Vps60 and Did2 [177, 178]. Interestingly, these interactions further potentiate its stimulatory activity towards Vps4, suggesting an allosteric effect [177].

The interaction between Vps60 and Vta1 is particularly intriguing, because the functional role of Vps60 appears to be unique among the ESCRT-III proteins. First, Vps60 is the only ESCRT-III protein that does not interact with Vps4 [118, 195]. Second, the endosomal association of Vps60 depends on Vta1, unlike other ESCRT-III proteins, which are targeted to the membrane prior to Vta1 and partially responsible for recruiting

Vta1 [177]. Finally, depletion of CHMP5 (Vps60 in mammals) leads to an increase in the release of infectious HIV-1 particles, in contrast to the effect of perturbing other ESCRT-III proteins function [194]. Deletion of the CHMP5 gene in mice results in early embryonic lethality, suggesting that CHMP5 plays a crucial function in higher eukaryotic species [112].

Vta1 has a modular structure with two ordered terminal domains linked by a long linker region (Figure 1.4G) [178]. Structures of all three sections have been characterized in our lab and will be discussed in more detail in Chapter 3. Briefly, its N-terminal domain (NTD) contains two MIT-like motifs, termed MIT1 and MIT2 respectively; and MIT2 is important for both Vps60 and Did2 binding. This finding suggests that MIT-like domains are generic ESCRT-III recognition motifs [196]. The C-terminal domain (CTD) of Vta1, which includes the VSL region, mediates dimerization of the full-length protein. Importantly, dimerization is critical for its *in vitro* and *in vivo* function as a Vps4 regulator. The long linker region, present in all Vta1 orthologs but showing no sequence conservation, contains little secondary structure. However, some preliminary observations suggest that this linker region might play an important role in communicating the structural changes at the two terminal domains, providing a structural basis for the observed allostery between ESCRT-III binding to NTD and Vps4 binding to CTD (discussed more in Chapter 3).

Regulation of Vps4 activity by Ist1

Ist1 is a newly identified player in the MVB pathway and binds directly to both Vps4 and Did2 [189, 197]. The endosome association of Ist1 depends on Did2, while

dissociation relies on the activity of Vps4. More importantly, it plays important inhibitory functions to Vps4 both *in vitro* and *in vivo*. It prevents the ATP-dependent oligomerization of Vps4 and therefore inhibits its ATPase activity [189]. Remarkably, this inhibitory effect is more potent than the Vta1-dependent stimulation of Vps4, since Ist1 causes inhibition even in the presence of Vta1. Furthermore, over-expression of Ist1 in yeast cells leads to a strong MVB sorting defect similar to deletion of Vps4, consistent with its inhibitory role. Although deletion of Ist1 by itself has no obvious effect on MVB function, synthetic deletions of Ist1 with either Vta1 or Vps60 significantly impair MVB sorting, leading to a typical class E phenotype [197]. In contrast, double deletion of Vta1 and Vps60 does not generate a similar phenotype. Similarly, deletion of Did2 is also synthetic with either Vta1 or Vps60, but not with Ist1. How these synthetic phenotypes should be interpreted is still controversial. Nevertheless, this suggests that regulation of Vps4 *in vivo* is an orchestrated process, and coordinated inputs from Vta1, Vps60, Ist1, and Did2 put Vps4 activity in check.

BLAST search reveals a clear Ist1 homolog in higher eukaryotes, referred as "KIAA0174" in human and many other species. The function of this protein is largely uncharacterized, but the sequence homology suggests that it likely acts in a way similar to Ist1 in yeast. Conserved domain analysis indicates Ist1 and all of its homologs contain a predicted DUF292 (domain of unknown function) domain at their N-termini [198, 199]. Besides the DUF292 domain, Ist1 also contains a canonical C-terminal Vps4-interacting MIM1 motif [189]. The sequence between the two well-conserved regions has little predicted secondary structure and displays a high degree of sequence variation, similar to the linker in Vta1. Further insights into the function of Ist1, however, are not available,

partly due to the absence of structural information, especially for the N-terminal DUF292 domain. In Chapter 4, I will examine the structural basis for Ist1 function. Briefly, I have found the N-terminal DUF292 domain has an ESCRT-III protein like structure (Figure 1.4H), which is remarkable considering they share little sequence identity. This provides insights into the functions of other proteins containing this domain, as well as raises an interesting possibility that Ist1 might inhibit the activity of Vps4 by functioning as a substrate mimetic. In addition, this domain specifically interacts with the MIM1 motif of Did2 via a novel non-MIT MIM-binding site. Therefore, the N-terminal domain of Ist1 represents a new class of MIM-interacting structure.

Finally, it is worth pointing out that the current list of Vps4 regulators is probably not complete. For example, there are several other proteins known to interact with Vps4, such as two members of the oxysterol binding protein family, Osh6 and Osh7, and a protein purported to be involved in intracellular cholesterol transport, NPC1 (Niemann-Pick disease, type C1) [200, 201]. Whether these interactions are relevant to the MVB sorting pathway and how they might affect the activity of Vps4 are interesting questions to be addressed in future studies.

ESCRT FUNCTIONS IN ENVELOPE VIRUS BUDDING, CYTOKINESIS, AND AUTOPHAGY-ASSOCIATED NEURODEGENERATION

The involvement of the ESCRT machinery in the MVB pathway predicts a role for these proteins in pathological conditions where down-regulation of the growth factor signaling is undermined, the most prominent being cancer. As described above,

dysfunction of Tsg101 of ESCRT-I, Vps25 of ESCRT-II, and CHMP1 of ESCRT-III have all been associated with cancer related cell overgrowth. In addition, the ESCRT machinery has been implicated in a myriad of other cellular processes including budding of envelope viruses, abscission in cytokinesis and autophagy.

For a mature enveloped virus to infect other cells, it has to escape from the previously infected host cell. Many viruses hijack the host ESCRT machinery to achieve this purpose [42, 43, 202]. These viruses encode specific domains in their structural proteins called the late assembly domains (L domains). To facilitate viral budding, the L domains often recruit cellular proteins by mimicking their genuine binding partners. The first late domain was identified in the HIV-1 p6 protein, which contains the P-T-A-P motif and recruits Tsg101 as described above. The same motif has subsequently been found in many other viruses, such as the Ebola virus, the human T cell leukemia virus type I (HTLV-I), and so on, suggesting a similar budding mechanism is common to many enveloped viruses [76, 203, 204]. Another well-characterized L domain has a Y-P-(x)n-L motif and recruits Alix/AIP1, first identified in the p9 protein of the equine infectious anemia virus (EIAV) [117, 148]. The p6 protein of HIV-1 also contains this motif and recruits Alix in parallel to Tsg101, suggesting a one-two punch mechanism in snatching the ESCRT system [148]. Interestingly, dominant negative ESCRT-III or Vps4 proteins are often potent inhibitors for budding of viruses that utilize the MVB pathway.

The connection between the ESCRT machinery and cytokinesis was first discovered in plant *Arabidopsis*, where mutation of gene *ELC* causes multiple nuclei in various cell types [205]. ELC was later demonstrated to be the homolog of Vps23/Tsg101 in plants. Subsequently, it was found in mammalian cells that Tsg101 and the ESCRT-

associated protein Alix are recruited to the midbody during cytokinesis, in part by their interactions with the centrosome protein 55 (Cep55) [139, 140, 206]. Furthermore, both Tsg101 and Alix are required for the final abscission stage of cell division. ESCRT-III and Vps4 are also recruited, and dominant negative mutants of these proteins again potently inhibit this process. Therefore, most of the ESCRT machinery seems to be involved. Interestingly, it appears that the ESCRT-III proteins and Vps4 may have homologs in some archaeal genomes, suggesting an ancient function might exist for these proteins before the endomembrane system evolved [174, 207, 208]. Their implications in cytokinesis would be an intriguing possibility [209].

Autophagy is a cellular self-digestion process involving the degradation of a cell's own components by the lysosome [210-212]. In one type of autophagy, macroautophagy, a cytosolic membrane structure called the phagophore engulfs part of the cytoplasm to form the autophagosome, which subsequently fuses with the lysosome, resulting in the degradation of their inner materials [213]. The ESCRT proteins have been previously reported to be implicated in autophagy [214, 215]. However, a definitive link between the MVB pathway and autophagy is first revealed by clinical discoveries. Specifically, mutations in the ESCRT-III protein CHMP2B gene were found to be associated with a rare form of autosomal dominant frontotemporal dementia (FTD) in a Danish pedigree [216], and in some patients with amyotrophic lateral sclerosis (ALS) [217]. Both FTD and ALS are neurodegenerative diseases related to impaired autophagy-mediated degradation process, suggesting CHMP2B and probably the ESCRT machinery are important for the autophagy function. In line with this discovery, it was recently found by several groups that functional disruption of the ESCRT proteins results in accumulation

of autophagosomes and inhibition of autophagic degradation [46, 218-220]. How the ESCRT machinery is involved is still unclear, but current data suggest the functional MVB pathway is necessary for autophagy. Elucidating the molecular mechanism underlying this process would be of particular interest for clinical treatments of autophagy-related neurodegenerative diseases.

SUMMARY

The ESCRT machinery functions in the MVB pathway and is essential in many physiological and pathological processes. Vps4 catalyzes the ESCRT disassembly, an event critical for regulating the ESCRT activity and perhaps directly involved in ILV formation. In the absence of Vps4 function, all the ESCRT components are trapped on the endosomal membrane, therefore shutting down the entire MVB pathway. Owing to its functional importance, the Vps4-dependent ESCRT disassembly reaction has generated great interest over the past few years. However, the detailed molecular mechanism that drives the action and regulation of Vps4 function, particularly with regard to the interplay between Vps4, Vta1, Ist1, and the regulatory ESCRT-III proteins Vps60 and Did2, is poorly defined. My thesis focuses on addressing these questions by a structural and biochemical approach. In Chapter 2, I will describe the ATPase reaction cycle of Vps4 and discuss its nucleotide-dependent conformational change and substrate interaction. In Chapter 3, I will present the structural basis of Vta1 function and illustrate how its structure contributes to its Vps4-regulating and Vps60/Did2-binding properties. In Chapter 4, I will provide functional insights of Ist1 by reporting its N-terminal domain

structure and characterizing its interaction with Did2. In Chapter 5, I will summarize and discuss the molecular mechanism of Vps4 function and regulation in the MVB pathway. Taken together, these results provide a better understanding for the function and regulation mechanism of Vps4 and enable us to evaluate the roles of these proteins in contributing to the overall function of the MVB pathway in the cell.

REFERENCES

1. Hurley, J.H., *ESCRT complexes and the biogenesis of multivesicular bodies.* Curr Opin Cell Biol, 2008. **20**(1): p. 4-11.

2. Saksena, S., et al., *ESCRTing proteins in the endocytic pathway.* Trends Biochem Sci, 2007. **32**(12): p. 561-73.

3. Williams, R.L. and S. Urbe, *The emerging shape of the ESCRT machinery.* Nat Rev Mol Cell Biol, 2007. **8**(5): p. 355-68.

4. Hurley, J.H. and S.D. Emr, *The ESCRT complexes: structure and mechanism of a membrane-trafficking network.* Annu Rev Biophys Biomol Struct, 2006. **35**: p. 277-98.

5. Piper, R.C. and D.J. Katzmann, *Biogenesis and function of multivesicular bodies.* Annu Rev Cell Dev Biol, 2007. **23**: p. 519-47.

6. Gruenberg, J. and H. Stenmark, *The biogenesis of multivesicular endosomes.* Nat Rev Mol Cell Biol, 2004. **5**(4): p. 317-23.

7. Schlessinger, J., *Cell signaling by receptor tyrosine kinases.* Cell, 2000. **103**(2): p. 211-25.

8. Yarden, Y. and M.X. Sliwkowski, *Untangling the ErbB signalling network.* Nat Rev Mol Cell Biol, 2001. **2**(2): p. 127-37.

9. Sorkin, A. and L.K. Goh, *Endocytosis and intracellular trafficking of ErbBs.* Exp Cell Res, 2008.

10. Katzmann, D.J., G. Odorizzi, and S.D. Emr, *Receptor downregulation and multivesicular-body sorting.* Nat Rev Mol Cell Biol, 2002. **3**(12): p. 893-905.

11. Miranda, M. and A. Sorkin, *Regulation of receptors and transporters by ubiquitination: new insights into surprisingly similar mechanisms.* Mol Interv, 2007. **7**(3): p. 157-67.

12. Tanaka, N., M. Kyuuma, and K. Sugamura, *Endosomal sorting complex required for transport proteins in cancer pathogenesis, vesicular transport, and non-endosomal functions.* Cancer Sci, 2008. **99**(7): p. 1293-303.

13. Mellman, I., *Endocytosis and molecular sorting.* Annu Rev Cell Dev Biol, 1996. **12**: p. 575-625.

14. Maxfield, F.R. and T.E. McGraw, *Endocytic recycling.* Nat Rev Mol Cell Biol, 2004. **5**(2): p. 121-32.

15. Piper, R.C. and J.P. Luzio, *Ubiquitin-dependent sorting of integral membrane proteins for degradation in lysosomes.* Curr Opin Cell Biol, 2007. **19**(4): p. 459-65.

16. Woodman, P.G. and C.E. Futter, *Multivesicular bodies: co-ordinated progression to maturity.* Curr Opin Cell Biol, 2008. **20**(4): p. 408-14.

17. Odorizzi, G., M. Babst, and S.D. Emr, *Phosphoinositide signaling and the regulation of membrane trafficking in yeast.* Trends Biochem Sci, 2000. **25**(5): p. 229-35.

18. Misra, S., G.J. Miller, and J.H. Hurley, *Recognizing phosphatidylinositol 3-phosphate.* Cell, 2001. **107**(5): p. 559-62.

19. Odorizzi, G., M. Babst, and S.D. Emr, *Fab1p PtdIns(3)P 5-kinase function essential for protein sorting in the multivesicular body.* Cell, 1998. **95**(6): p. 847-58.

20. Matsuo, H., et al., *Role of LBPA and Alix in multivesicular liposome formation and endosome organization.* Science, 2004. **303**(5657): p. 531-4.

21. Trajkovic, K., et al., *Ceramide triggers budding of exosome vesicles into multivesicular endosomes.* Science, 2008. **319**(5867): p. 1244-7.

22. Bishop, N. and P. Woodman, *ATPase-defective mammalian VPS4 localizes to aberrant endosomes and impairs cholesterol trafficking.* Mol Biol Cell, 2000. **11**(1): p. 227-39.

23. Yang, M., et al., *The Plasmodium falciparum Vps4 homolog mediates multivesicular body formation.* J Cell Sci, 2004. **117**(Pt 17): p. 3831-8.

24. Peck, J.W., E.T. Bowden, and P.D. Burbelo, *Structure and function of human Vps20 and Snf7 proteins.* Biochem J, 2004. **377**(Pt 3): p. 693-700.

25. Raymond, C.K., et al., *Morphological classification of the yeast vacuolar protein sorting mutants: evidence for a prevacuolar compartment in class E vps mutants.* Mol Biol Cell, 1992. **3**(12): p. 1389-402.

26. Katzmann, D.J., M. Babst, and S.D. Emr, *Ubiquitin-dependent sorting into the multivesicular body pathway requires the function of a conserved endosomal protein sorting complex, ESCRT-I.* Cell, 2001. **106**(2): p. 145-55.

27. Babst, M., et al., *Endosome-associated complex, ESCRT-II, recruits transport machinery for protein sorting at the multivesicular body.* Dev Cell, 2002. **3**(2): p. 283-9.

28. Babst, M., et al., *Escrt-III: an endosome-associated heterooligomeric protein complex required for mvb sorting.* Dev Cell, 2002. **3**(2): p. 271-82.

29. Bilodeau, P.S., et al., *The Vps27p Hse1p complex binds ubiquitin and mediates endosomal protein sorting.* Nat Cell Biol, 2002. **4**(7): p. 534-9.

30. Bache, K.G., et al., *STAM and Hrs are subunits of a multivalent ubiquitin-binding complex on early endosomes.* J Biol Chem, 2003. **278**(14): p. 12513-21.

31. Asao, H., et al., *Hrs is associated with STAM, a signal-transducing adaptor molecule. Its suppressive effect on cytokine-induced cell growth.* J Biol Chem, 1997. **272**(52): p. 32785-91.

32. Babst, M., et al., *Endosomal transport function in yeast requires a novel AAA-type ATPase, Vps4p.* EMBO J, 1997. **16**(8): p. 1820-31.

33. Babst, M., et al., *The Vps4p AAA ATPase regulates membrane association of a Vps protein complex required for normal endosome function.* EMBO J, 1998. **17**(11): p. 2982-93.

34. Babst, M., *A protein's final ESCRT.* Traffic, 2005. **6**(1): p. 2-9.

35. Hochstrasser, M., *Ubiquitin-dependent protein degradation.* Annu Rev Genet, 1996. **30**: p. 405-39.

36. Pickart, C.M., *Ubiquitin in chains.* Trends Biochem Sci, 2000. **25**(11): p. 544-8.

37. Hicke, L. and R. Dunn, *Regulation of membrane protein transport by ubiquitin and ubiquitin-binding proteins.* Annu Rev Cell Dev Biol, 2003. **19**: p. 141-72.

38. Huang, F., et al., *Differential regulation of EGF receptor internalization and degradation by multiubiquitination within the kinase domain.* Mol Cell, 2006. **21**(6): p. 737-48.

39. Duncan, L.M., et al., *Lysine-63-linked ubiquitination is required for endolysosomal degradation of class I molecules.* EMBO J, 2006. **25**(8): p. 1635-45.

40. Winter, V. and M.T. Hauser, *Exploring the ESCRTing machinery in eukaryotes.* Trends Plant Sci, 2006. **11**(3): p. 115-23.

41. Leung, K.F., J.B. Dacks, and M.C. Field, *Evolution of the multivesicular body ESCRT machinery; retention across the eukaryotic lineage.* Traffic, 2008. **9**(10): p. 1698-716.

42. Morita, E. and W.I. Sundquist, *Retrovirus budding.* Annu Rev Cell Dev Biol, 2004. **20**: p. 395-425.

43. Calistri, A., et al., *Role of multivesicular bodies and their components in the egress of enveloped RNA viruses.* Rev Med Virol, 2008.

44. Montoya, M., *An ESCRT for daughters.* Nat Struct Mol Biol, 2007. **14**(7): p. 579.

45. Rusten, T.E. and A. Simonsen, *ESCRT functions in autophagy and associated disease.* Cell Cycle, 2008. **7**(9): p. 1166-72.

46. Lee, J.A. and F.B. Gao, *Roles of ESCRT in autophagy-associated neurodegeneration.* Autophagy, 2008. **4**(2): p. 230-2.

47. Misra, S. and J.H. Hurley, *Crystal structure of a phosphatidylinositol 3-phosphate-specific membrane-targeting motif, the FYVE domain of Vps27p.* Cell, 1999. **97**(5): p. 657-66.

48. Raiborg, C., et al., *FYVE and coiled-coil domains determine the specific localisation of Hrs to early endosomes.* J Cell Sci, 2001. **114**(Pt 12): p. 2255-63.

49. Gaullier, J.M., et al., *FYVE fingers bind PtdIns(3)P.* Nature, 1998. **394**(6692): p. 432-3.

50. Shih, S.C., et al., *Epsins and Vps27p/Hrs contain ubiquitin-binding domains that function in receptor endocytosis.* Nat Cell Biol, 2002. **4**(5): p. 389-93.

51. Swanson, K.A., et al., *Solution structure of Vps27 UIM-ubiquitin complex important for endosomal sorting and receptor downregulation.* EMBO J, 2003. **22**(18): p. 4597-606.

52. Fisher, R.D., et al., *Structure and ubiquitin binding of the ubiquitin-interacting motif.* J Biol Chem, 2003. **278**(31): p. 28976-84.

53. Mizuno, E., et al., *STAM proteins bind ubiquitinated proteins on the early endosome via the VHS domain and ubiquitin-interacting motif.* Mol Biol Cell, 2003. **14**(9): p. 3675-89.

54. McCullough, J., et al., *Activation of the endosome-associated ubiquitin isopeptidase AMSH by STAM, a component of the multivesicular body-sorting machinery.* Curr Biol, 2006. **16**(2): p. 160-5.

55. Ren, J., et al., *Hse1, a component of the yeast Hrs-STAM ubiquitin-sorting complex, associates with ubiquitin peptidases and a ligase to control sorting efficiency into multivesicular bodies.* Mol Biol Cell, 2007. **18**(1): p. 324-35.

56. Kato, M., K. Miyazawa, and N. Kitamura, *A deubiquitinating enzyme UBPY interacts with the Src homology 3 domain of Hrs-binding protein via a novel binding motif PX(V/I)(D/N)RXXKP*. J Biol Chem, 2000. **275**(48): p. 37481-7.

57. Raiborg, C., et al., *Hrs sorts ubiquitinated proteins into clathrin-coated microdomains of early endosomes.* Nat Cell Biol, 2002. **4**(5): p. 394-8.

58. Raiborg, C., et al., *Hrs recruits clathrin to early endosomes.* EMBO J, 2001. **20**(17): p. 5008-21.

59. Ungewickell, E.J. and L. Hinrichsen, *Endocytosis: clathrin-mediated membrane budding.* Curr Opin Cell Biol, 2007. **19**(4): p. 417-25.

60. Hirano, S., et al., *Double-sided ubiquitin binding of Hrs-UIM in endosomal protein sorting.* Nat Struct Mol Biol, 2006. **13**(3): p. 272-7.

61. Mao, Y., et al., *Crystal structure of the VHS and FYVE tandem domains of Hrs, a protein involved in membrane trafficking and signal transduction.* Cell, 2000. **100**(4): p. 447-56.

62. Kaneko, T., et al., *Structural insight into modest binding of a non-PXXP ligand to the signal transducing adaptor molecule-2 Src homology 3 domain.* J Biol Chem, 2003. **278**(48): p. 48162-8.

63. Prag, G., et al., *The Vps27/Hse1 complex is a GAT domain-based scaffold for ubiquitin-dependent sorting.* Dev Cell, 2007. **12**(6): p. 973-86.

64. Kostelansky, M.S., et al., *Molecular architecture and functional model of the complete yeast ESCRT-I heterotetramer.* Cell, 2007. **129**(3): p. 485-98.

65. Bache, K.G., et al., *Hrs regulates multivesicular body formation via ESCRT recruitment to endosomes.* J Cell Biol, 2003. **162**(3): p. 435-42.

66. Katzmann, D.J., et al., *Vps27 recruits ESCRT machinery to endosomes during MVB sorting.* J Cell Biol, 2003. **162**(3): p. 413-23.

67. Bilodeau, P.S., et al., *Vps27-Hse1 and ESCRT-I complexes cooperate to increase efficiency of sorting ubiquitinated proteins at the endosome.* J Cell Biol, 2003. **163**(2): p. 237-43.

68. Sundquist, W.I., et al., *Ubiquitin recognition by the human TSG101 protein.* Mol Cell, 2004. **13**(6): p. 783-9.

69. Teo, H., D.B. Veprintsev, and R.L. Williams, *Structural insights into endosomal sorting complex required for transport (ESCRT-I) recognition of ubiquitinated proteins.* J Biol Chem, 2004. **279**(27): p. 28689-96.

70. Li, L. and S.N. Cohen, *Tsg101: a novel tumor susceptibility gene isolated by controlled homozygous functional knockout of allelic loci in mammalian cells.* Cell, 1996. **85**(3): p. 319-29.

71. Li, L., et al., *The TSG101 tumor susceptibility gene is located in chromosome 11 band p15 and is mutated in human breast cancer.* Cell, 1997. **88**(1): p. 143-54.

72. Moberg, K.H., et al., *Mutations in erupted, the Drosophila ortholog of mammalian tumor susceptibility gene 101, elicit non-cell-autonomous overgrowth.* Dev Cell, 2005. **9**(5): p. 699-710.

73. Pornillos, O., et al., *HIV Gag mimics the Tsg101-recruiting activity of the human Hrs protein.* J Cell Biol, 2003. **162**(3): p. 425-34.

74. Garrus, J.E., et al., *Tsg101 and the vacuolar protein sorting pathway are essential for HIV-1 budding.* Cell, 2001. **107**(1): p. 55-65.

75. Perez, O.D. and G.P. Nolan, *Resistance is futile: assimilation of cellular machinery by HIV-1.* Immunity, 2001. **15**(5): p. 687-90.

76. Martin-Serrano, J., T. Zang, and P.D. Bieniasz, *HIV-1 and Ebola virus encode small peptide motifs that recruit Tsg101 to sites of particle assembly to facilitate egress.* Nat Med, 2001. **7**(12): p. 1313-9.

77. VerPlank, L., et al., *Tsg101, a homologue of ubiquitin-conjugating (E2) enzymes, binds the L domain in HIV type 1 Pr55(Gag).* Proc Natl Acad Sci U S A, 2001. **98**(14): p. 7724-9.

78. Teo, H., et al., *ESCRT-I core and ESCRT-II GLUE domain structures reveal role for GLUE in linking to ESCRT-I and membranes.* Cell, 2006. **125**(1): p. 99-111.

79. Nickerson, D.P., M.R. Russell, and G. Odorizzi, *A concentric circle model of multivesicular body cargo sorting.* EMBO Rep, 2007. **8**(7): p. 644-50.

80. Kostelansky, M.S., et al., *Structural and functional organization of the ESCRT-I trafficking complex.* Cell, 2006. **125**(1): p. 113-26.

81. Chu, T., et al., *New component of ESCRT-I regulates endosomal sorting complex assembly.* J Cell Biol, 2006. **175**(5): p. 815-23.

82. Curtiss, M., C. Jones, and M. Babst, *Efficient cargo sorting by ESCRT-I and the subsequent release of ESCRT-I from multivesicular bodies requires the subunit Mvb12.* Mol Biol Cell, 2007. **18**(2): p. 636-45.

83. Morita, E., et al., *Identification of human MVB12 proteins as ESCRT-I subunits that function in HIV budding.* Cell Host Microbe, 2007. **2**(1): p. 41-53.

84. Oestreich, A.J., et al., *Mvb12 is a novel member of ESCRT-I involved in cargo selection by the multivesicular body pathway.* Mol Biol Cell, 2007. **18**(2): p. 646-57.

85. Audhya, A., et al., *MVB-12, a fourth subunit of metazoan ESCRT-I, functions in receptor downregulation.* PLoS ONE, 2007. **2**(9): p. e956.

86. Bowers, K., et al., *Degradation of endocytosed epidermal growth factor and virally ubiquitinated major histocompatibility complex class I is independent of mammalian ESCRTII.* J Biol Chem, 2006. **281**(8): p. 5094-105.

87. Pornillos, O., et al., *Structure of the Tsg101 UEV domain in complex with the PTAP motif of the HIV-1 p6 protein.* Nat Struct Biol, 2002. **9**(11): p. 812-7.

88. Pineda-Molina, E., et al., *The crystal structure of the C-terminal domain of Vps28 reveals a conserved surface required for Vps20 recruitment.* Traffic, 2006. **7**(8): p. 1007-16.

89. Stuchell, M.D., et al., *The human endosomal sorting complex required for transport (ESCRT-I) and its role in HIV-1 budding.* J Biol Chem, 2004. **279**(34): p. 36059-71.

90. Kamura, T., et al., *Cloning and characterization of ELL-associated proteins EAP45 and EAP20. a role for yeast EAP-like proteins in regulation of gene expression by glucose.* J Biol Chem, 2001. **276**(19): p. 16528-33.

91. Thompson, B.J., et al., *Tumor suppressor properties of the ESCRT-II complex component Vps25 in Drosophila.* Dev Cell, 2005. **9**(5): p. 711-20.

92. Vaccari, T. and D. Bilder, *The Drosophila tumor suppressor vps25 prevents nonautonomous overproliferation by regulating notch trafficking.* Dev Cell, 2005. **9**(5): p. 687-98.

93. Herz, H.M., et al., *vps25 mosaics display non-autonomous cell survival and overgrowth, and autonomous apoptosis.* Development, 2006. **133**(10): p. 1871-80.

94. Teo, H., et al., *ESCRT-II, an endosome-associated complex required for protein sorting: crystal structure and interactions with ESCRT-III and membranes.* Dev Cell, 2004. **7**(4): p. 559-69.

95. Bowers, K., et al., *Protein-protein interactions of ESCRT complexes in the yeast Saccharomyces cerevisiae.* Traffic, 2004. **5**(3): p. 194-210.

96. Wang, T. and W. Hong, *RILP interacts with VPS22 and VPS36 of ESCRT-II and regulates their membrane recruitment.* Biochem Biophys Res Commun, 2006. **350**(2): p. 413-23.

97. Progida, C., et al., *RILP interacts with the VPS22 component of the ESCRT-II complex.* Biochem Biophys Res Commun, 2006. **347**(4): p. 1074-9.

98. Progida, C., et al., *RILP is required for the proper morphology and function of late endosomes.* J Cell Sci, 2007. **120**(Pt 21): p. 3729-37.

99. Slagsvold, T., et al., *Eap45 in mammalian ESCRT-II binds ubiquitin via a phosphoinositide-interacting GLUE domain.* J Biol Chem, 2005. **280**(20): p. 19600-6.

100. Alam, S.L., et al., *Structural basis for ubiquitin recognition by the human ESCRT-II EAP45 GLUE domain.* Nat Struct Mol Biol, 2006. **13**(11): p. 1029-30.

101. Hirano, S., et al., *Structural basis of ubiquitin recognition by mammalian Eap45 GLUE domain.* Nat Struct Mol Biol, 2006. **13**(11): p. 1031-2.

102. Im, Y.J. and J.H. Hurley, *Integrated structural model and membrane targeting mechanism of the human ESCRT-II complex.* Dev Cell, 2008. **14**(6): p. 902-13.

103. Gill, D.J., et al., *Structural insight into the ESCRT-I/-II link and its role in MVB trafficking.* EMBO J, 2007. **26**(2): p. 600-12.

104. Alam, S.L., et al., *Ubiquitin interactions of NZF zinc fingers.* EMBO J, 2004. **23**(7): p. 1411-21.

105. Hierro, A., et al., *Structure of the ESCRT-II endosomal trafficking complex.* Nature, 2004. **431**(7005): p. 221-5.

106. Yorikawa, C., et al., *Human CHMP6, a myristoylated ESCRT-III protein, interacts directly with an ESCRT-II component EAP20 and regulates endosomal cargo sorting.* Biochem J, 2005. **387**(Pt 1): p. 17-26.

107. Whitley, P., et al., *Identification of mammalian Vps24p as an effector of phosphatidylinositol 3,5-bisphosphate-dependent endosome compartmentalization.* J Biol Chem, 2003. **278**(40): p. 38786-95.

108. Lin, Y., et al., *Interaction of the mammalian endosomal sorting complex required for transport (ESCRT) III protein hSnf7-1 with itself, membranes, and the AAA+ ATPase SKD1.* J Biol Chem, 2005. **280**(13): p. 12799-809.

109. Nickerson, D.P., M. West, and G. Odorizzi, *Did2 coordinates Vps4-mediated dissociation of ESCRT-III from endosomes.* J Cell Biol, 2006. **175**(5): p. 715-20.

110. Teis, D., S. Saksena, and S.D. Emr, *Ordered Assembly of the ESCRT-III Complex on Endosomes Is Required to Sequester Cargo during MVB Formation.* Dev Cell, 2008. **15**(4): p. 578-89.

111. Bache, K.G., et al., *The ESCRT-III subunit hVps24 is required for degradation but not silencing of the epidermal growth factor receptor.* Mol Biol Cell, 2006. **17**(6): p. 2513-23.

112. Shim, J.H., et al., *CHMP5 is essential for late endosome function and down-regulation of receptor signaling during mouse embryogenesis.* J Cell Biol, 2006. **172**(7): p. 1045-56.

113. Li, J., et al., *Chmp1A functions as a novel tumor suppressor gene in human embryonic kidney and ductal pancreatic tumor cells.* Cell Cycle, 2008. **7**(18): p. 2886-93.

114. Carlton, J.G., M. Agromayor, and J. Martin-Serrano, *Differential requirements for Alix and ESCRT-III in cytokinesis and HIV-1 release.* Proc Natl Acad Sci U S A, 2008. **105**(30): p. 10541-6.

115. Horii, M., et al., *CHMP7, a novel ESCRT-III-related protein, associates with CHMP4b and functions in the endosomal sorting pathway.* Biochem J, 2006. **400**(1): p. 23-32.

116. Zamborlini, A., et al., *Release of autoinhibition converts ESCRT-III components into potent inhibitors of HIV-1 budding.* Proc Natl Acad Sci U S A, 2006. **103**(50): p. 19140-5.

117. Martin-Serrano, J., et al., *Divergent retroviral late-budding domains recruit vacuolar protein sorting factors by using alternative adaptor proteins.* Proc Natl Acad Sci U S A, 2003. **100**(21): p. 12414-9.

118. von Schwedler, U.K., et al., *The protein network of HIV budding.* Cell, 2003. **114**(6): p. 701-13.

119. Muziol, T., et al., *Structural basis for budding by the ESCRT-III factor CHMP3.* Dev Cell, 2006. **10**(6): p. 821-30.

120. Shim, S., L.A. Kimpler, and P.I. Hanson, *Structure/function analysis of four core ESCRT-III proteins reveals common regulatory role for extreme C-terminal domain.* Traffic, 2007. **8**(8): p. 1068-79.

121. Hanson, P.I., et al., *Plasma membrane deformation by circular arrays of ESCRT-III protein filaments.* J Cell Biol, 2008. **180**(2): p. 389-402.

122. Lata, S., et al., *Helical structures of ESCRT-III are disassembled by VPS4.* Science, 2008. **321**(5894): p. 1354-7.

123. Ghazi-Tabatabai, S., et al., *Structure and disassembly of filaments formed by the ESCRT-III subunit Vps24.* Structure, 2008. **16**(9): p. 1345-56.

124. Shimada, A., et al., *Curved EFC/F-BAR-domain dimers are joined end to end into a filament for membrane invagination in endocytosis.* Cell, 2007. **129**(4): p. 761-72.

125. Frost, A., et al., *Structural basis of membrane invagination by F-BAR domains.* Cell, 2008. **132**(5): p. 807-17.

126. Dawson, J.C., J.A. Legg, and L.M. Machesky, *Bar domain proteins: a role in tubulation, scission and actin assembly in clathrin-mediated endocytosis.* Trends Cell Biol, 2006. **16**(10): p. 493-8.

127. Itoh, T. and P. De Camilli, *BAR, F-BAR (EFC) and ENTH/ANTH domains in the regulation of membrane-cytosol interfaces and membrane curvature.* Biochim Biophys Acta, 2006. **1761**(8): p. 897-912.

128. Dikic, I., *ALIX-ing phospholipids with endosome biogenesis.* Bioessays, 2004. **26**(6): p. 604-7.

129. Pons, V., et al., *Hrs and SNX3 Functions in Sorting and Membrane Invagination within Multivesicular Bodies.* PLoS Biol, 2008. **6**(9): p. e214.

130. Luhtala, N. and G. Odorizzi, *Bro1 coordinates deubiquitination in the multivesicular body pathway by recruiting Doa4 to endosomes.* J Cell Biol, 2004. **166**(5): p. 717-29.

131. Richter, C., M. West, and G. Odorizzi, *Dual mechanisms specify Doa4-mediated deubiquitination at multivesicular bodies.* EMBO J, 2007. **26**(10): p. 2454-64.

132. Agromayor, M. and J. Martin-Serrano, *Interaction of AMSH with ESCRT-III and deubiquitination of endosomal cargo.* J Biol Chem, 2006. **281**(32): p. 23083-91.

133. Ma, Y.M., et al., *Targeting of AMSH to endosomes is required for epidermal growth factor receptor degradation.* J Biol Chem, 2007. **282**(13): p. 9805-12.

134. Row, P.E., et al., *The MIT domain of UBPY constitutes a CHMP binding and endosomal localization signal required for efficient epidermal growth factor receptor degradation.* J Biol Chem, 2007. **282**(42): p. 30929-37.

135. Vito, P., et al., *Cloning of AIP1, a novel protein that associates with the apoptosis-linked gene ALG-2 in a Ca2+-dependent reaction.* J Biol Chem, 1999. **274**(3): p. 1533-40.

136. Missotten, M., et al., *Alix, a novel mouse protein undergoing calcium-dependent interaction with the apoptosis-linked-gene 2 (ALG-2) protein.* Cell Death Differ, 1999. **6**(2): p. 124-9.

137. Odorizzi, G., *The multiple personalities of Alix.* J Cell Sci, 2006. **119**(Pt 15): p. 3025-32.

138. Fujii, K., J.H. Hurley, and E.O. Freed, *Beyond Tsg101: the role of Alix in 'ESCRTing' HIV-1.* Nat Rev Microbiol, 2007. **5**(12): p. 912-6.

139. Carlton, J.G. and J. Martin-Serrano, *Parallels between cytokinesis and retroviral budding: a role for the ESCRT machinery.* Science, 2007. **316**(5833): p. 1908-12.

140. Morita, E., et al., *Human ESCRT and ALIX proteins interact with proteins of the midbody and function in cytokinesis.* EMBO J, 2007. **26**(19): p. 4215-27.

141. Katoh, K., et al., *The ALG-2-interacting protein Alix associates with CHMP4b, a human homologue of yeast Snf7 that is involved in multivesicular body sorting.* J Biol Chem, 2003. **278**(40): p. 39104-13.

142. Kim, J., et al., *Structural basis for endosomal targeting by the Bro1 domain.* Dev Cell, 2005. **8**(6): p. 937-47.

143. Usami, Y., S. Popov, and H.G. Gottlinger, *Potent rescue of human immunodeficiency virus type 1 late domain mutants by ALIX/AIP1 depends on its CHMP4 binding site.* J Virol, 2007. **81**(12): p. 6614-22.

144. McCullough, J., et al., *ALIX-CHMP4 interactions in the human ESCRT pathway.* Proc Natl Acad Sci U S A, 2008. **105**(22): p. 7687-91.

145. Lee, S., et al., *Structural basis for viral late-domain binding to Alix.* Nat Struct Mol Biol, 2007. **14**(3): p. 194-9.

146. Zhai, Q., et al., *Structural and functional studies of ALIX interactions with YPX(n)L late domains of HIV-1 and EIAV.* Nat Struct Mol Biol, 2008. **15**(1): p. 43-9.

147. Fisher, R.D., et al., *Structural and biochemical studies of ALIX/AIP1 and its role in retrovirus budding.* Cell, 2007. **128**(5): p. 841-52.

148. Strack, B., et al., *AIP1/ALIX is a binding partner for HIV-1 p6 and EIAV p9 functioning in virus budding.* Cell, 2003. **114**(6): p. 689-99.

149. Fujita, H., et al., *A dominant negative form of the AAA ATPase SKD1/VPS4 impairs membrane trafficking out of endosomal/lysosomal compartments: class E vps phenotype in mammalian cells.* J Cell Sci, 2003. **116**(Pt 2): p. 401-14.

150. Scheuring, S., et al., *Mammalian cells express two VPS4 proteins both of which are involved in intracellular protein trafficking.* J Mol Biol, 2001. **312**(3): p. 469-80.

151. Scheuring, S., et al., *Cloning, characterisation, and functional expression of the Mus musculus SKD1 gene in yeast demonstrates that the mouse SKD1 and the yeast VPS4 genes are orthologues and involved in intracellular protein trafficking.* Gene, 1999. **234**(1): p. 149-59.

152. Lupas, A.N. and J. Martin, *AAA proteins.* Curr Opin Struct Biol, 2002. **12**(6): p. 746-53.

153. Frickey, T. and A.N. Lupas, *Phylogenetic analysis of AAA proteins.* J Struct Biol, 2004. **146**(1-2): p. 2-10.

154. Erzberger, J.P. and J.M. Berger, *Evolutionary relationships and structural mechanisms of AAA+ proteins.* Annu Rev Biophys Biomol Struct, 2006. **35**: p. 93-114.

155. Hanson, P.I. and S.W. Whiteheart, *AAA+ proteins: have engine, will work.* Nat Rev Mol Cell Biol, 2005. **6**(7): p. 519-29.

156. Ogura, T. and A.J. Wilkinson, *AAA+ superfamily ATPases: common structure--diverse function.* Genes Cells, 2001. **6**(7): p. 575-97.

157. Maurizi, M.R. and C.C. Li, *AAA proteins: in search of a common molecular basis. International Meeting on Cellular Functions of AAA Proteins.* EMBO Rep, 2001. **2**(11): p. 980-5.

158. Salinas, S., et al., *Spastin and microtubules: Functions in health and disease.* J Neurosci Res, 2007. **85**(12): p. 2778-82.

159. Quarmby, L., *Cellular Samurai: katanin and the severing of microtubules.* J Cell Sci, 2000. **113 (Pt 16)**: p. 2821-7.

160. Brunger, A.T., *Structure of proteins involved in synaptic vesicle fusion in neurons.* Annu Rev Biophys Biomol Struct, 2001. **30**: p. 157-71.

161. Scott, A., et al., *Structural and mechanistic studies of VPS4 proteins.* EMBO J, 2005. **24**(20): p. 3658-69.

162. Xiao, J., et al., *Structural characterization of the ATPase reaction cycle of endosomal AAA protein Vps4.* J Mol Biol, 2007. **374**(3): p. 655-70.

163. Hartmann, C., et al., *Vacuolar protein sorting: two different functional states of the AAA-ATPase Vps4p.* J Mol Biol, 2008. **377**(2): p. 352-63.

164. Inoue, M., et al., *Nucleotide-dependent conformational changes and assembly of the AAA ATPase SKD1/VPS4B.* Traffic, 2008.

165. Gonciarz, M.D., et al., *Biochemical and Structural Studies of Yeast Vps4 Oligomerization.* J Mol Biol, 2008.

166. Roll-Mecak, A. and R.D. Vale, *Structural basis of microtubule severing by the hereditary spastic paraplegia protein spastin.* Nature, 2008. **451**(7176): p. 363-7.

167. Davies, J.M., A.T. Brunger, and W.I. Weis, *Improved structures of full-length p97, an AAA ATPase: implications for mechanisms of nucleotide-dependent conformational change.* Structure, 2008. **16**(5): p. 715-26.

168. Vale, R.D., *AAA proteins. Lords of the ring.* J Cell Biol, 2000. **150**(1): p. F13-9.

169. Brunger, A.T. and B. DeLaBarre, *NSF and p97/VCP: similar at first, different at last.* FEBS Lett, 2003. **555**(1): p. 126-33.

170. Yu, Z., et al., *Cryo-EM structure of dodecameric Vps4p and its 2:1 complex with Vta1p.* J Mol Biol, 2008. **377**(2): p. 364-77.

171. Ciccarelli, F.D., et al., *The identification of a conserved domain in both spartin and spastin, mutated in hereditary spastic paraplegia.* Genomics, 2003. **81**(4): p. 437-41.

172. Scott, A., et al., *Structure and ESCRT-III protein interactions of the MIT domain of human VPS4A.* Proc Natl Acad Sci U S A, 2005. **102**(39): p. 13813-8.

173. Takasu, H., et al., *Structural characterization of the MIT domain from human Vps4b.* Biochem Biophys Res Commun, 2005. **334**(2): p. 460-5.

174. Obita, T., et al., *Structural basis for selective recognition of ESCRT-III by the AAA ATPase Vps4.* Nature, 2007. **449**(7163): p. 735-9.

175. Stuchell-Brereton, M.D., et al., *ESCRT-III recognition by VPS4 ATPases.* Nature, 2007. **449**(7163): p. 740-4.

176. Kieffer, C., et al., *Two distinct modes of ESCRT-III recognition are required for VPS4 functions in lysosomal protein targeting and HIV-1 budding.* Dev Cell, 2008. **15**(1): p. 62-73.

177. Azmi, I.F., et al., *ESCRT-III family members stimulate Vps4 ATPase activity directly or via Vta1*. Dev Cell, 2008. **14**(1): p. 50-61.

178. Xiao, J., et al., *Structural basis of Vta1 function in the multivesicular body sorting pathway*. Dev Cell, 2008. **14**(1): p. 37-49.

179. Shim, S., S.A. Merrill, and P.I. Hanson, *Novel interactions of ESCRT-III with LIP5 and VPS4 and their implications for ESCRT-III disassembly*. Mol Biol Cell, 2008. **19**(6): p. 2661-72.

180. Zolkiewski, M., *A camel passes through the eye of a needle: protein unfolding activity of Clp ATPases.* Mol Microbiol, 2006. **61**(5): p. 1094-100.

181. DeLaBarre, B., et al., *Central pore residues mediate the p97/VCP activity required for ERAD.* Mol Cell, 2006. **22**(4): p. 451-62.

182. White, S.R., et al., *Recognition of C-terminal amino acids in tubulin by pore loops in Spastin is important for microtubule severing.* J Cell Biol, 2007. **176**(7): p. 995-1005.

183. Tessarz, P., A. Mogk, and B. Bukau, *Substrate threading through the central pore of the Hsp104 chaperone as a common mechanism for protein disaggregation and prion propagation.* Mol Microbiol, 2008. **68**(1): p. 87-97.

184. Singleton, M.R., M.S. Dillingham, and D.B. Wigley, *Structure and mechanism of helicases and nucleic acid translocases.* Annu Rev Biochem, 2007. **76**: p. 23-50.

185. Praefcke, G.J. and H.T. McMahon, *The dynamin superfamily: universal membrane tubulation and fission molecules?* Nat Rev Mol Cell Biol, 2004. **5**(2): p. 133-47.

186. Roux, A., et al., *GTP-dependent twisting of dynamin implicates constriction and tension in membrane fission.* Nature, 2006. **441**(7092): p. 528-31.

187. Azmi, I., et al., *Recycling of ESCRTs by the AAA-ATPase Vps4 is regulated by a conserved VSL region in Vta1*. J Cell Biol, 2006. **172**(5): p. 705-17.

188. Lottridge, J.M., et al., *Vta1p and Vps46p regulate the membrane association and ATPase activity of Vps4p at the yeast multivesicular body.* Proc Natl Acad Sci U S A, 2006. **103**(16): p. 6202-7.

189. Dimaano, C., et al., *Ist1 regulates Vps4 localization and assembly.* Mol Biol Cell, 2008. **19**(2): p. 465-74.

190. Yeo, S.C., et al., *Vps20p and Vta1p interact with Vps4p and function in multivesicular body sorting and endosomal transport in Saccharomyces cerevisiae.* J Cell Sci, 2003. **116**(Pt 19): p. 3957-70.

191. Fujita, H., et al., *Mammalian class E Vps proteins, SBP1 and mVps2/CHMP2A, interact with and regulate the function of an AAA-ATPase SKD1/Vps4B.* J Cell Sci, 2004. **117**(Pt 14): p. 2997-3009.

192. Haas, T.J., et al., *The Arabidopsis AAA ATPase SKD1 is involved in multivesicular endosome function and interacts with its positive regulator LYST-INTERACTING PROTEIN5.* Plant Cell, 2007. **19**(4): p. 1295-312.

193. Shiflett, S.L., et al., *Characterization of Vta1p, a class E Vps protein in Saccharomyces cerevisiae.* J Biol Chem, 2004. **279**(12): p. 10982-90.

194. Ward, D.M., et al., *The role of LIP5 and CHMP5 in multivesicular body formation and HIV-1 budding in mammalian cells.* J Biol Chem, 2005. **280**(11): p. 10548-55.

195. Tsang, H.T., et al., *A systematic analysis of human CHMP protein interactions: additional MIT domain-containing proteins bind to multiple components of the human ESCRT III complex.* Genomics, 2006. **88**(3): p. 333-46.

196. Hurley, J.H. and D. Yang, *MIT domainia.* Dev Cell, 2008. **14**(1): p. 6-8.

197. Rue, S.M., et al., *Novel Ist1-Did2 complex functions at a late step in multivesicular body sorting.* Mol Biol Cell, 2008. **19**(2): p. 475-84.

198. Marchler-Bauer, A., et al., *CDD: a Conserved Domain Database for protein classification.* Nucleic Acids Res, 2005. **33**(Database issue): p. D192-6.

199. Marchler-Bauer, A., et al., *CDD: a conserved domain database for interactive domain family analysis.* Nucleic Acids Res, 2007. **35**(Database issue): p. D237-40.

200. Wang, P., et al., *AAA ATPases regulate membrane association of yeast oxysterol binding proteins and sterol metabolism.* EMBO J, 2005. **24**(17): p. 2989-99.

201. Ohsaki, Y., et al., *Cholesterol depletion facilitates ubiquitylation of NPC1 and its association with SKD1/Vps4.* J Cell Sci, 2006. **119**(Pt 13): p. 2643-53.

202. Chen, B.J. and R.A. Lamb, *Mechanisms for enveloped virus budding: can some viruses do without an ESCRT?* Virology, 2008. **372**(2): p. 221-32.

203. Licata, J.M., et al., *Overlapping motifs (PTAP and PPEY) within the Ebola virus VP40 protein function independently as late budding domains: involvement of host proteins TSG101 and VPS-4.* J Virol, 2003. **77**(3): p. 1812-9.

204. Bouamr, F., et al., *PPPYVEPTAP motif is the late domain of human T-cell leukemia virus type 1 Gag and mediates its functional interaction with cellular proteins Nedd4 and Tsg101 [corrected].* J Virol, 2003. **77**(22): p. 11882-95.

205. Spitzer, C., et al., *The Arabidopsis elch mutant reveals functions of an ESCRT component in cytokinesis.* Development, 2006. **133**(23): p. 4679-89.

206. Lee, H.H., et al., *Midbody targeting of the ESCRT machinery by a noncanonical coiled coil in CEP55.* Science, 2008. **322**(5901): p. 576-80.

207. Hobel, C.F., et al., *The Sulfolobus solfataricus AAA protein Sso0909, a homologue of the eukaryotic ESCRT Vps4 ATPase.* Biochem Soc Trans, 2008. **36**(Pt 1): p. 94-8.

208. Ellen, A.F., et al., *Proteomic analysis of secreted membrane vesicles of archaeal Sulfolobus species reveals the presence of endosome sorting complex components.* Extremophiles, 2008.

209. Lindas, A.C., et al., *A unique cell division machinery in the Archaea.* Proc Natl Acad Sci U S A, 2008.

210. Mizushima, N., et al., *Autophagy fights disease through cellular self-digestion.* Nature, 2008. **451**(7182): p. 1069-75.

211. Shintani, T. and D.J. Klionsky, *Autophagy in health and disease: a double-edged sword.* Science, 2004. **306**(5698): p. 990-5.

212. Klionsky, D.J. and S.D. Emr, *Autophagy as a regulated pathway of cellular degradation.* Science, 2000. **290**(5497): p. 1717-21.

213. Xie, Z. and D.J. Klionsky, *Autophagosome formation: core machinery and adaptations.* Nat Cell Biol, 2007. **9**(10): p. 1102-9.

214. Shirahama, K., T. Noda, and Y. Ohsumi, *Mutational analysis of Csc1/Vps4p: involvement of endosome in regulation of autophagy in yeast.* Cell Struct Funct, 1997. **22**(5): p. 501-9.

215. Roudier, N., C. Lefebvre, and R. Legouis, *CeVPS-27 is an endosomal protein required for the molting and the endocytic trafficking of the low-density lipoprotein receptor-related protein 1 in Caenorhabditis elegans.* Traffic, 2005. **6**(8): p. 695-705.

216. Skibinski, G., et al., *Mutations in the endosomal ESCRTIII-complex subunit CHMP2B in frontotemporal dementia.* Nat Genet, 2005. **37**(8): p. 806-8.

217. Parkinson, N., et al., *ALS phenotypes with mutations in CHMP2B (charged multivesicular body protein 2B).* Neurology, 2006. **67**(6): p. 1074-7.

218. Lee, J.A., et al., *ESCRT-III dysfunction causes autophagosome accumulation and neurodegeneration.* Curr Biol, 2007. **17**(18): p. 1561-7.

219. Rusten, T.E., et al., *ESCRTs and Fab1 regulate distinct steps of autophagy.* Curr Biol, 2007. **17**(20): p. 1817-25.

220. Filimonenko, M., et al., *Functional multivesicular bodies are required for autophagic clearance of protein aggregates associated with neurodegenerative disease.* J Cell Biol, 2007. **179**(3): p. 485-500.

CHAPTER 2

STRUCTURAL CHARACTERIZATION OF THE ATPASE REACTION CYCLE OF ENDOSOMAL AAA-PROTEIN VPS4

ABSTRACT

The Multi-Vesicular Body (MVB) pathway functions in multiple cellular processes including cell surface receptor down-regulation and viral budding from host cells. An important step in the MVB pathway is the correct sorting of cargo molecules, which requires the assembly and disassembly of Endosomal Sorting Complexes Required for Transport (ESCRTs) on the endosomal membrane. Disassembly of the ESCRTs is catalyzed by AAA-protein (ATPase Associated with various cellular Activities) Vps4. Vps4 contains a single AAA domain and undergoes ATP-dependent quaternary structural change to disassemble the ESCRTs. Structural and biochemical analyses of the Vps4 ATPase reaction cycle are reported here. Crystal structures of *S. cerevisiae* Vps4 in both the nucleotide-free form and the ADP-bound form provide the first structural view illustrating how nucleotide binding might induce conformational changes within Vps4 that leads to oligomerization and binding to its substrate ESCRT-III subunits. In contrast to previous models, characterization of the Vps4 structure now supports a model where the ground state of Vps4 in the ATPase reaction cycle is predominantly a monomer and the activated state is a dodecamer. Comparison with a previously reported human VPS4B

structure suggests that Vps4 functions in the MVB pathway via a highly conserved mechanism supported by similar protein-protein interactions during its ATPase reaction cycle.

INTRODUCTION

A significant number of activated cell surface receptors are down-regulated through endocytosis and delivery to the hydrolytic organelle the lysosome for degradation [1]. This process is mediated by a special form of the late endosome called the multi-vesicular body (MVB). During MVB formation, MVB cargoes are sorted into invaginating vesicles, which further bud into the lumen of the endosome. Fusion of the MVBs with the lysosome delivers the cargo-carrying intralumenal vesicles to the hydrolytic activity of the lysosome for degradation [2-4]. Sorting of proteins into the MVB pathway is not limited to endocytic cargoes. Lysosomal resident proteins are sorted directly from the Golgi apparatus into the lysosome without transiting the cell surface. In addition to facilitating delivery of proteins to the lysosome, the MVB machinery also participates in the budding of retroviruses from the host cell [5] and more recently has been implicated in abscission, the final stage of cytokinesis [6].

MVB cargoes are sorted into the MVB pathway via the action of class E Vps (Vacuolar Protein Sorting) proteins, a majority of which are subunits of three distinct protein complexes called ESCRTs (Endosomal Sorting Complexes Required for Transport, -I, -II and –III) [7, 8]. These complexes are transiently recruited from the cytoplasm to the endosomal membrane where they function sequentially in the sorting of cargo proteins into the MVB pathway and possibly in the formation of MVB vesicles [3].

After protein sorting is completed, the ESCRTs are disassembled and released from the endosomal membrane for further rounds of action [3]. Disassembly of the ESCRTs requires the activity of Vps4, a member of the AAA-protein (ATPase Associated with various cellular Activities) family [9, 10]. The functional importance of Vps4 is underscored by the fact that loss of Vps4 activity results in accumulation of the ESCRTs on the endosomal membrane, impairment of cargo sorting and blockage of viral budding [11-17].

The ESCRT disassembly activity of Vps4 is tightly coupled to the ATPase reaction cycle of Vps4. Disruption of Vps4 ATPase activity through point mutations resulted in the accumulation of ESCRT on the endosomal membrane [9]. Upon binding ATP, Vps4 undergoes protein oligomerization which enables its binding to the ESCRTs [10]. When ATP is hydrolyzed into ADP, the stability of the oligomer decreases and it disassembles into a lower molecular weight species *in vitro*. In order to understand the molecular mechanism by which Vps4 catalyzes the disassembly of the ESCRTs, it is necessary to define the detailed conformational changes within the Vps4 structure during its ATPase reaction cycle. To this end, we have now determined the crystal structures of *S. cerevisiae* Vps4 both in the absence of nucleotide and in the presence of ADP. This study provides the first structural view detailing how adenine nucleotide binding might trigger conformational changes within Vps4 leading to protein oligomerization and ESCRT binding. Given the importance of quaternary structural change in the mechanism of Vps4 action, our structural and biochemical characterization now supports a model of Vps4 monomer as the ground state in the ATPase reaction cycle in contrast to a prior notion that Vps4 is a molecular dimer in the absence of ATP binding. Together with a

previously reported nucleotide-free human VPS4B structure [18], our study suggests that Vps4 functions in the MVB pathway via a highly conserved mechanism supported by similar protein-protein interactions during its ATPase reaction cycle.

RESULTS

Structure determination

The crystal structure of Vps4 from the budding yeast *S. cerevisiae* was determined using an ATPase deficient mutant (E233Q) fragment that encompasses residues 83-437. The missing 82 residues are known to fold into an independent domain responsible for binding protein substrates including subunits of ESCRT-III [19]. Deletion of these residues, however, does not affect the ATPase activity or ATP-dependent oligomerization of Vps4, suggesting that the N-terminal domain is dispensable for the ATPase reaction cycle of Vps4. Two different crystal forms were obtained, one in the absence and the other in the presence of 5 mM ADP. The nucleotide-free form belongs to the $P6_522$ space group with one molecule in the asymmetric unit and the ADP-bound form belongs to the $P2_12_12_1$ space group with three molecules in the asymmetric unit. Final structure of the nucleotide-free form was refined to a resolution of 2.9Å with an R-factor of 25.9% and an R_{free} of 28.8% and that of the ADP-bound form was refined to a resolution of 3.2Å with an R-factor of 25.5% and an R_{free} of 30.5% (Table 2.1). Residues not included in the final structural models have no observable electron density and are presumably disordered.

Overall structure

Table 2.1 Crystallographic Data Statistics

	Crystal form I (apo)				Crystal form II (ADP)
	Native	SeMet			Native
Data collection statistics					
Wavelength		0.9799 Å	0.9801Å	0.9499Å	
Space group	$P6_522$		$P6_522$		$P2_12_12_1$
Unit cell (Å)	a = b = 86.55 Å c = 236.06 Å		a = b = 87.20 Å c = 235.59 Å		a = 75.63 Å, b = 120.64 Å, c = 157.33 Å
Resolution (Å)	2.9	3.2	3.2	3.2	3.2
Completeness (%)	98.1 (99.2)	99.6 (97.8)	99.4 (95.9)	99.3 (94.8)	99.4 (97.3)
I/σ[a]	37.5 (3.8)	38.7 (3.6)	37.3 (3.0)	37.0 (2.6)	26.9 (2.5)
R_{merge} (%)[a]	6.3 (60.6)	8.1 (50.5)	6.8 (55.9)	6.8 (50.5)	4.2 (47.5)
Redundancy	13.2	13.3	13.3	13.2	3.7
Unique reflections	10,792	9,425	9,428	9,466	24,259

MAD phasing statistics for Crystal form I

	Peak		Edge		Remote	
	Isomorphous	Anomalous	Isomorphous	Anomalous	Isomorphous	Anomalous
Phasing power[b]						
Centric	-	-	0.888	-	1.011	-
Acentric	-	2.438	0.928	1.552	1.159	1.524
FOM[c]						
Centric	0.346					
Acentric	0.507					
FOM after DM[d]	0.820					

Refinement statistics (Native data set)		
R_{work}/ R_{free}(%)[e]	25.8/28.8	25.5/30.5
Rmsd, bonds (Å)	0.009	0.008
Rmsd, angles (°)	1.135	1.281
Mean B ($Å^2$)	61.8	120.0
Ramachandran	86.2%/13.0%/0.4%/0.4%	73.8%/24.8%/1.4%/0%
Molecules/ASU	1	3

[a]Values in parentheses are for the highest resolution bin.
[b]Phasing power = < [| Fh(calc) | / phase-integrated lack of closure] >.
[c]Figure of merit.
[d]Figure of merit after solvent flattening in the program DM.
[e]$R = \Sigma(|F_{obs}| - |F_{calc}|)/|F_{obs}|$. R_{free} is the R value obtained for a test set of reflections that consisted of a randomly selected 5% subset of the diffraction data used during refinement.

The structure of yeast Vps4 contains a single canonical AAA-domain fold [20, 21] that can be further divided into a large subdomain and a small subdomain (Figure 2.1A). The large subdomain has an α/β fold that includes α-helices α1-α6 and β-strands β0-β5. Strands β1-β5 form a parallel β-sheet in the order of β2-β3-β4-β1-β5 with the additional strand β0 running anti-parallel next to strand β2. Six helices are distributed on both sides of the sheet with α1-α2 on one side and α3-α6 on the other. The small subdomain has an all-α fold that includes four α-helices α7-α10. Sequence alignment of Vps4 homologs reveals two unique structural features not seen in other AAA-family proteins, a stretch of 42 to 48 residues inserted between α9 and α10 in the small subdomain (colored pink) and a stretch of extra 23 residues at the C-terminus of the protein (colored green) (Figure 2.1B). In yeast Vps4, the small subdomain insertion sequence folds into an independent anti-parallel β-strand-containing domain (β6-β8) that has few interactions with the rest of the protein. This domain has been shown to interact with Vps4 regulator Vta1 [18]. The C-terminal sequence is structured as a four-turn α-helix (α11) that packs itself onto the large subdomain at the same side of the parallel β-sheet as helices α3-α6. Deletion of the C-terminal helix resulted in an insoluble and unstable mutant protein suggesting that the helix is an integral part of the large subdomain structure (data not shown). The function of the helix is not known but it is thought to participate in subunit interaction upon Vps4 oligomerization [5]. Vps4 belongs to the “meiotic” clade of the AAA protein family that also includes katanin, spastin and fidgetin [22]. Like Vps4, these proteins all contain a single AAA domain in their sequences. While the β-domain insertion appears to be a unique feature in Vps4 proteins

Figure 2.1 Crystal structure of yeast Vps4 and sequence alignment of Vps4 proteins. (**A**) Stereo view of the monomeric yeast Vps4 structure in a ribbon representation. The large AAA ATPase subdomain is colored blue; the small AAA ATPase subdomain is colored orange; the β domain is colored pink; and the C-terminal helix is colored green. Structurally disordered regions are represented as dash lines. α-Helices are labeled as α1-α11 and β-strands β0-β8. The N- and C-termini of the structure are also indicated. (**B**) Sequence alignments of Vps4 proteins from *S. cerevisiae*, *S. pombe*, *C. elegans*, *D. melanogaster* and *H. sapiens*. Secondary structural elements identified in the crystal structure of yeast Vps4 are displayed above its sequence. α-Helices shown as cylinders, β-strands arrows and loops as lines. They are labeled and colored using a same scheme as in **A**. Structurally disordered regions are shown as dash lines. Conserved residues are shaded with gray boxes.

A

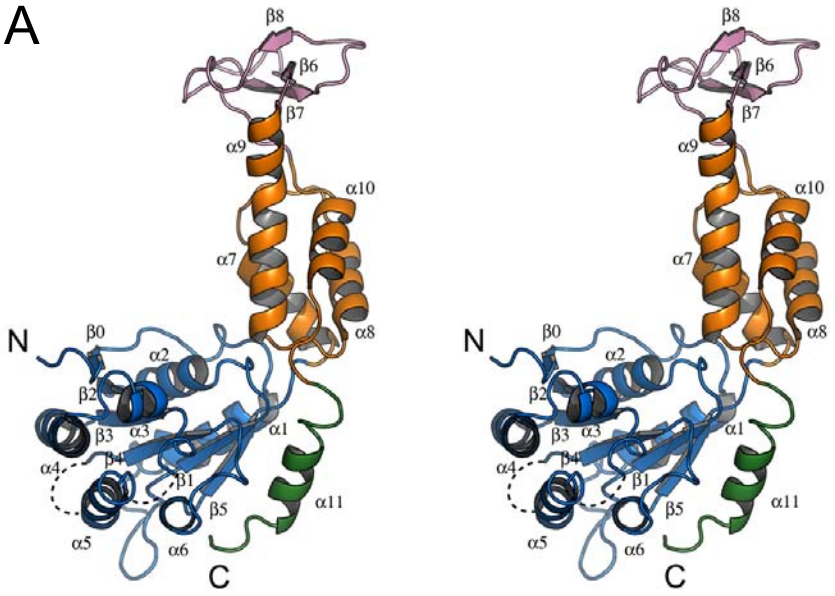
β8
β6
β7
α9
α10
α7
α8
N
β0
α2
β2
β3
α3
α1
α4
β4
β1
β5
α11
α5
α6
C

B

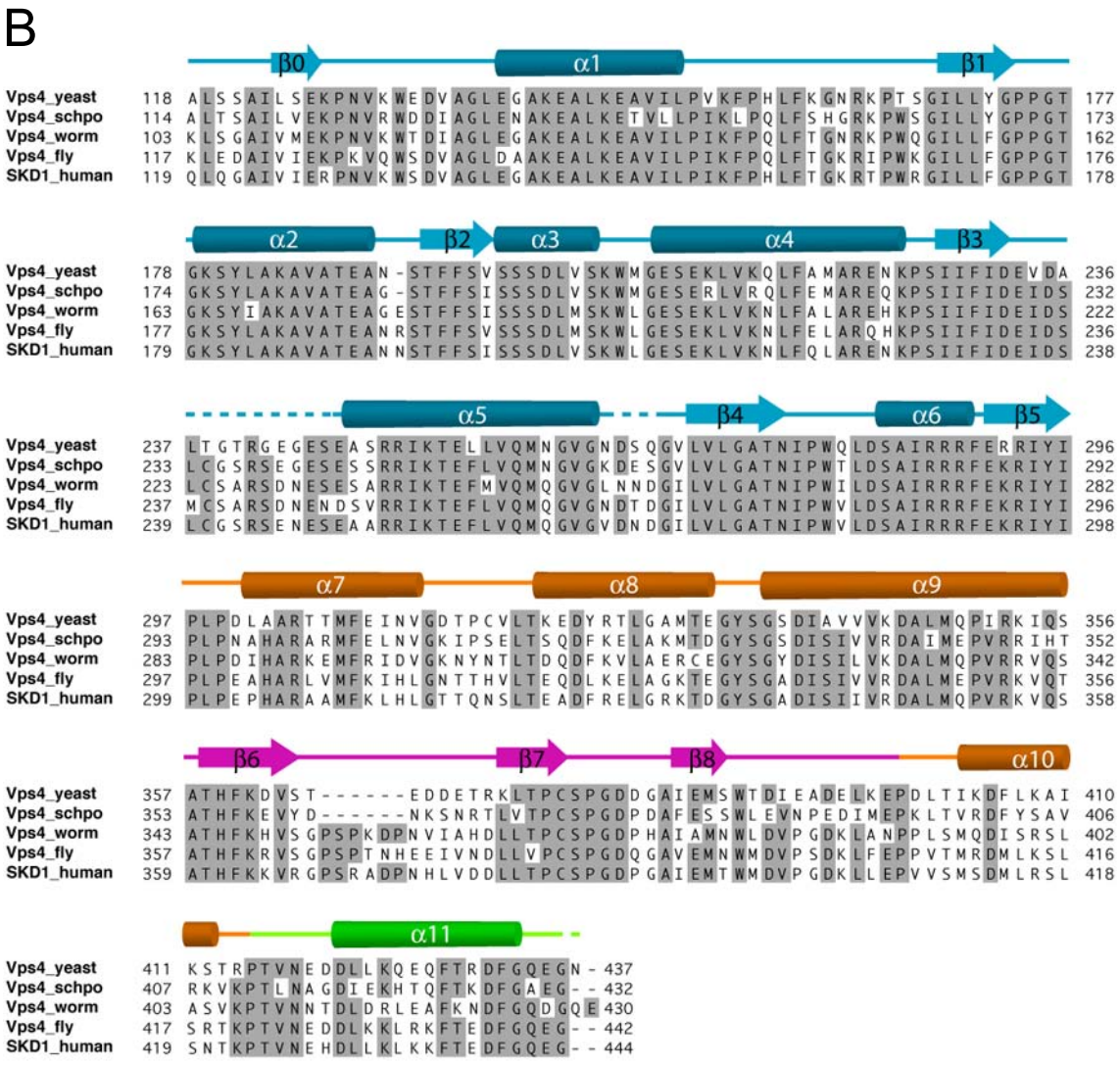
β0 α1 β1
Vps4_yeast 118 ALSSAILSEKPNVKWEDVAGLEGAKEALKEAVILPVKFPHLFKGNRKPTSGILLYGPPGT 177
Vps4_schpo 114 ALTSAILVEKPNVRWDDIAGLENAKEALKETVLLPIKLPQLFSHGRKPWSGILLYGPPGT 173
Vps4_worm 103 KLSGAIVMEKPNVKWTDIAGLEGAKEALKEAVILPIKFPQLFTGNRKPWQGILLFGPPGT 162
Vps4_fly 117 KLEDAIVIEKPKVQWSDVAGLDAAKEALKEAVILPIKFPQLFTGKRIPWKGILLFGPPGT 176
SKD1_human 119 QLQGAIVIERPNVKWSDVAGLEGAKEALKEAVILPIKFPHLFTGKRTPWRGILLFGPPGT 178
α2 β2 α3 α4 β3
Vps4_yeast 178 GKSYLAKAVATEAN-STFFSVSSSDLVSKWMGESEKLVKQLFAMARENKPSIIFIDEVDA 236
Vps4_schpo 174 GKSYLAKAVATEAG-STFFSISSSDLVSKWMGESERLVRQLFEMAREQKPSIIFIDEIDS 232
Vps4_worm 163 GKSYIAKAVATEAGESTFFSISSSDLMSKWLGESEKLVKNLFALAREHKPSIIFIDEIDS 222
Vps4_fly 177 GKSYLAKAVATEANRSTFFSVSSSDLMSKWLGESEKLVKNLFELARQHKPSIIFIDEIDS 236
SKD1_human 179 GKSYLAKAVATEANNSTFFSISSSDLVSKWLGESEKLVKNLFQLARENKPSIIFIDEIDS 238
α5 β4 α6 β5
Vps4_yeast 237 LTGTRGEGESEASRRIKTELLVQMNGVGNDSQGVLVLGATNIPWQLDSAIRRRFERRIYI 296
Vps4_schpo 233 LCGSRSEGESESSRRIKTEFLVQMNGVGKDESGVLVLGATNIPWTLDSAIRRRFEKRIYI 292
Vps4_worm 223 LCSARSDNESESARRIKTEFMVQMQGVGLNNDGILVLGATNIPWILDSAIRRRFEKRIYI 282
Vps4_fly 237 MCSARSDNENDSVRRIKTEFLVQMQGVGNDTDGILVLGATNIPWVLDSAIRRRFEKRIYI 296
SKD1_human 239 LCGSRSENESEAARRIKTEFLVQMQGVGVDNDGILVLGATNIPWVLDSAIRRRFEKRIYI 298
α7 α8 α9
Vps4_yeast 297 PLPDLAARTTMFEINVGDTPCVLTKEDYRTLGAMTEGYSGSDIAVVVKDALMQPIRKIQS 356
Vps4_schpo 293 PLPNAHARARMFELNVGKIPSELTSQDFKELAKMTDGYSGSDISIVVRDAIMEPVRRIHT 352
Vps4_worm 283 PLPDIHARKEMFRIDVGKNYNTLTDQDFKVLAERCEGYSGYDISILVKDALMQPVRRVQS 342
Vps4_fly 297 PLPEAHARLVMFKIHLGNTTHVLTEQDLKELAGKTEGYSGADISIVVRDALMEPVRKVQT 356
SKD1_human 299 PLPEPHARAAMFKLHLGTTQNSLTEADFRELGRKTDGYSGADISIIVRDALMQPVRKVQS 358
β6 β7 β8 α10
Vps4_yeast 357 ATHFKDVST------EDDETRKLTPCSPGDDGAIEMSWTDIEADELKEPDLTIKDFLKAI 410
Vps4_schpo 353 ATHFKEVYD------NKSNRTLVTPCSPGDPDAFESSWLEVNPEDIMEPKLTVRDFYSAV 406
Vps4_worm 343 ATHFKHVSGPSPKDPNVIAHDLLTPCSPGDPHAIAMNWLDVPGDKLANPPLSMQDISRSL 402
Vps4_fly 357 ATHFKRVSGPSPTNHEEIVNDLLVPCSPGDQGAVEMNWMDVPSDKLFEPPVTMRDMLKSL 416
SKD1_human 359 ATHFKKVRGPSRADPNHLVDDLLTPCSPGDPGAIEMTWMDVPGDKLLEPVVSMSDMLRSL 418
α11
Vps4_yeast 411 KSTRPTVNEDDLLKQEQFTRDFGQEGN- 437
Vps4_schpo 407 RKVKPTLNAGDIEKHTQFTKDFGAEG-- 432
Vps4_worm 403 ASVKPTVNNTDLDRLEAFKNDFGQDGQE 430
Vps4_fly 417 SRTKPTVNEDDLKKLRKFTEDFGQEG-- 442
SKD1_human 419 SNTKPTVNEHDLLKLKKFTEDFGQEG-- 444

only, the conserved C-terminal helix has been observed in these other members of the clade suggesting a common mechanism for protein oligomerization [23].

Comparison to human VPS4B structure

The human genome contains two Vps4 genes, VPS4A and VPS4B [24]. Of the two, VPS4B has an overall 60% sequence identity to that of yeast Vps4 and is able to complement the MVB sorting defect in *vps4*-null yeast cells [24]. Comparison between the structures of yeast Vps4 and human VPS4B (in its nucleotide-free form) showed that the overall similarity between the two protein structures is high [18]. The root mean square difference between the two structures based on 285 Cα positions is 2.2 Å. Each of the eleven α-helices and nine β-strands in yeast Vps4 corresponds closely to one of the secondary structural elements in VPS4B, except for the short two-turn helix α3 where the sequence in VPS4B adopts a more extended loop conformation (Figure 2.1B). In addition, VPS4B has a slightly larger β insertion domain where a six-residue insertion was seen in the loop that connects strands β6 and β7. The high degree of structural similarity between the two proteins supports the genetic complementation results that the structure and function of Vps4 is well preserved during evolution.

The quaternary structure of Vps4 in its nucleotide-free form

The most apparent structural change of Vps4 during its ATPase reaction cycle is the change in its quaternary structure. Based on results from gel filtration and chemical cross-linking analyses and the fact that Vps4 is an AAA-protein, it has been suggested that the protein inter-converts between a dimer in the absence of nucleotide and a

dodecamer in the presence of ATP [10, 18]. If the ground state of Vps4 in the ATPase reaction cycle is indeed a dimer, the dimer structure should exist in both the nucleotide-free and the ADP-bound Vps4 crystals. Examination of crystal packing within the two crystal forms showed a "crystallographic dimer" structure. However, we reasoned that it could not represent a structure of a molecular dimer for the following reasons. Each "subunit" in this pair buries 3% of its total solvent-accessible surface and residues at the interface are not conserved. More importantly, mutagenesis of interface residues (M330D/L407D) resulted in a mutant protein whose gel filtration profile did not change appreciably as compared with the wild-type protein (data not shown).

Since the mechanism and regulation of Vps4 ATPase cycle depend on its ground state structure, we asked whether the predominant species of Vps4 in the absence of nucleotide binding is a dimer. To address this, we co-expressed and co-purified $Vps4^{E233Q}$ with C-terminal S-tagged $Vps4^{E233Q}$ from bacteria *E. coli*. If Vps4 forms a stable dimer, mixing the co-purified proteins with S-protein agarose should lead to retention of both S-tagged and non-tagged proteins due to interaction between the two proteins. The result showed that only S-tagged Vps4 is retained on the beads suggesting that protein-protein interaction between Vps4 in the absence of nucleotide is weak (Figure 2.2). As a positive control, we also preformed the same experiment in the presence of ATP. Both proteins were retained on the beads indicating protein-protein interaction in the presence of ATP (Figure 2.2). In addition, we co-expressed N-terminal His-tagged Vps4 together with wild-type Vps4 and performed pull-down experiments using Ni^{2+}-NTA resin. Again, only the His-tagged Vps4 is retained on the beads (data not shown). These results strongly

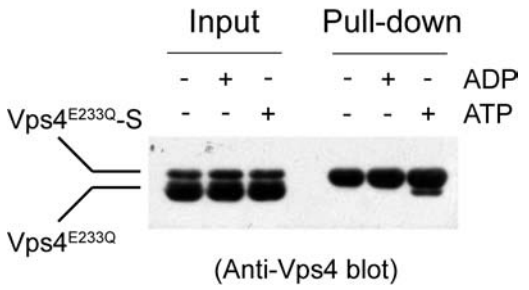

Figure 2.2 Yeast Vps4 e xists as a monomer in the absence of ATP.
Untagged Vps4 and C-terminal S-tagged Vps4 were co-expressed and co-purified from *E. coli*. Protein samples were applied to S-protein agarose under different nucleotide conditions as indicated. After extensive wash, bound proteins were separated on SDS-PAGE and detected by western blotting using anti-Vps4 antibody.

argue that the predominant species of Vps4 in the ground state of its ATPase reaction cycle is a monomer.

The quaternary structure of Vps4 in its ADP-bound form

Analysis of protein-protein interaction within the lattice of the ADP-bound Vps4 crystal shows that the protein aggregates into a form that suggests the molecular symmetry for the oligomerized species of Vps4. There are three molecules in the asymmetric unit of the ADP-bound Vps4 crystal. Together with other molecules related by crystallographic symmetry, they form a left-handed helix with a pseudo six-fold screw axis along the z-axis. Each molecule is related to its neighbor by a 60° rotation and 1/6 of unit cell translation along the z axis (Figure 2.3A). Therefore, if viewed along the z-axis, the projection of these molecules forms a hexameric ring (Figure 2.3B).

Although AAA-ATPase with a helical, open assembly has been described [25], overwhelming majority of them assemble into ring-shaped assemblies [25]. However, it is not uncommon that ring-shaped AAA-ATPases crystallize in a helical packing arrangement similar to what is seen in Vps4. For example, bacterial molecular chaperone ClpB crystallizes into a similar helix but forms a ring structure in solution in the presence of ATP as determined by cryo-EM imaging [26]. Therefore, the molecular arrangement within Vps4-ADP crystal provides strong evidence that supports a hexameric/dodecameric model previously proposed based on structural similarity of Vps4 to the D1 domain of AAA-protein p97 [18].

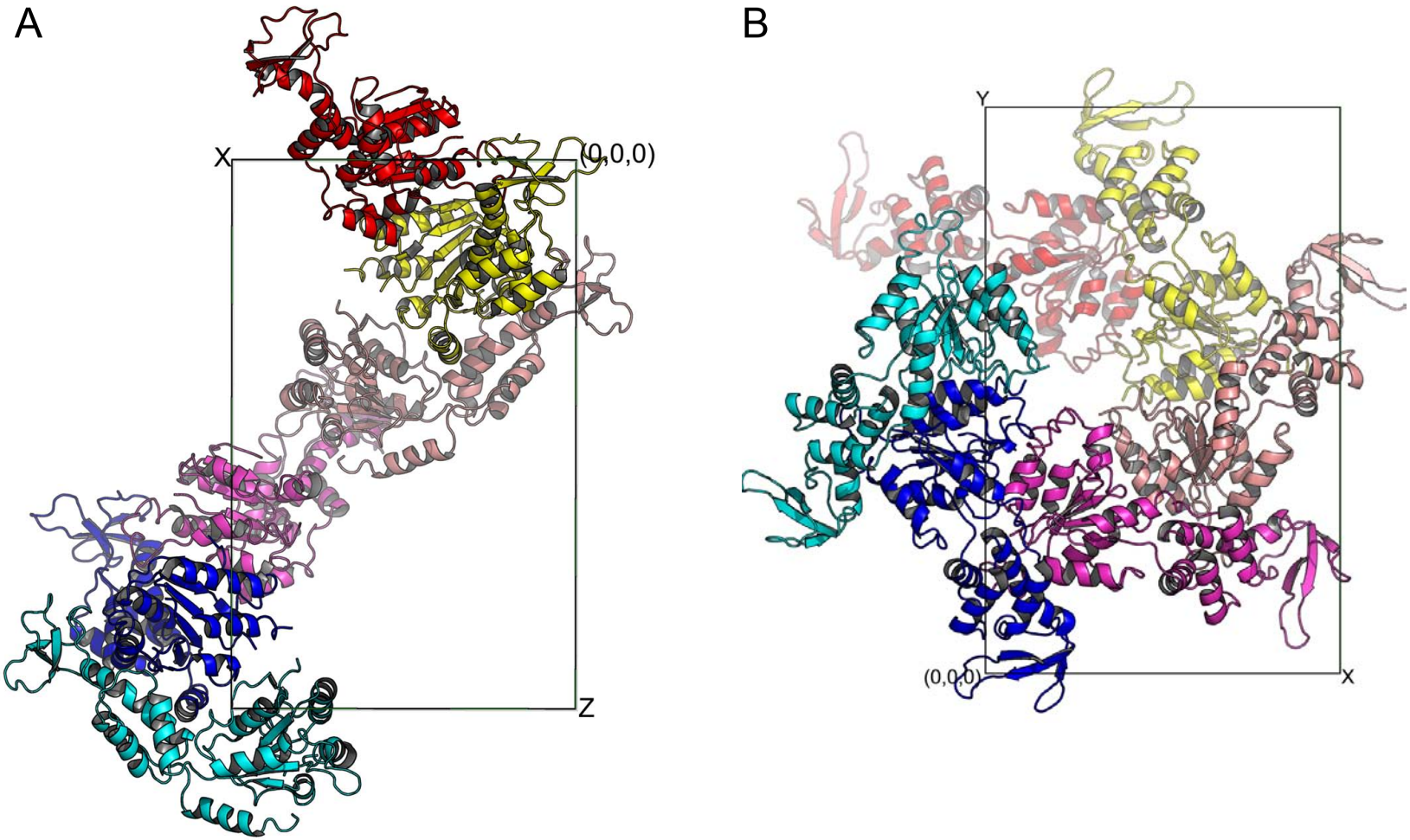

Figure 2.3 Crystal packing within the lattice of the ADP-bound Vps4 structure. Six Vps4 molecules along the z-axis in the $P2_12_12_1$ space group are shown either down the z-axis **(A)** or y-axis **(B)**. These six molecules form a pseudo-left-handed helix with a 6-fold screw symmetry.

ADP binding

Consistent with what have been observed in other AAA-protein systems [20], ADP is bound in a shallow cleft located between the large and small AAA subdomains (Figure 2.4A). It adopts a rather extended conformation with the ribose ring arching over the P-loop, a structurally conserved motif with an invariant GPPGTG sequence between strand β1 and helix α2. The di-phosphate sits in a pocket formed by C-terminal residues of the parallel β-strands β1, β3 and β4 as well as residues from helix α1. Specifically, the oxygen atoms of the β-phosphate form electro-static and/or hydrogen bond interactions with the side chains of highly conserved Lys179, Asp232 and Asn277 (Figure 2.4B). Lys179 is a Walker A motif (GxxxxGKT, x = any residue) residue and a K179A mutation has been shown to result in a loss in nucleotide binding [10]. Asp232 is a Walker B motif (hhhhDExx, h = hydrophobic residue) residue and its neighbor Glu233 is catalytically important [10]. In the ADP-bound structure, Glu233 has been mutated to glutamine. The corresponding residue is about 4.3Å away from the β-phosphate oxygen and is poised to catalyze the cleavage of the β-γ phosphate bond. In addition to afore-mentioned side chain interactions, the β-phosphate is also engaged in hydrogen bond interactions with backbone amide nitrogen atoms of Lys179 and Ser180.

Interactions between the rest of ADP and Vps4 are dominated by van der Waals forces with only a few specific hydrogen bonds. The adenine-binding pocket is largely hydrophobic and is formed by residues from the loop preceding helix α1, helix α2 and small subdomain helix α7 and the loop between α8 and α9 (Figure 2.4B). Ring stacking interaction is observed between the purine ring and the side chain of the conserved Tyr181, together with a hydrogen bond between the 6'-amine nitrogen and the backbone

Figure 2.4 ADP binding causes conformational changes in Vps4.
(**A**) Ribbon representation of the yeast Vps4 structure in complex with ADP. The structure is shown in the same orientation as in Figure 2.1A. ADP molecule bound in the cleft between the large AAA and small subdomains is shown as a stick model and colored based on its atomic property.
(**B**) Stereo view of the nucleotide-binding pocket of Vps4 showing interactions between the protein and the ADP molecule. The P-loop is highlighted in magenta. Potential hydrogen bond interactions are shown as dash lines.
(**C**) Conformational changes in yeast Vps4 as induced by nucleotide binding. The nucleotide-free structure is colored yellow and the ADP-bound structure is white. Residues 119-128, which forms the β0 strand in the ADP-bound structure are disordered in the nucleotide-free structure therefore not present in the model.

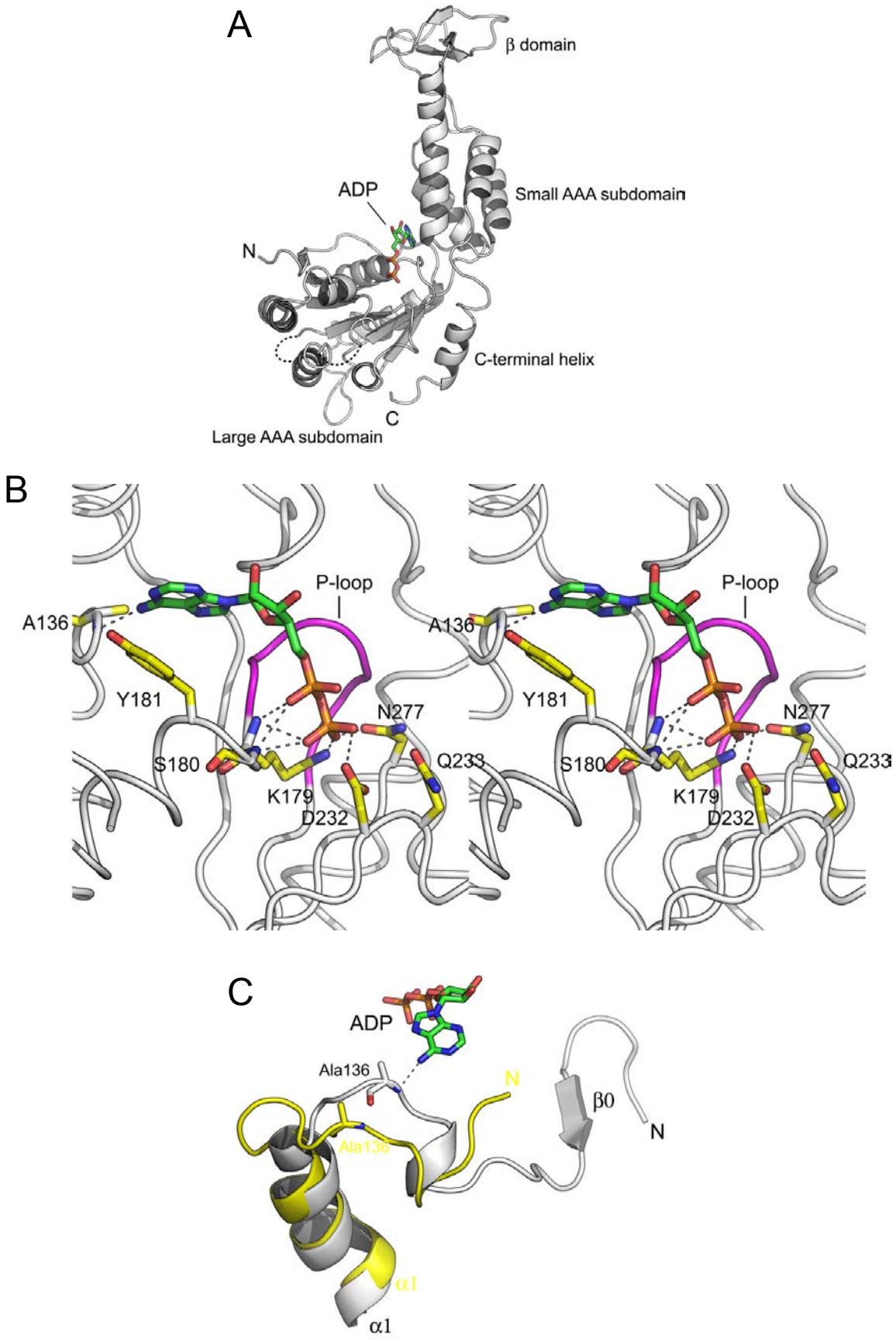
A
β domain
ADP
Small AAA subdomain
N
C-terminal helix
C
Large AAA subdomain
B
P-loop
A136
Y181
N277
S180
Q233
K179
D232
P-loop
A136
Y181
N277
S180
Q233
K179
D232
C
ADP
Ala136
N
β0
N
Ala136
α1
α1

amide nitrogen of Ala136. Interaction between the adenine and Ala136 appears to be important in communicating the presence of nucleotide in the binding pocket to the N-terminus of Vps4 through which the protein binds substrates including the ESCRT-III subunits. In the absence of ADP, helix α1 bends near its N-terminus and pulls the preceding loop away from the adenine-binding pocket (Figure 2.4C). As a result, residues 119-129 that form an anti-parallel β-strand (β0) in the ADP-bound structure become disordered in the nucleotide-free structure.

Structural flexibility within Vps4

Comparison of the four independently determined Vps4 structures in our study shows that there is significant structural flexibility within the molecule (Figure 2.5A). The flexibility is displayed as *en bloc* domain movements as there is little conformational change within the individual domains of Vps4. Two general hinge regions can be identified in the structure. One is located between the large AAA sub-domain and the small AAA sub-domain, consisting of residues Pro299 and Pro415. The other is located between the small AAA sub-domain and the β-domain, consisting of residues Pro350 and Pro399 (Figure 2.5B). These four proline residues are highly conserved among Vps4 homologs, suggesting that the observed structural flexibility is a general feature inherent to the function of Vps4. The *en bloc* motion involves an 11° swing between the large and small AAA subdomains and an 18° swing between the small AAA subdomain and the β domain around axes defined by respective hinge residues.

The four Vps4 structures display a progressive opening of the nucleotide-binding site. As a consequence, interactions between the protein and ADP in particular those

Figure 2.5 Structural flexibility within Vps4.
(A) Superimposition of the four independently determined Vps4 structures in the current study. The three molecules (ADP-bound) in the asymmetric unit of the $P2_12_12_1$ space group are colored white, cyan, and red, respectively. The one molecule (nucleotide-free) in the asymmetric unit of $P6_522$ space group is colored yellow. The magnitude of the en bloc motions between the large AAA subdomain and small AAA subdomain and between the small AAA subdomain and the β domain is illustrated schematically.
(**B**) Two potential hinge regions within Vps4 structure. The conserved proline residues in the hinge regions are shown as spheres and highlighted in brown.

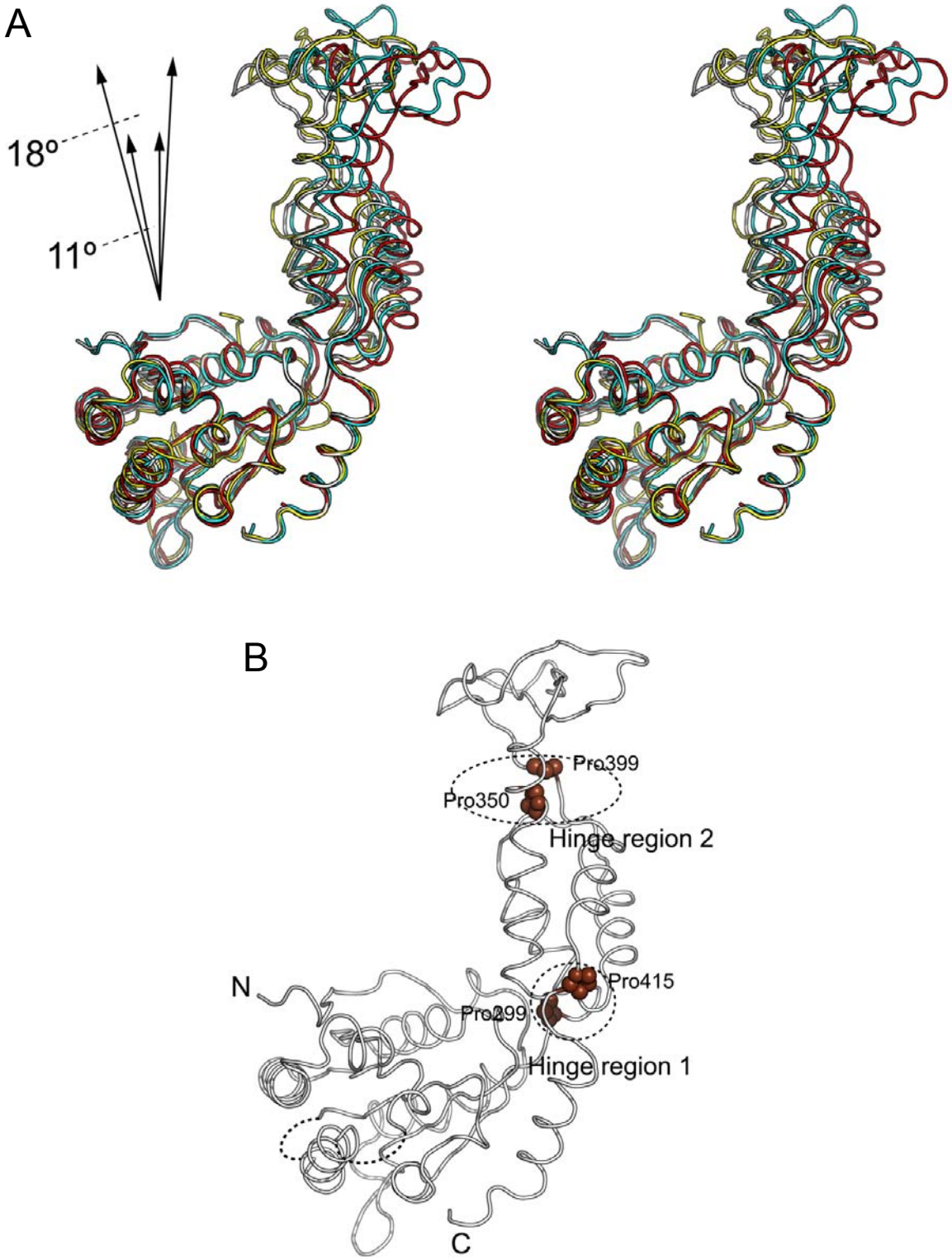
A
18°
11°
B
Pro399
Pro350
Hinge region 2
N
Pro415
Pro299
Hinge region 1
C

involving the ribose and adenine rings vary considerably. Although clear electron-density is observed for the di-phosphate in all three ADP-bound molecules, density for the rest of the nucleotide is poor in the two more open structures. This observation suggests that structural flexibility of Vps4 is important for the nucleotide-binding induced conformational change within the molecule.

Structural basis of ATP-dependent ESCRT-III binding

The N-terminal domain of Vps4, whose structure is missing in our current model, has been shown to be responsible for ESCRT-III binding [19]. To determine whether the interactions are ATP dependent, GST-tagged ESCRT-III proteins (Vps2, Vps20, Vps24 and Snf7) were expressed and purified from *E. coli* and their interactions with $Vps4^{E233Q}$ were examined using a GST pull-down assay in the absence and presence of ATP. As shown in Figure 2.6A, it is evident that these interactions either require ATP or are strongly enhanced by ATP.

There are two possible explanations for the ATP dependency of these interactions. The N-terminal domain might not be accessible to the ESCRT-III protein in the absence of ATP. Alternatively, stable association may require the ESCRT-III protein to simultaneously bind to more than one Vps4 subunit; a condition only met in the ATP-induced Vps4 oligomeric structure. To distinguish between these two possibilities, we expressed and purified two Vps4 N-terminal fragments, $Vps4^{1-82}$ and $Vps4^{1-120}$. Both protein fragments were able to bind to the ESCRT-III subunit Vps2 and Vps20 though the interaction with $Vps4^{1-120}$ appears to be stronger (Figure 2.6B). Purified $Vps4^{1-120}$ also effectively competes with full-length $Vps4^{E233Q}$ for binding to Vps2 as shown by

Figure 2.6 Nucleotide binding induces conformational change within the N-terminal region of Vps4.
(**A**) The ESCRT-III subunits interact with Vps4 in the presence of ATP. ESCRT-III subunits Vps2, Vps20, Vps24 and Snaf7 were expressed as GST-tagged fusion proteins and bound to glutathione-agarose beads (left panel). Purified $Vps4^{E233Q}$ was loaded onto the ESCRT-III subunit-bound matrix either in the absence (-) or presence (+) of ATP. Proteins retained on the matrix after extensive washes were separated on 12% SDS-PAGE gel and stained with Coomassie Blue (right panel).
(B) The N-terminal domain of Vps4 interacts with the ESCRT-III subunits. Vps2 and Vps20 were expressed as GST-tagged fusion proteins and bound to glutathione-agarose beads. Cell lysate containing His_8-$Vps4^{1-82}$ or His_8-$Vps4^{1-120}$ was loaded onto GST-Vps2 or GST-Vps20 bound matrix. Proteins retained on the matrix after extensive washes were separated on the SDS-PAGE gel and detected by either Ponceau S staining (top panel) or anti-His antibody (bottom panel).
(C) $Vps4^{1-120}$ competes with full-length Vps4 for binding to the ESCRT-III subunit Vps2. GST-Vps2 was bound to glutathione-agarose beads. Purified $Vps4^{E233Q}$ was loaded onto Vps2-bound matrix in the presence of ATP and increasing amounts of BSA or $Vps4^{1-120}$. Proteins retained on the matrix were separated on SDS-PAGE gel and detected by western blotting with anit-Vps4 antibody. The amount of $Vps4^{E233Q}$ was quantified by program ImageJ and shown in a bar diagram (the amount in the first lane was set as 100%).
(D) Vps4 undergoes conformational change at the linker region upon ATP binding. $Vps4^{E233Q}$ was incubated with increasing amounts of subtilisin at 4°C for 30 min with different nucleotides. Digestion products were separated on 15% SDS-PAGE, followed by Coomassie staining.

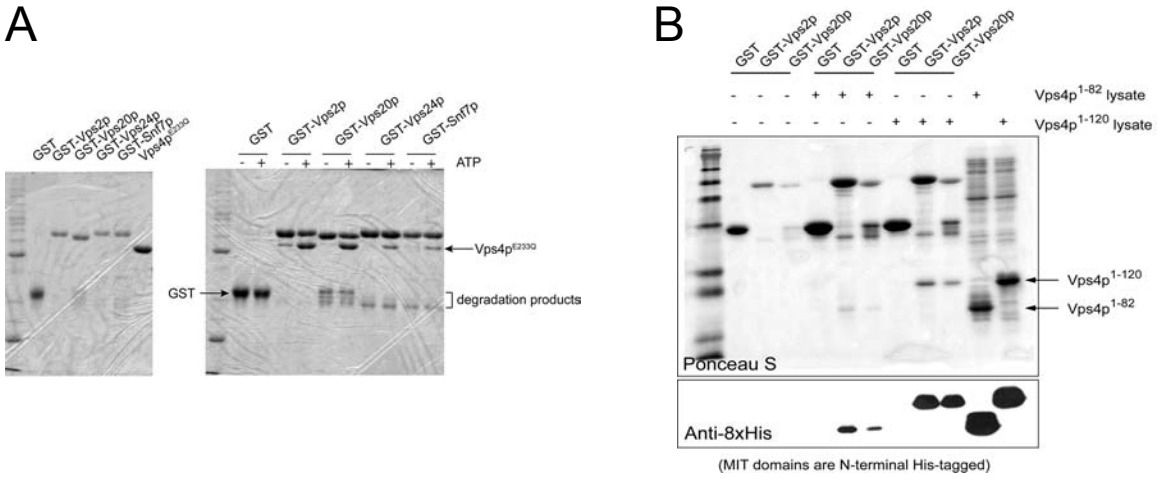
A
GST
GST-Vps2p
GST-Vps20p
GST-Vps24p
GST-Snf7p
Vps4p^E233Q
ATP
Vps4p^E233Q
GST
degradation products
B
Vps4p^1-82 lysate
Vps4p^1-120 lysate
Vps4p^1-120
Vps4p^1-82
Ponceau S
Anti-8xHis
(MIT domains are N-terminal His-tagged)

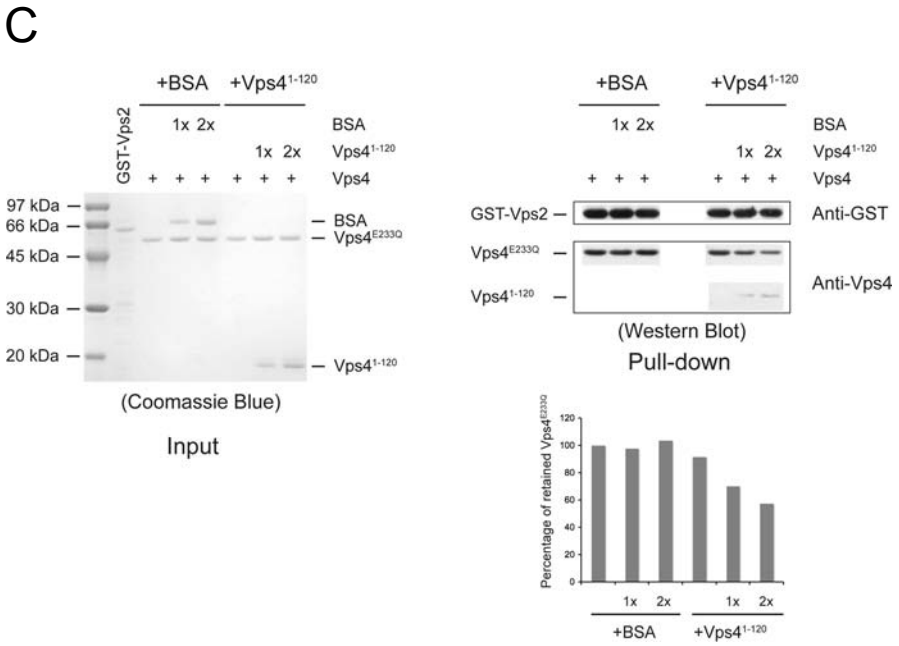
C
+BSA
+Vps4^1-120
GST-Vps2
1x 2x
BSA
Vps4^1-120
Vps4
97 kDa
66 kDa
45 kDa
30 kDa
20 kDa
BSA
Vps4^E233Q
Vps4^1-120
(Coomassie Blue)
Input
GST-Vps2
Vps4^E233Q
Vps4^1-120
Anti-GST
Anti-Vps4
(Western Blot)
Pull-down
Percentage of retained Vps4^E233Q
120
100
80
60
40
20
0

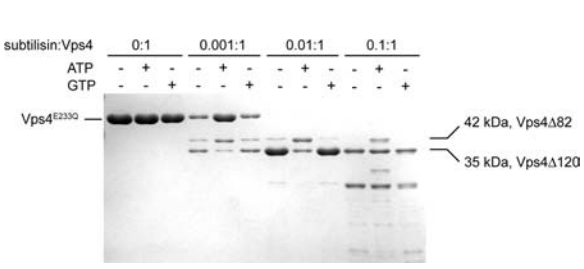
D
subtilisin:Vps4
0:1
0.001:1
0.01:1
0.1:1
ATP
GTP
Vps4^E233Q
42 kDa, Vps4Δ82
35 kDa, Vps4Δ120

decreased amounts of full-length Vps4^{E233Q} retained by GST-Vps2 when Vps4$^{1-120}$ was included in the binding assay (Figure 2.6C). These results showed that an isolated, monomeric N-terminal domain is sufficient for binding to the ESCRT-III protein. Rather than the valency requirement, it is the ATP-binding induced conformational change in Vps4 structure that leads to the increased accessibility of the N-terminal domain. Similar ATP-binding induced conformational change in the substrate-binding domain has been observed in other AAA protein systems such as p97 [27, 28].

To probe ATP-binding induced conformational change within Vps4 structure, we subjected Vps4 to mild protease treatment in the absence and presence of ATP. Purified proteins were incubated with increasing amounts of subtilisin and the reaction was stopped after 30 minutes on ice. As can be seen in Figure 2.6D, in the absence of ATP, Vps4 was quickly converted into a fragment of 35 kDa that corresponds to residues 121 to the C-terminus (Vps4Δ120). In contrast, a stable fragment of 42 kDa accumulated before the appearance of the 35 kDa fragment in the presence of ATP. The new fragment contains residues 83 to the C-terminus (Vps4pΔ82). Interestingly, this region corresponds to the linker that connects the ESCRT-III binding domain and the ATP-binding AAA domain. This effect was specific for ATP, as inclusion of GTP in the digestion mixture did not lead to the accumulation of Vps4pΔ82 (Figure 2.6D). As expected, ATP had no effect on the subtilisin digestion pattern of trigger factor, a molecular chaperone that does not bind to ATP [29] (data not shown). Together, these results demonstrated that the linker undergoes conformational change in response to ATP binding and this is likely the structural basis for the ATP-dependent ESCRT-III binding to the full-length Vps4.

DISCUSSION

Vps4 catalyzes the dissociation of the ESCRTs from the endosomal membrane in the MVB pathway. This function is critical to a number of cell biology processes including cell surface growth hormone receptor down-regulation and budding of retroviral particles from host cells as dysfunction of Vps4 will lead to the blockage of these processes. Among proteins that have been implicated in the proper function of the MVB pathway, Vps4 is one of the most conserved proteins with a high level of sequence identity between yeast and human proteins. Comparison of yeast and human Vps4 crystal structures confirms the structural conservation suggesting that all Vps4 proteins likely function through a common mechanism.

As a member of the AAA protein family, Vps4 derives its ability to dissociate and remodel protein complexes from ATP binding and hydrolysis driven conformational changes within its structure. While most AAA proteins contain two AAA domains with one defective in ATP hydrolysis thus enabling the formation of a stable protein assembly, Vps4 has only one AAA domain [23]. As ATP is hydrolyzed, the assembly is weakened resulting in cyclic quaternary structural change. Based on results from gel filtration and cross-linking experiments, it has been proposed that Vps4 cycles between a dimer structure and a structure containing 10-12 subunits [10]. Molecular packing within the Vps4-ADP crystal favors a model of Vps4 high-order oligomer with a six-fold symmetry. Therefore, it is likely that the high-order oligomer contains 12 subunits arranged as two hexameric rings as observed in most AAA proteins. Our structural and biochemical analysis, however, does not support that Vps4 oligomer dissociates into a stable dimmer

upon ATP hydrolysis and subsequent release of the nucleotide. Instead, it suggested that the ground state structure of Vps4 ATPase reaction cycle is predominantly a monomer. Our results, however, does not rule out weak protein-protein interaction between Vps4 subunits in the absence of nucleotide. In deed, analytical ultracentrifugation analysis suggests that the solution behavior of Vps4 is complicated and cannot be fitted into a simple one species model (data not shown).

While ADP binding to Vps4 is not sufficient to support a stable oligomeric structure as would ATP, insights regarding conformational change of Vps4 induced by ATP binding can be gained from the Vps4-ADP structure. It is likely that ATP binding results in similar *en bloc* domain movements within the Vps4 structure, albeit larger in magnitude, which favors protein-protein interactions between Vps4 subunits leading to protein oligomerization. The reason that ADP is unable to support a closed ring structure may be due to the lack of additional inter-subunit interactions stabilized by the presence of the γ-phosphate [19]. Interestingly, nucleotide binding also causes *en bloc* movement of the β domain relative to the core AAA domain (Figure 2.5A). Given that the β domain is responsible for binding to Vta1 in the presence of ATP, this observation suggests that ATP binding to Vps4 not only causes local conformational changes at the lower portion of the molecule but its effect is also propagated to the distant part of Vps4 resulting conformational changes that support its interaction with Vta1 as well.

Examination of yeast Vps4 structure reveals several highly conserved surface patches. They are mostly located on the large AAA subdomain but the small AAA subdomain and the β domain each contains one prominent patch (Figure 2.7). A significant fraction of the conserved surfaces on the large subdomain are involved in

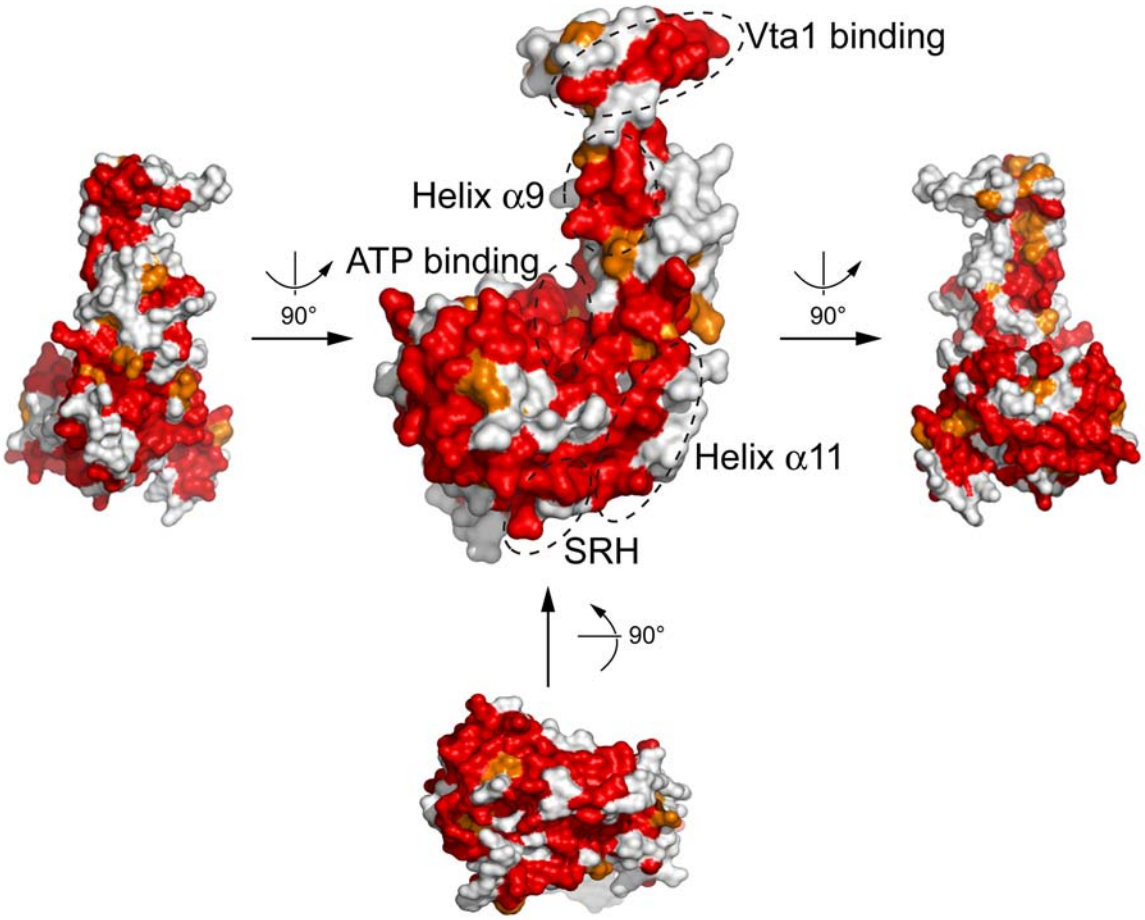

Figure 2.7 Conserved surface patches on Vps4.
Surface representation of yeast Vps4 is shown in several different orientations as indicated. They are colored based on the conservation of underlying residues as presented in Figure 2.1B: identical residues red and homologous ones orange. Surface patches known to be involved in ATP binding and Vta1 binding are indicated. In addition, those formed by residues from helix α9 and α11 as well as SRH (Second Region of Homology, a region likely involved in inter-subunit interactions) are also highlighted.

binding nucleotide as has been shown in the ADP-bound Vps4 structure. The function for the rest of the conserved surfaces is less clear but probably involved in ATP-dependent oligomerization. Similarly, the conserved patch on the small subdomain formed by residues of helix α9 is probably also involved in protein oligomerization. The conserved patch on the β domain formed by loop residues between strands β7 and β8 is likely involved in Vta1 binding as mutation of Ser377 and Asp380 of Vps4 in the region abolishes its ability to bind to its regulator [18].

In summary, our structural and biochemical analyses of yeast Vps4 structure suggest that Vps4 likely functions in the MVB pathway via a highly conserved mechanism supported by similar protein-protein interactions through its ATPase reaction cycle. Our study provides the first structural view illustrating how nucleotide binding might induce conformational changes within Vps4 that leads to oligomerization and binding to its substrate ESCRT-III. In addition, inherent hinged domain movements within the Vps4 structure may also play a role in supporting nucleotide binding. In contrast to previous models, our characterization of Vps4 now supports a model where the ground state structure of Vps4 ATPase reaction cycle is predominantly a monomer and the activated state structure is a dodecamer. While a high-resolution structure of Vps4 oligomer will ultimately be required to define the ATP driven structural changes within Vps4, our study provides a platform where these changes can now be probed experimentally by mutagenesis and other methods.

METHODS

Cloning, expression and purification

DNA fragment encoding Vps4 was amplified from the *Saccharomyces cerevisiae* genomic DNA and cloned into the BamHI/XhoI sites of a modified pET21a vector that contains an N-terminal His_8-tag and a TEV protease cleavage site. *E. coli* strain Rosetta(DE3) harboring the His_8-TEV-Vps4 expression plasmid was grown at 37°C in LB medium to an OD_{600} of 0.6-0.8 before induced with 0.4 mM IPTG at 25°C for 4 hours. The cells were harvested by centrifugation and frozen at -80°C.

All protein purification steps were performed at 4°C. Frozen cell pastes were resuspended in 100 ml buffer A (50 mM Tris, pH 8.0, 300 mM NaCl, 1 mM $MgCl_2$) supplemented with 10 μg/ml PMSF and disrupted by sonication. Supernatant from centrifugation was loaded on a Ni^{2+}-NTA affinity column. After the column was washed extensively with buffer A, His_8-TEV-Vps4 was eluted with a 0-250 mM imidazole gradient in buffer A. Fractions containing Vps4 were pooled, incubated with TEV protease (100:1), and dialyzed against 50 mM Tris, pH 8.0, 50 mM NaCl, 1 mM $MgCl_2$ overnight. A second Ni^{2+}-NTA step removed the tag and TEV protease. Vps4-containing fractions was then placed into buffer C (25 mM Tris, pH 7.5, 100 mM NaCl, 5 mM $MgCl_2$) and further purified using an anion exchange Resource-Q column (Amersham Pharmacia) with a 0.1-0.5 M NaCl gradient. For MAD phasing, selenomethionyl protein were expressed in *E. coli* B834(DE3) using a minimal medium where methionines were replaced with selenomethionines [30]. Derivative proteins were purified in a similar way as native proteins.

Crystallization and data collection

For crystallization, purified protein was stored in a final buffer containing 20 mM Tris, pH 7.5, 400 mM NaCl, 5 mM $MgCl_2$ and concentrated to 25 mg/ml. The nucleotide-free crystal form was obtained by the sitting drop method at 20°C. Proteins were mixed in a 1:1 ratio with a reservoir solution containing 1.0 M sodium acetate, 0.2-0.25 M cadmium sulfate, and 0.1 M PIPES, pH 6.5 in a final volume of 4 μl and equilibrated against the reservoir solution. Crystals grew to full size in several days and were transferred into 1.05 M sodium acetate, 0.25 M cadmium sulfate, 0.1 M HEPES, pH 7.0, and 35% sucrose and equilibrated against the same solution for several hours before flash-frozen under liquid nitrogen. The adjustment of buffer, pH and the soaking step improved the diffraction quality of the crystal. Selenomethionyl crystals were prepared in a similar manner.

The ADP crystal form was also grown by the sitting drop method at 20°C. Proteins in the presence of 5mM ADP were mixed in a 1:1 ratio with a reservoir solution of 1.3-1.4 M Na/K-phosphate, pH 5.8, 10% glycerol, 5% glucose in a final volume of 4 μl and equilibrated against the reservoir solution. Crystals grew to full size in a week and were often clustered. Single crystals used for data collection were obtained by seeding. Crystals were transferred into 1.6 M Na/K-phosphate, pH 5.8, 1 mM ADP, and 35% sucrose and flash-frozen in liquid nitrogen before data collection. All diffraction data were collected at Advanced Photon Source beam line 23-ID. Diffraction data were integrated and scaled by using the program HKL2000 (HKL Research).

Structure determination and refinement

The nucleotide-free structure was solved initially at 3.2 Å resolution using the MAD method [31]. Four of the seven expected selenium sites were found with SnB [32]. Two additional sites were identified using anomalous difference Fourier method as implemented in SHARP [33]. Parameters for these six sites were refined and MAD phases were calculated and improved by solvent flattening with SHARP. The resulting experimental map was interpretable to allow the building of a polyalanine model in O [34]. Cycles of rebuilding and refinement were carried out using the program O and CNS [35], while phases were extended to 2.9 Å resolution using a native data set. Initial refinement was carried out with torsion angle dynamics simulated annealing using the maximum likelihood target function with the experimental phases as a prior phase distribution (MLHL). A randomly selected 5% of the total reflections were used for cross-validation. Later rounds of refinement were performed with REFMAC5 in the CCP4 suite with TLS parameters incorporated [36]. The final structure contains residues 129-206, 210-239, 246-264, 268-365, and 371-433. The refined model has 86.2% of the residues with the most favored backbone conformations and only one residue with disallowed conformation on the Ramachandran plot.

The ADP structure was determined by the molecular replacement method with the program PHASER [37] using the partially refine nucleotide-free structure as a search model. The β-domain and most of the loop regions were removed during the molecular replacement process. The model was refined using CNS with intersperse manual rebuilding with O. Three Vps4 molecules were found in the asymmetric unit and they were initially refined with strict non-crystallographic symmetry (NCS) constraint. However, as the refinement progressed, it was clear that they differ from each other quite

significantly therefore only weak NCS restraint was applied during the later stage of the refinement. The final structure contains residues 119-237, 249-262, and 270-435 for molecule A and B, and 123-237, 249-262, and 270-432 for molecule C. A complete ADP molecule was built in molecule A but only a phosphate group was built in molecule B and C due to poor electron density quality for the rest of the ADP molecule.

In vitro binding experiments

For the S-tag pull-down experiments, untagged Vps4^{E233Q} and C-terminal S-tagged Vps4 ^{E233Q} were co-expressed using pETDuet-1 vector (Novagen) and co-purified by anion-exchange chromatography followed by gel filtration chromatography. Protein samples were applied to S-protein agarose (Novagen) in the absence or presence of 1 mM adenosine nucleotides. After extensive wash, bound proteins were separated by SDS-PAGE and detected by Western blotting with anti-Vps4 antibody (Santa Cruz, sc-21821).

For GST pull-down experiments, DNAs encoding yeast Vps2, Vps20, Vps24, and Snf7 were amplified from the *S. cerevisiae* genomic DNA and cloned into a modified pET41a vector (Novagen). GST tagged proteins were expressed in *E. coli* BL21(DE3) cells, induced with 0.4 mM IPTG at 16°C overnight. These cells were resuspended in PBS (140 mM NaCl, 2.7 mM KCl, 10 mM Na_2HPO_4, 1.8 mM KH_2PO_4, pH 7.3) supplemented with 1 mM DTT and 0.1% Triton X-100 and lysed by mild sonication. 20 ml glutathione-agarose (Sigma) pre-equilibrated with PBS/DTT buffer was incubated with soluble cell lysates at 4°C for 40 minutes. The beads were subsequently washed with the above buffer and incubated with purified Vps4^{E233Q} proteins or cell lysates containing His_8-tagged Vps4 N-terminal domains at 4°C for 40 minutes. ATP was added to a final concentration of 1 mM where indicated. Bound proteins were analyzed by SDS-PAGE.

Limited proteolysis

Subtilisin was used in the assay with protease to protein ratios in the following order: 0/1, 0.001/1, 0.01/1, and 0.1/1. For a typical reaction, 1 mg/ml $Vps4^{E233Q}$ protein was incubated with subtilisin in the reaction buffer (20 mM HEPES, pH 7.5, 200 mM NaCl, 10% glycerol). Reactions were allowed to proceed for 30 minutes on ice before terminated by addition of protease inhibitor PMSF. Samples were boiled in SDS-loading buffer, subjected to SDS-PAGE and visualized by Coomassie staining.

Protein Data Bank accession number

Atomic coordinates and structure factors for yeast Vps4 have been deposited in the RCSB Protein Data Bank with accession code 2QP9 for the nucleotide-free form and 2QPA for the ADP-bound form.

REFERENCES

1. Katzmann, D.J., G. Odorizzi, and S.D. Emr, *Receptor downregulation and multivesicular-body sorting.* Nat Rev Mol Cell Biol, 2002. **3**(12): p. 893-905.

2. Raiborg, C., T.E. Rusten, and H. Stenmark, *Protein sorting into multivesicular endosomes.* Curr Opin Cell Biol, 2003. **15**(4): p. 446-55.

3. Babst, M., *A protein's final ESCRT.* Traffic, 2005. **6**(1): p. 2-9.

4. Gruenberg, J. and H. Stenmark, *The biogenesis of multivesicular endosomes.* Nat Rev Mol Cell Biol, 2004. **5**(4): p. 317-23.

5. Morita, E. and W.I. Sundquist, *Retrovirus budding.* Annu Rev Cell Dev Biol, 2004. **20**: p. 395-425.

6. Carlton, J.G. and J. Martin-Serrano, *Parallels between cytokinesis and retroviral budding: a role for the ESCRT machinery.* Science, 2007. **316**(5833): p. 1908-12.

7. Hurley, J.H. and S.D. Emr, *The ESCRT Complexes: Structure and Mechanism of a Membrane-Trafficking Network.* Annu Rev Biophys Biomol Struct, 2006.

8. Williams, R.L. and S. Urbe, *The emerging shape of the ESCRT machinery.* Nat Rev Mol Cell Biol, 2007. **8**(5): p. 355-68.

9. Babst, M., et al., *Endosomal transport function in yeast requires a novel AAA-type ATPase, Vps4p.* Embo J, 1997. **16**(8): p. 1820-31.

10. Babst, M., et al., *The Vps4p AAA ATPase regulates membrane association of a Vps protein complex required for normal endosome function.* Embo J, 1998. **17**(11): p. 2982-93.

11. Babst, M., et al., *Escrt-III: an endosome-associated heterooligomeric protein complex required for mvb sorting.* Dev Cell, 2002. **3**(2): p. 271-82.

12. Nickerson, D.P., M. West, and G. Odorizzi, *Did2 coordinates Vps4-mediated dissociation of ESCRT-III from endosomes.* J Cell Biol, 2006. **175**(5): p. 715-20.

13. Azmi, I., et al., *Recycling of ESCRTs by the AAA-ATPase Vps4 is regulated by a conserved VSL region in Vta1.* J Cell Biol, 2006. **172**(5): p. 705-17.

14. Bishop, N. and P. Woodman, *TSG101/mammalian VPS23 and mammalian VPS28 interact directly and are recruited to VPS4-induced endosomes.* J Biol Chem, 2001. **276**(15): p. 11735-42.

15. von Schwedler, U.K., et al., *The protein network of HIV budding.* Cell, 2003. **114**(6): p. 701-13.

16. Sachse, M., G.J. Strous, and J. Klumperman, *ATPase-deficient hVPS4 impairs formation of internal endosomal vesicles and stabilizes bilayered clathrin coats on endosomal vacuoles.* J Cell Sci, 2004. **117**(Pt 9): p. 1699-708.

17. Fujita, H., et al., *A dominant negative form of the AAA ATPase SKD1/VPS4 impairs membrane trafficking out of endosomal/lysosomal compartments: class E vps phenotype in mammalian cells.* J Cell Sci, 2003. **116**(Pt 2): p. 401-14.

18. Scott, A., et al., *Structural and mechanistic studies of VPS4 proteins.* Embo J, 2005. **24**(20): p. 3658-69.

19. Scott, A., et al., *Structure and ESCRT-III protein interactions of the MIT domain of human VPS4A.* Proc Natl Acad Sci U S A, 2005. **102**(39): p. 13813-12818.

20. Ogura, T. and A.J. Wilkinson, *AAA+ superfamily ATPases: common structure--diverse function.* Genes Cells, 2001. **6**(7): p. 575-97.

21. Hanson, P.I. and S.W. Whiteheart, *AAA+ proteins: have engine, will work.* Nat Rev Mol Cell Biol, 2005. **6**(7): p. 519-29.

22. Frickey, T. and A.N. Lupas, *Phylogenetic analysis of AAA proteins.* J Struct Biol, 2004. **146**(1-2): p. 2-10.

23. Vale, R.D., *AAA proteins. Lords of the ring.* J Cell Biol, 2000. **150**(1): p. F13-9.

24. Scheuring, S., et al., *Mammalian cells express two VPS4 proteins both of which are involved in intracellular protein trafficking.* J Mol Biol, 2001. **312**(3): p. 469-80.

25. Erzberger, J.P., M.L. Mott, and J.M. Berger, *Structural basis for ATP-dependent DnaA assembly and replication-origin remodeling.* Nat Struct Mol Biol, 2006. **13**(8): p. 676-83.

26. Lee, S., et al., *The structure of ClpB: a molecular chaperone that rescues proteins from an aggregated state.* Cell, 2003. **115**(2): p. 229-40.

27. DeLaBarre, B. and A.T. Brunger, *Nucleotide Dependent Motion and Mechanism of Action of p97/VCP.* J Mol Biol, 2005. **347**(2): p. 437-452.

28. Davies, J.M., et al., *Conformational changes of p97 during nucleotide hydrolysis determined by small-angle X-Ray scattering.* Structure (Camb), 2005. **13**(2): p. 183-95.

29. Ludlam, A.V., B.A. Moore, and Z. Xu, *The crystal structure of ribosomal chaperone trigger factor from Vibrio cholerae.* Proc Natl Acad Sci U S A, 2004. **101**(37): p. 13436-41.

30. Xu, Z., J.D. Knafels, and K. Yoshino, *Crystal structure of the bacterial protein export chaperone secB.* Nat Struct Biol, 2000. **7**(12): p. 1172-7.

31. Hendrickson, W.A. and C.M. Ogata, *Phase Determination from Multiwavelength Anomalous Diffraction Measurements.* Methods in Enzymology, 1997. **276**: p. 494-523.

32. Weeks, C.M. and R. Miller, *The design and implementation of SnB v2.0.* J Appl Cryst, 1999. **32**: p. 120-124.

33. Fortelle, E.d.l.B., G., *Maximum-Likelihood Heavy-Atom Parameter Refinement for Multiple Isomorphous Replacement and Multiwavelength Anomalous Diffraction Methods.* Methods in Enzymology, 1997. **276**.

34. Jones, T.A., et al., *Improved methods for building protein models in electron density maps and the location of errors in these models.* Acta Crystallogr A, 1991. **47 (Pt 2)**: p. 110-9.

35. Brunger, A.T., et al., *Crystallography & NMR system: A new software suite for macromolecular structure determination.* Acta Crystallogr D Biol Crystallogr, 1998. **54**(Pt 5): p. 905-21.

36. Winn, M.D., G.N. Murshudov, and M.Z. Papiz, *Macromolecular TLS refinement in REFMAC at moderate resolutions.* Methods Enzymol, 2003. **374**: p. 300-21.

37. McCoy, A.J., et al., *Likelihood-enhanced fast translation functions.* Acta Crystallogr D Biol Crystallogr, 2005. **61**(Pt 4): p. 458-64.

CHAPTER 3

STRUCTURAL BASIS OF VTA1 FUNCTION IN THE MULTIVESICULAR BODY SORTING PATHWAY

ABSTRACT

The MVB pathway plays essential roles in several eukaryotic cellular processes. Proper function of the MVB pathway requires reversible membrane association of the ESCRTs, a process catalyzed by Vps4 ATPase. Vta1 regulates the Vps4 activity but its mechanism of action was poorly understood. We report the high-resolution crystal structures of the Did2- and Vps60-binding N-terminal domain and the Vps4-binding C-terminal domain of *S. cerevisiae* Vta1. The C-terminal domain also mediates Vta1 dimerization and both subunits are required for its function as a Vps4 regulator. Emerging from our analysis is a mechanism of regulation by Vta1 in which the C-terminal domain stabilizes the ATP-dependent double ring assembly of Vps4. In addition, the MIT motif containing N-terminal domain, projected by a long disordered linker, allows contact between the Vps4 disassembly machinery and the accessory ESCRT-III proteins. This provides an additional level of regulation and coordination for ESCRT-III assembly and disassembly.

INTRODUCTION

The multivesicular body (MVB) is a special form of the late endosome, generated when the limiting membrane of the endosome invaginates and buds into its own lumen. During this process, proteins residing in the endosomal membrane are sorted into the forming vesicles. Subsequent fusion of MVBs with the lysosome results in the delivery of cargo-containing intralumenal vesicles to the hydrolytic environment of the lysosome (for reviews see [1-4]). The MVB pathway plays key roles in eukaryotic cellular processes such as cell surface growth factor receptor down-regulation (for reviews see [1, 4]), budding of retroviruses from the host cell (for a review see [5]) and cytokinesis [6, 7]. Entry into the MVB pathway is a tightly regulated process and depends on the action of class E Vps (Vacuolar Protein Sorting) proteins, a majority of which are subunits of three distinct protein complexes called Endosomal Sorting Complexes Required for Transport (ESCRT-I, -II, and -III, for reviews see [1, 4, 8, 9]). These complexes transiently assemble on the endosomal membrane during the cargo sorting process. For sustained protein trafficking through the MVB pathway, the ESCRTs need to be dissociated and disassembled from the membrane and recycled back into the cytoplasm. Vps4, together with its regulator Vta1, catalyzes the process of ESCRT disassembly in an ATP-dependent reaction [10].

Vps4 is a member of the AAA-protein (ATPase associated with a variety of activities) family [11, 12]. It cycles between alternate molecular assembly states *in vitro* depending on the state of ATP binding and hydrolysis [13]. The protein exists as a 90 kDa molecular species that upon ATP binding oligomerizes into a large molecular complex of 440 kDa, which also has a higher affinity for the substrate ESCRT-III

subunits [14]. ATP hydrolysis by Vps4 in turn results in the disassembly of the oligomer, coincident with the release of the ESCRTs from the endosomal membrane. Since ATP hydrolysis represents an irreversible step in the MVB pathway, regulation of the Vps4 ATPase activity is critical for the proper function of the MVB sorting reaction. Vta1 has been recently shown to act as a positive regulator of Vps4 by stimulating its ATPase activity [15, 16]. Furthermore, this mechanism of regulation appears to be conserved during evolution, since Vta1 orthologs have been identified from yeast to humans and contain highly homologous sequence motifs that are thought to mediate interactions with Vps4 [17-19]. In addition, Vta1 also interacts with other proteins acting in the late stage of the MVB pathway, such as the accessory ESCRT-III proteins Vps60 and Vps46/Did2 [15, 16, 20]. These interactions are also important for the MVB sorting and the retrovirus release processes [21]. However, the structural basis for the function of Vta1 remains elusive.

Here we report biochemical and high-resolution structural characterization of *S. cerevisiae* Vta1. We show that Vta1 has a modular structure with two well-folded terminal domains bridged by a region dominated by random-coil structure. Crystal structures of the Vps60- and Did2-binding N-terminal domain and the Vps4-binding C-terminal domain reveal the structural details for the respective binding sites. The C-terminal domain also mediates Vta1 dimerization, and mutagenesis studies demonstrate that both subunits in the dimer are necessary for the function of Vta1 as a Vps4 regulator. Our study suggests a mechanism of regulation by Vta1 in which the C-terminal domain promotes the ATP-dependent double ring assembly of Vps4, while the N-terminal domain, projected by the disordered middle linker region, allows contact between the

Vps4 disassembly machinery and accessory ESCRT-III proteins to coordinate ESCRT-III assembly and disassembly.

RESULTS

Structure determination

Initial attempt to crystallize the intact *S. cerevisiae* Vta1 was not successful. Limited proteolysis of Vta1 by chymotrypsin cleaved the protein after Tyr279 and resulted in two major fragments; of which the C-terminal fragment $Vta1^{280-330}$ was readily crystallized. Secondary structure prediction for Vta1 suggested that the region between residues 168 and 279 contains little regular structure. Therefore, an N-terminal fragment $Vta1^{1-167}$ was generated and crystals were subsequently obtained. In the following sections, we will refer $Vta1^{1-167}$ as Vta1NTD and $Vta1^{280-330}$ as Vta1CTD.

The structure of Vta1NTD was determined by single isomorphous replacement with anomalous scattering (SIRAS) from a native crystal and a selenomethionyl crystal. The protein structure was refined against the native data to a working R factor of 21.5% and a free R factor of 26.0% at 2.9 Å (Table 3.1). The entire structure can be visualized except for residues 65-75, which are presumed disordered. There are two polypeptide chains, related by a non-crystallographic 2-fold symmetry, in the asymmetric unit. However, gel filtration and sedimentation equilibrium analytical ultracentrifugation experiments suggested that Vta1NTD is a monomer in solution. The structure of Vta1CTD was determined by multi-wavelength anomalous dispersion (MAD) from a selenomethionyl crystal at 1.8 Å and later refined against a native data set to a working R factor of 22.0% and a free R factor of 24.9% at 1.5 Å (Table 3.1). There are a total of six

Table 3.1 Data collection and refinement statistics

	Vta1-NTD		Vta1-CTD			
	Native	SeMet	Native	SeMet		
Wavelength	0.9787 Å	0.9787 Å		0.9793 Å	0.9794Å	0.9566Å
Space group	I4	I4	$P2_12_12$	$P2_12_12$		
Unit cell (Å)	a=b=126.169 Å, c=70.252 Å	a=b=126.623 Å, c=69.046 Å	a=102.420 Å b=50.707 c=74.353 Å	a=102.429 Å, b=50.695, c=74.317 Å		
Resolution (Å)	2.9	3.0	1.5	1.8	1.8	1.8
Completeness (%)	99.5 (96.7)	95.2 (73.0)	94.2 (91.3)	99.9 (100.0)	99.9 (100.0)	99.7 (100.0)
I / σ	37.6 (3.3)	34.5 (2.4)	23.7 (5.2)	38.8 (9.9)	39.6 (11.0)	41.2 (11.6)
R_{merge} (%)	6.2 (41.8)	8.1 (48.7)	6.2 (20.2)	6.5 (21.2)	5.8 (19.4)	5.4 (17.9)
Redundancy	7.4	9.7	4.0	8.1	8.1	8.2
Unique reflections	12,169	10,527	59,057	36,525	36,514	36,570
Refinement						
R_{work}/ R_{free}	21.5/26.0 (CNS)		22.0/24.9 (REFMAC)			
Rmsd, bonds (Å)	0.009		0.014			
Rmsd, angles (°)	1.108		1.240			
Mean B ($Å^2$)	81.8		19.8 (residue B after TLS refinement)			
Ramachandran	92.5% core 7.5% allow		96.7% core 3.3% allow			

polypeptide chains that form three dimer pairs in the asymmetric unit. While the C-termini of the six molecules are all well defined, the N-termini show great structural variability among the six molecules and the region between residues 280 and 289 must be modeled into several alternative positions.

The crystal structure of Vta1NTD

Vta1NTD contains seven α-helices (α1-α7) arranged into two anti-parallel three-helix bundle modules (Figure 3.1A). Helices α1 (1-18), α2 (22-36) and α3 (42-64) form the first module; and helices α5 (86-110), α6 (115-135) and α7 (141-163) form the second module. A short helix α4 (76-84) and a disordered loop between α3 and α4 connect α3 and α5 at one end of the molecule. The two modules have an overall very similar structure and are related by a pseudo-dyad with α1/α5, α2/α6, and α3/α7 forming the corresponding pairs. They stack together via α1-α2 and α5-α6 with their helical axes perpendicular to each other. Extensive hydrophobic interactions exist between module 1, α4 and module 2 such that a total of 1809 $Å^2$ is buried at the interface of the three structural elements. Therefore the entire assembly should be considered as a single domain. This explains the fact that attempts to express the two modules separately lead to either no or aggregated protein expression (data not shown).

Vta1NTD consists of two MIT motifs

When the two structural modules within Vta1NTD were used to search for proteins of similar structure in the protein database, the N-terminal ESCRT-III binding domains of Vps4 were among the best matches (PDB ID: 1YXR and 2CPT, for human

Figure 3.1 The crystal structure of Vta1NTD.
(**A**) A ribbon representation of the Vta1NTD structure. Helices α1, α2, and α3 (MIT1) are colored blue; helix α4 is colored green; and helices α5, α6, and α7 (MIT2) are colored orange. The disordered loop region connecting helices α3 and α4 is drawn as a dash line. The N- and C-termini of the molecule are indicated.
(**B**) Structural overlay of Vta1NTD-MIT1 with the MIT domain of human Vps4A (PDB ID: 1YXR). Vta1NTD is colored gray. Vps4 MIT is colored red. The N- and C-termini for both molecules are indicated.
(**C**) Structural Overlay of Vta1NTD-MIT2 with the MIT domain of human Vps4A.
(**D**) *In vitro* analysis of Vta1-Vps60/Did2 interaction. GST or GST-tagged Vps60/Did2 was used to pull down purified Vta1NTD or $Vta1^{165-330}$ as indicated. Proteins retained on the beads were analyzed by SDS-PAGE and visualized by Coomassie blue staining.
Figures 3.1A, 3.1B and 3.1C are prepared with Pymol (DeLano Scientific LLC).

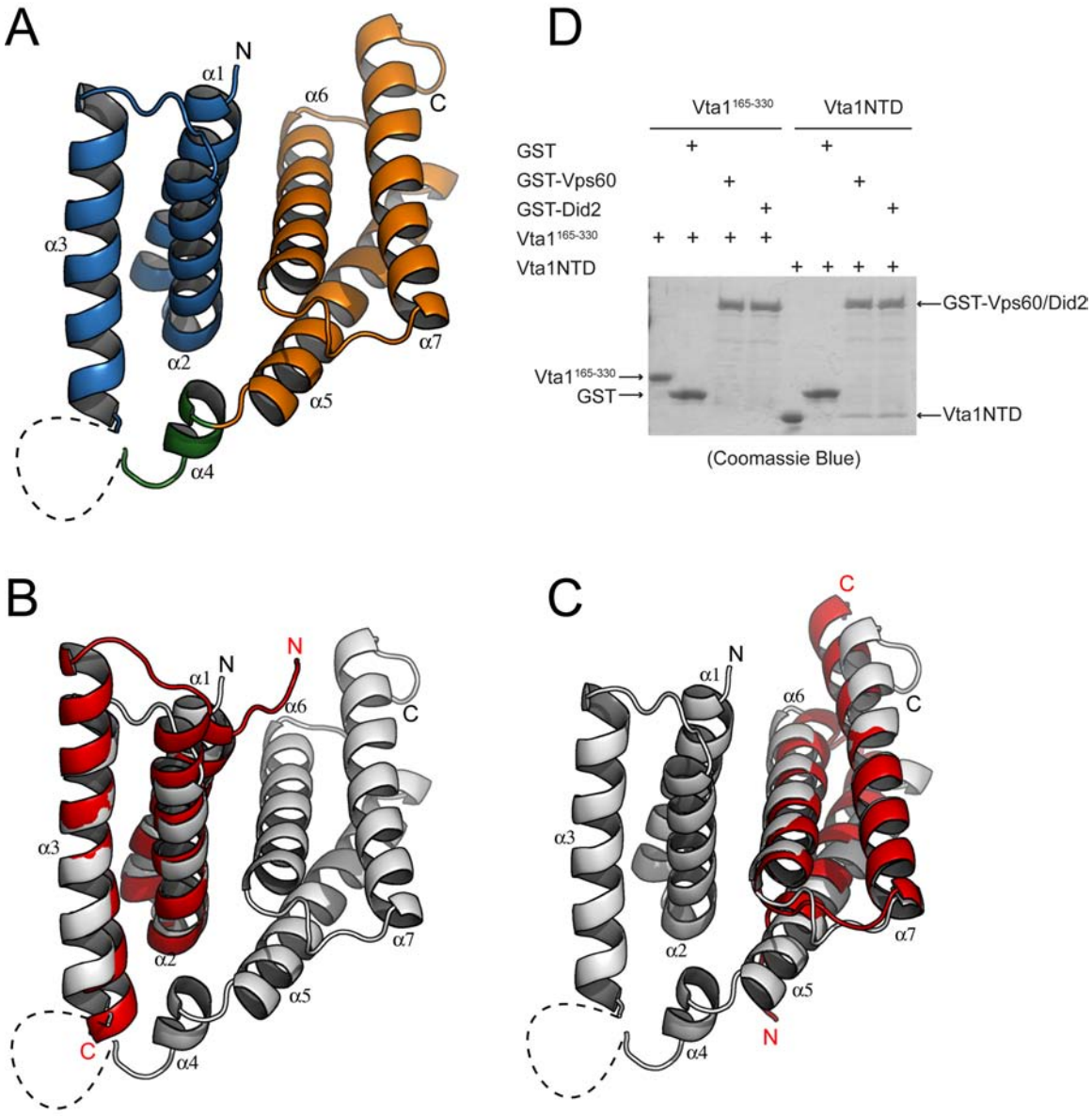
A
N
α1
α6
C
α3
α2
α7
α5
α4
D
Vta1165-330
Vta1NTD
GST
GST-Vps60
GST-Did2
Vta1165-330
Vta1NTD
GST-Vps60/Did2
Vta1165-330
GST
Vta1NTD
(Coomassie Blue)
B
N
N
α1
α6
C
α3
α7
α2
α5
C
α4
C
N
α1
α6
C
α3
α7
α2
α5
N
α4

Vps4A and Vps4B, respectively). This domain contains a fold of three helices also known as the microtubule interacting and transport (MIT) motif [22, 23]. When the three MIT domain helices of Vps4 were aligned with those in the two modules of Vta1NTD (MIT1 and MIT2), root mean square deviations for the Cα atoms are 1.3 Å and 1.7 Å over 52 and 54 residues, respectively, for human Vps4A (Figure 3.1B, 3.1C).

The MIT domain of Vps4 mediates its interaction with the ESCRT-III subunits. The site of interaction involves a surface groove formed by helix 2 and helix 3 of the MIT domain [22]. The ESCRT-III subunits interact with Vps4 by providing a fourth helix to complete a non-canonical tetratricopeptide repeat (TPR) fold. Although Vta1 does not bind to the ESCRT-III subunits, it does interact with two ESCRT-III like proteins, Vps60 and Vps46/Did2 [16, 20]. Given the structural similarity between Vta1NTD and Vps4 MIT domain, it is likely that Vta1 interacts with Vps60 and Vps46/Did2 via Vta1NTD in a manner similar to that between Vps4 and ESCRT-III. Indeed, purified Vta1NTD alone is sufficient to bind to GST-Vps60 and GST-Did2, while purified Vta1 lacking the NTD fails to bind to either (Figure 3.1D). This *in vitro* result is also consistent with an earlier finding that deletion of the N-terminal 68 residues of Vta1 abolishes its *in vivo* interaction with Vps60 [15].

Potential Vps60 and Did2 binding surface on Vta1NTD

Since the site of protein-protein interaction in the Vps4 MIT domain involves a surface groove formed by helix 2 and helix 3 of the motif, we examined the two corresponding surface areas in Vta1NTD. Both surfaces contain a hydrophobic center surrounded by polar/charged regions. Surface 1 in MIT1 is formed by conserved

hydrophobic residues Leu-29, Val-32, Leu-36, Leu-53, and Ile-56, and conserved charged/polar residues Glu-33, Arg-41, Thr-46, Thr-50, Asp-54, Glu-57, Lys-60, and Lys-61 (Figure 3.2A, 3.2B). In fact, this region on MIT1 represents the largest conserved area on the surface of Vta1NTD. The corresponding residues for Leu-29, Val-32, Leu-36, Leu-53, Ile-56, Glu-33, Thr-46, Asp-54, Glu-57 and Lys-60 in the Vps4 MIT domain (Y34, L37, M41, L64, A67, D38, R57, N65, E68 and K71) were shown to be involved in its interaction with the ESCRT-III subunit Vps2 [22]. Compared with surface 1, surface 2 on MIT2 is much less conserved (Figure 3.2A, 3.2C). Residues that form the surface include hydrophobic residues Trp-122, Ile-125, Leu-132 and Ile151, and charged/polar residues Lys-118, Ser-129, His-133, Lys-136, Glu-137, Glu-141, Thr-144, Gln-148, Lys-152 and Lys155. Of these, only Trp-122, Leu-132, Glu-137, Glu-141 and Lys-152 appear to be conserved in other Vta1 proteins.

In the lattice of Vta1NTD crystals, each Vta1NTD non-crystallographic “dimer” interacts with four neighboring molecules. Three of these interactions involve a helix from a neighboring molecule binding to the potential Vps60 binding surface in either MIT1 or MIT2 (Figure 3.2D). In all three cases, a majority of the above-described conserved residues are buried at the interface. These findings suggest that surface grooves formed by helix 2 and helix 3 of the MIT motifs in Vta1NTD are capable of participating in protein-protein interactions and therefore are excellent candidates for binding to Vps60 and Vps46/Did2.

To address this possibility, mutational analysis of the putative Vps60 and Did2 binding surface(s) of Vta1 was performed. Conserved surface residues within MIT1 (Leu-29, Leu-36, Leu-53, Ile-56, Glu-57) and MIT2 (Trp-122, Leu-132, Glu-137, Lys-

Figure 3.2 Potential Vps60 binding sites on Vta1NTD.
(**A**) Structure-based sequence alignment for the MIT domains in Vps4 and the two MIT motifs in Vta1. Secondary structure elements are shown above the sequences. Residues conserved in all MIT domains are colored red and yellow. Residues conserved only in MIT1 are colored green; and residues conserved only in MIT2 are colored blue. Residues involved in the potential functional surfaces of MIT1 and MIT2 are marked by white and black triangles, respectively.
(**B, C**) Conserved molecular surfaces on MIT1 (**B**) and MIT2 (**C**). Surface and ribbon representations of molecules in the same orientation are shown on the left and right panels, respectively. MIT1 is colored blue; helix α4 is colored green; and MIT2 is colored orange. Conserved molecular surfaces are colored red and underlying residues are labeled.
(**D**) The two conserved surfaces are involved in interacting with an α-helix from molecules in the crystal lattice. MIT1 is colored blue and MIT2 is colored orange. The helices they interact with in the crystal lattice are colored red, magenta, and cyan, respectively.
(E) Residues in MIT2 are important for Vps60 and Did2 binding. GST or GST-tagged Vps60/Did2 was used to pull down purified wild-type Vta1 or mutants as indicated. Proteins retained on the beads were analyzed by SDS-PAGE and visualized by Coomassie blue staining or western blotting with anti-Vta1 antibody (see the accompanying study (Azmi et al., 2007) for anti-Vta1 polyclonal antibody production). Figures 3.2B, 3.2C and 3.2D are prepared with Pymol (DeLano Scientific LLC).

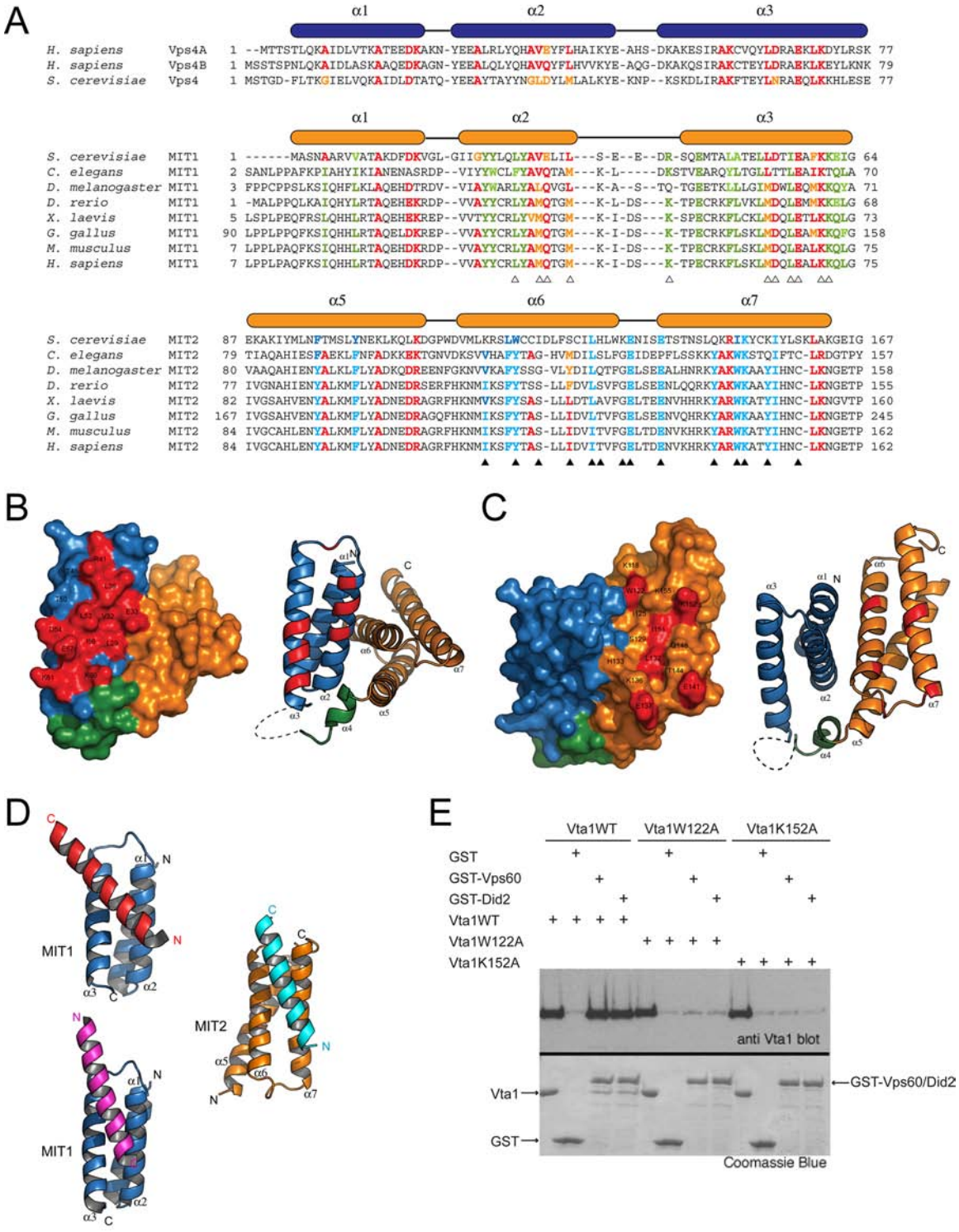
A
α1
α2
α3
H. sapiens Vps4A 1 --MTTSTLQKAIDLVTKATEEDKAKN-YEEALRLYQHAVEYFLHAIKYE-AHS-DKAKESIRAKCVQYLDRAEKLKDYLRSK 77
H. sapiens Vps4B 1 MSSTSPNLQKAIDLASKAAQEDKAGN-YEEALQLYQHAVQYFLHVVKYE-AQG-DKAKQSIRAKCTEYLDRAEKLKEYLKNK 79
S. cerevisiae Vps4 1 MSTGD-FLTKGIELVQKAIDLDTATQ-YEEAYTAYYNGLDYLMLALKYE-KNP--KSKDLIRAKFTEYLNRAEQLKKHLESE 77
α1
α2
α3
S. cerevisiae MIT1 1 ------MASNAARVVATAKDFDKVGL-GIIGYYLQLYAVELIL---S-E--E--DR-SQEMTALATELLDTIEAFKKEIG 64
C. elegans MIT1 2 SANLPPAFKPIAHYIKIANENASRDP--VIYYWCLFYAVQTAM---K-L-----DKSTVEARQYLTGLLTTLEAIKTQLA 70
D. melanogaster MIT1 3 FPPCPPSLKSIQHFLKLAQEHDTRDV--VIAYWARLYALQVGL---K-A--S--TQ-TGEETKLLLGIMDWLEQMKKQYA 71
D. rerio MIT1 1 -MALPPQLKAIQHYLRTAQEHEKRDP--VVAYYCRLYAMQTGM---K-L-DS---K-TPECRKFLVKLMDQLEMMKKELG 68
X. laevis MIT1 5 LSPLPEQFRSLQHHLRTAQEHEKREP--VVTYYCRLYVMQTGM---K-I-DS---K-SPECRKFLCKLMDQLETLKKQLG 73
G. gallus MIT1 90 LPPLPPQFKSIQHHLRTAQELDKREP--VVAYYCRLYAMQTGM---K-I-DS---K-TPECRKFLSKLMDQLEAMKKQFG 158
M. musculus MIT1 7 LPPLPAQFKSIQHHLRTAQEHDKRDP--VVAYYCRLYAMQTGM---K-I-DS---K-TPECRKFLSKLMDQLEALKKQLG 75
H. sapiens MIT1 7 LPPLPAQFKSIQHHLRTAQEHDKRDP--VVAYYCRLYAMQTGM---K-I-DS---K-TPECRKFLSKLMDQLEALKKQLG 75
α5
α6
α7
S. cerevisiae MIT2 87 EKAKIYMLNFTMSLYNEKLKQLKDGPWDVMLKRSLWCCIDLFSCILHLWKENISETSTNSLQKRIKYCKIYLSKLAKGEIG 167
C. elegans MIT2 79 TIAQAHIESFAEKLFNFADKKEKTGNVDKSVVHAFYTAG-HVMDILSLFGEIDEPFLSSKKYAKWKSTQIFTC-LRDGTPY 157
D. melanogaster MIT2 80 VAAQAHIENYALKLFLYADKQDREENFGKNVVKAFYSSG-VLYDILQTFGELSEEALHNRKYAKWKAAYIHNC-LKNGETP 158
D. rerio MIT2 77 IVGNAHIENYALKMFLYADNEDRSERFHKNMIKSFYTSS-LLFDVLSVFGELSEENLQQRKYAKWKAAYIHNC-LKNGETP 155
X. laevis MIT2 82 IVGSAHVENYALKMFLYADNEDRAGRFHKNMVKSFYSAS-LLLDTLAVFGELTEENVHHRKYARWKATYIHNC-LKNGVTP 160
G. gallus MIT2 167 IVGSAHVENYALKMFLYADNEDRAGQFHKNMIKSFYTAS-LLIDVLTVFGELSEENVQHRKYARWKAAYIHNC-LKNGETP 245
M. musculus MIT2 84 IVGCAHLENYALKMFLYADNEDRAGRFHKNMIKSFYTAS-LLIDVITVFGELTDENVKHRKYARWKATYIHNC-LKNGETP 162
H. sapiens MIT2 84 IVGCAHLENYALKMFLYADNEDRAGRFHKNMIKSFYTAS-LLIDVITVFGELTDENVKHRKYARWKATYIHNC-LKNGETP 162
B
C
D
MIT1
MIT2
MIT1
E
Vta1WT
Vta1W122A
Vta1K152A
GST
GST-Vps60
GST-Did2
Vta1WT
Vta1W122A
Vta1K152A
anti Vta1 blot
Vta1
GST
GST-Vps60/Did2
Coomassie Blue

149, Lys-152) were mutated to alanines, the mutant proteins were expressed in bacteria, and the purified proteins were examined for binding to GST-Did2 and GST-Vps60. While most mutations did not dramatically reduce binding (data not shown), this analysis identified 2 residues, Trp-122 and Lys-152, as important for Vta1 interaction with both Did2 and Vps60 (Figure 3.2E). This result implicated the surface groove formed by helix 2 (α6) and helix 3 (α7) of MIT2 as the putative binding site for both Vps60 and Did2. Functional analysis of this interaction is presented in the accompanying study [24].

The crystal structure of Vta1CTD

Vta1CTD is organized into a pair of anti-parallel α-helices (α8-α9) (Figure 3.3A). Helix α8 (281-310) is significantly longer than helix α9 (312-330) such that inter-helical interactions only exist between α9 and the C-terminal half of α8. As will be discussed in more detail, the structure where inter-helical interaction occurs is also involved in protein dimerization. Therefore, it should be considered as the structural core of Vta1CTD. Interestingly, regions outside the core display great conformational variability. Of the six independently determined Vta1CTD molecules in the asymmetric unit, helix α8 displays different degrees of bending at Arg-290, ranging from -30° to 14° (Figure 3.3B). These results suggest that the N-terminal part of helix α8 is highly flexible relative to the core of Vta1CTD.

Oligomerization state of Vta1

The crystal structure of Vta1CTD shows that the molecule forms a dimeric structure in the crystal lattice where three independent dimer pairs were observed. This is

Figure 3.3. The crystal structure of Vta1CTD.
(**A**) A ribbon representation of the monomer structure of Vta1CTD. The N- and C-termini of the molecule are indicated.
(**B**) Structure flexibility within Vta1CTD. Three Vta1CTD molecules that represent the largest differences among the six molecules in the asymmetric unit are shown as ribbons and colored green, pink, and cyan, respectively. Top right insert: a schematic diagram illustrating different degrees of helix α8 bending at Arg-290.
(**C**) LnA vs R^2 plot of sedimentation equilibrium analytical ultracentrifugation data. The slope of the plot is proportional to the molecular weight of the protein. Data is plotted alongside simulations using theoretical values for the molecular weight of a dimer (solid line) or a monomer (dash line) species, with an arbitrary Y-axis for direct comparison.
(**D**) Stereo view of the dimer structure of Vta1CTD. One molecule is colored pink, the other colored green. Residues located at the dimer interface are labeled. Leu-320 and Leu-327 are highlighted in magenta.
(**E**) Gel filtration analysis. Gel filtration experiments were performed on a Superdex^{TM} 200 column (Amersham). Compared with the wild-type protein (red), L320E (cyan) and L327E (pink) eluted at a monomer position; while Y303A (blue) and Y310A (green) maintained their dimeric structures. Figures 3.2A, 3.2B and 3.2D are prepared with Pymol (DeLano Scientific LLC).

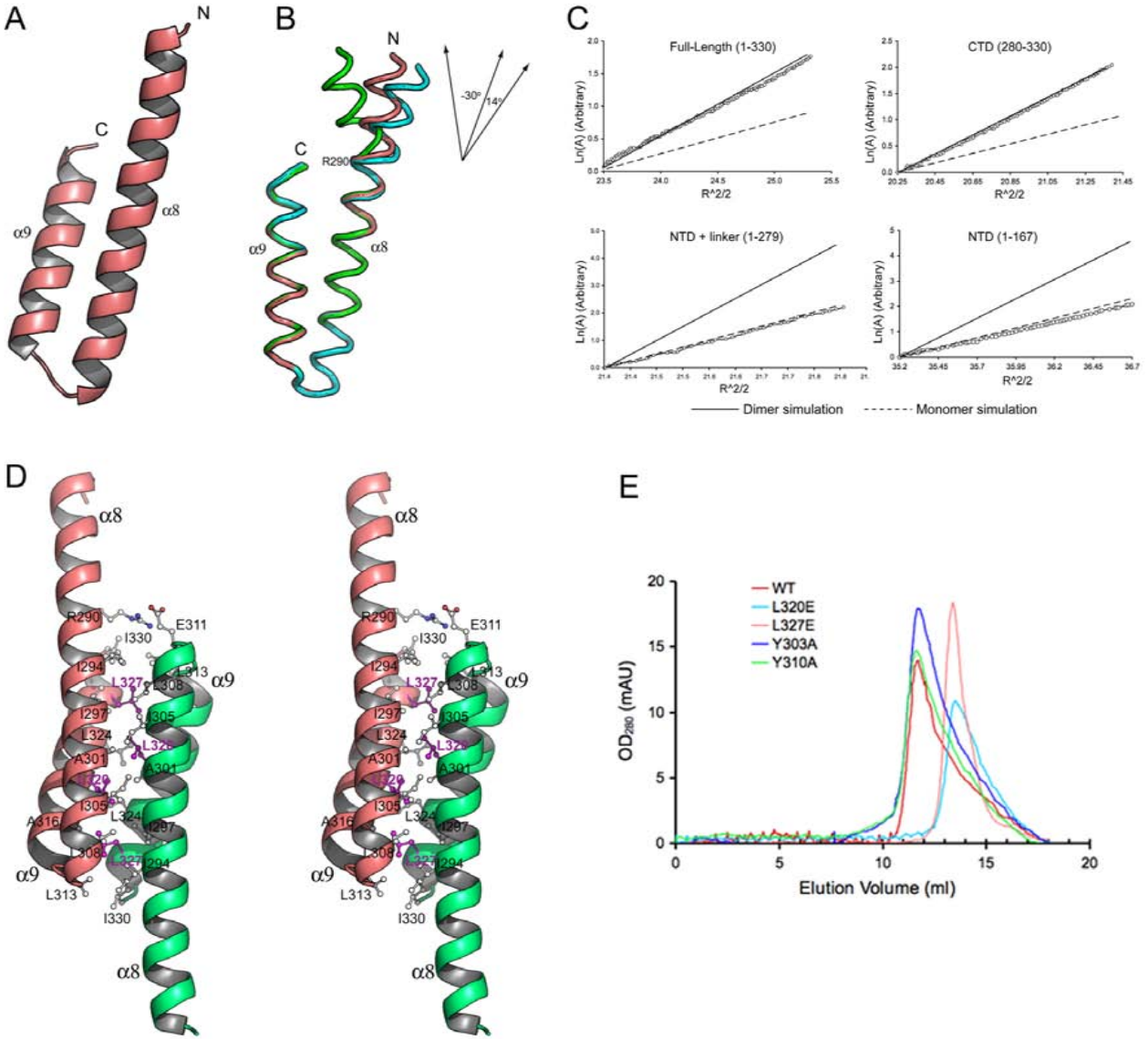
A
N
C
α8
α9
B
N
C
R290
α9
α8
-30°
14°
C
Full-Length (1-330)
CTD (280-330)
NTD + linker (1-279)
NTD (1-167)
Ln(A) (Arbitrary)
R^2/2
Dimer simulation
Monomer simulation
D
α8
R290
E311
I330
I294
L327
L313
I308
α9
I297
I305
L324
A301
A316
L313
I330
α8
E
WT
L320E
L327E
Y303A
Y310A
OD280 (mAU)
Elution Volume (ml)

consistent with previous findings that Vta1 is molecular dimer in solution and the C-terminal region is required for dimerization [15]. To determine whether Vta1CTD alone is sufficient for dimerization, the oligomerization state of Vta1CTD was analyzed using sedimentation equilibrium analytical ultracentrifugation (Figure 3.3C). The results showed that, like Vta1, Vta1CTD is a dimer in solution. In contrast, only a monomer species was observed for Vta1 lacking the C-terminal domain ($Vta1^{1-279}$), consistent with results from previous studies using an *in vivo* assay [15]. Therefore, Vta1CTD is necessary and sufficient for protein dimerization.

In forming the dimer, the anti-parallel α-helices within each Vta1CTD subunit interacts with their helical axes aligned to create a four-helix bundle dimer structure (Figure 3.3D). In the four-helix bundle, symmetry-related helices are packed against each other and the molecular dyad is perpendicular to the helical axes. As a result, the N-terminal ends of the two subunits point way from the four-helix bundle and in opposite directions. The dimer interface covers 21% of the solvent accessible surface for each subunit. The interface is predominantly hydrophobic with many highly conserved residues involved, including Ala-304, Leu-308, Leu-313, Ala-316, Leu-320, Leu-324 and Leu-327. At the periphery of the interface, a few polar interactions are also observed including a pair of salt bridges between Arg-290 and a highly conserved Glu-311.

To assess the contribution of the conserved residues at the Vta1CTD dimer interface to the stability of Vta1 dimer structure, two single point mutants, L320E and L327E, were generated. Both residues are in the central region of the hydrophobic dimer interface, and we predicted that substitution of them with charged glutamic acids would disrupt the packing within the dimer structure. Mutant proteins were purified and their

oligomerization states were analyzed using gel-filtration chromatography. Indeed, compared with the wild type Vta1 dimer, the elution profile of the L320E and L327E mutants were shifted towards the monomeric species on gel filtration (Figure 3.3E). These biochemical results confirmed that the conserved interface observed in Vta1CTD structure is responsible for Vta1 dimerization.

Vps4 binding surface on Vta1CTD

The C-terminal region of Vta1 has been previously shown to interact with Vps4 [15]. With purified $Vps4^{E233Q}$ (an ATPase deficient mutant), we further demonstrated that Vta1 interacts with Vps4 in an adenine nucleotide dependent manner (Figure 3.4A). Interestingly, the N-terminal region of Vta1 appears to have an effect on this interaction as Vta1CTD displays a stronger ADP-dependent binding to Vps4.

Sequence alignment of Vta1 proteins revealed a high degree of overall conservation for Vta1CTD among representative members from yeast, plants, and mammals (Figure 3.4B). Many of the conserved residues are located at the dimer interface and are important for supporting the dimer structure. There are, however, a few conserved surface exposed residues including Lys-299, Lys-302, Tyr-303, Ser-306, Tyr-310, Glu-311, Asp-312, Thr-315 and Lys-322 (Figure 3.4C). Previous studies showed that mutations in Lys-299 and Lys-302 completely abolished the ability of Vta1 to stimulate the ATPase activity of Vps4 while mutation in Lys-322 had no effect [15]. Since Lys-299 and Lys-302 are located on helix α8 and Lys-322 is located on helix α9, these results suggest that α8 is the site of Vps4 binding.

Figure 3.4. Vps4 binding sites on Vta1CTD.
(**A**) *In vitro* analysis of Vta1-Vps4 interaction. Glutathione agarose beads pre-loaded with GST, GST-Vta1 or GST-Vta1CTD were incubated with purified $Vps4^{E233Q}$ under indicated conditions. Proteins retained on the beads were analyzed by SDS-PAGE and visualized by Coomassie blue staining.
(**B**) Sequence alignment of Vta1CTD. Triangles indicate conserved residues involved in the dimer formation. Stars indicate conserved surface residues. Secondary structure elements are shown above the sequences.
(**C**) Stereo view of the conserved surface residues on Vta1CTD. The residues demonstrated to be important for Vps4 interaction are highlighted in red.
(**D**) Interactions between Vps4 and mutant Vta1 proteins. Purified $Vps4^{E233Q}$ were incubated with GST-tagged wild-type or point mutant Vta1 proteins in the presence of 2 mM ATP. Materials bound to glutathione agarose beads were analyzed by SDS PAGE and visualized by Coomassie blue staining.
(**E**) ATPase activity of Vps4 in the presence of Vta1 proteins. The activity was normalized to Vps4 alone to compare the stimulation effects of different Vta1 proteins (error bars represent standard deviation of results from three independent measurements).
(**F**) Interactions between Vps4 and Vta1 heterodimers. Vta1 heterodimers were co-expressed in pETDuet-1 vector such that the N-terminal His-tagged wild-type protein is in the first expression cassette and the C-terminal S-tagged wild-type or mutant protein is in the second expression cassette. Heterodimer proteins were isolated by tandem purification with Ni^{++}-NTA resin and S-protein resin (left panel). Heterodimers retained on the S-protein resin were then used to pull down $Vps4^{E233Q}$ in the presence of 2mM ATP. Bound Vps4 proteins were analyzed on SDS-PAGE and detected by Western blotting with anti-Vps4 antibody (right panel). Figure 3.4C is prepared with Pymol (DeLano Scientific LLC).

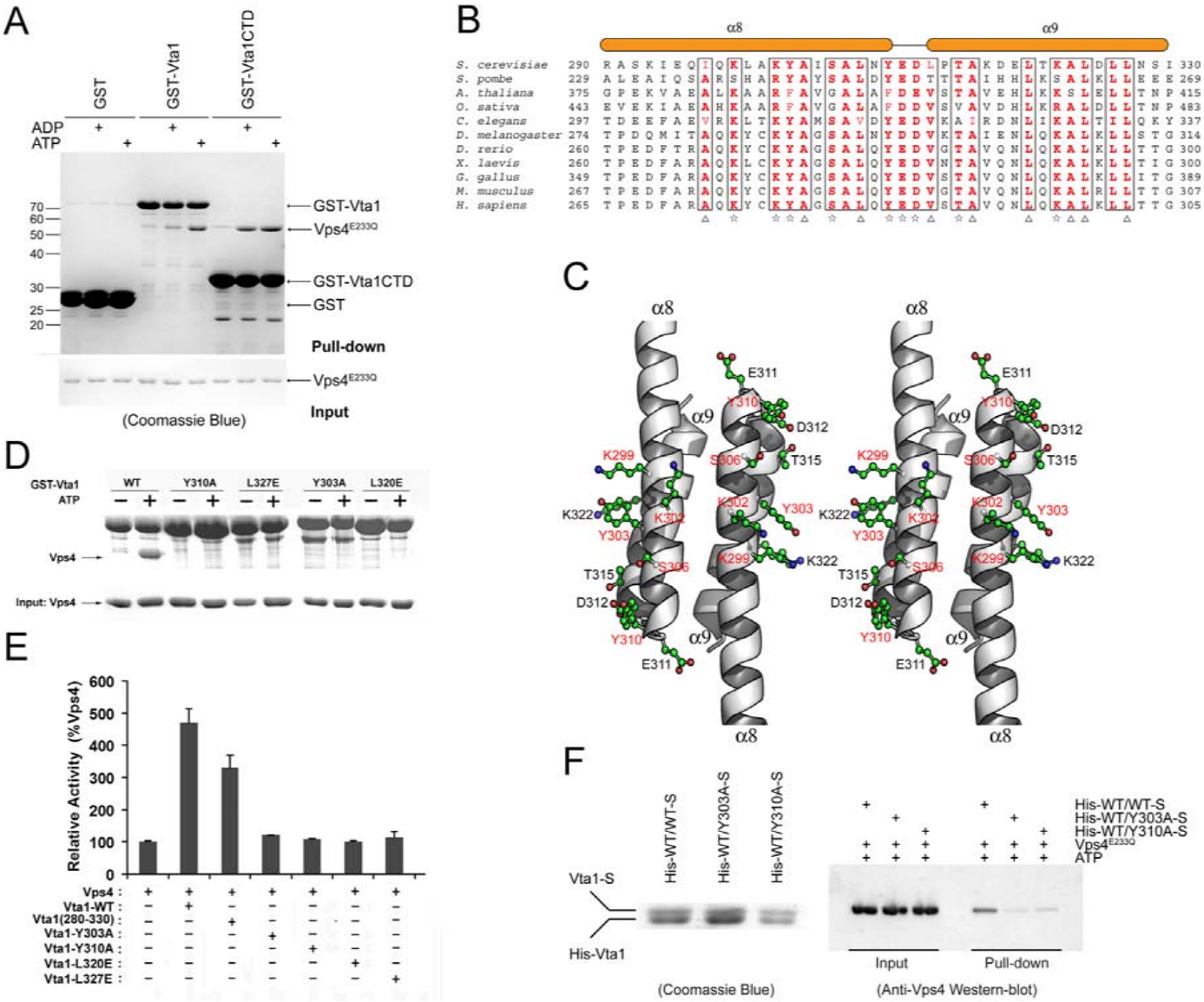
A
GST
GST-Vta1
GST-Vta1CTD
ADP
ATP
70
60
50
40
30
25
20
GST-Vta1
Vps4E233Q
GST-Vta1CTD
GST
Pull-down
Vps4E233Q
Input
(Coomassie Blue)
B
α8
α9
S. cerevisiae 290 R A S K I E Q I Q K L A K Y A I S A L N Y E D L P T A K D E L T K A L D L L N S I 330
S. pombe 229 A L E A I Q S A R S H A R Y A Y S A L D Y E D T T T A I H H L K S A L K L L E E E 269
A. thaliana 375 G P E K V A E A L K A A R F A V G A L A F D E V S T A V E H L K K S L E L L T N P 415
O. sativa 443 E V E K I A E A H K A A R F A V G A L A F D D V S V A V D H L K R A L D L L T N P 483
C. elegans 297 T D E E F A E V R K L T K Y A M S A V D Y E D V K A I R D N L I K A L T I L Q K Y 337
D. melanogaster 274 T P D Q M I T A Q K Y C K Y A G S A L N Y D D V K T A I E N L Q K A L K L L S T G 314
D. rerio 260 T P E D F T R A Q K Y C K Y A G S A L Q Y E D V G T A V Q N L Q K A L K L L T T G 300
X. laevis 260 T P E D F A R A Q K L C K Y A G S A L Q Y E D V N T A V Q N L Q K A L K L L T I G 300
G. gallus 349 T P E D F A R A Q K Y C K Y A G S A L Q Y E D V S T A V Q N L Q K A L K L L I T G 389
M. musculus 267 T P E D F A R A Q K Y C K Y A G S A L Q Y E D V G T A V Q N L Q K A L R L L T T G 307
H. sapiens 265 T P E D F A R A Q K Y C K Y A G S A L Q Y E D V S T A V Q N L Q K A L K L L T T G 305
C
α8
α9
E311
Y310
D312
T315
S306
K299
K302
Y303
K322
D
GST-Vta1
ATP
WT
Y310A
L327E
Y303A
L320E
Vps4
Input: Vps4
E
Relative Activity (%Vps4)
600
500
400
300
200
100
0
Vps4 :
Vta1-WT :
Vta1(280-330) :
Vta1-Y303A :
Vta1-Y310A :
Vta1-L320E :
Vta1-L327E :
F
His-WT/WT-S
His-WT/Y303A-S
His-WT/Y310A-S
Vps4E233Q
ATP
Vta1-S
His-Vta1
(Coomassie Blue)
Input
Pull-down
(Anti-Vps4 Western-blot)

Four more conserved residues on α8 and the short linker between α8 and α9, residues Tyr-303, Tyr-310, Glu-311, and Asp-312, were mutated into alanines to assess their roles in mediating Vps4 interaction. Of the four, Y303A and Y310A were deficient in interaction with Vps4 as demonstrated in a GST pull-down assay while maintaining their dimeric structures (Figure 3.4D, 3.3E). In addition, when the mutant proteins were purified and used in the ATPase assay, they failed to stimulate the ATPase activity of Vps4, in contrast to the wild type protein (Figure 3.4E). Therefore, it is likely that these two residues are directly involved in Vps4 interaction as well. The other two mutants, E311A and D312A, also did not bind to Vps4 but they were monomers in solution (data not shown). Hence it is not clear whether they directly participate in binding to the ATPase. Taken together, these results showed that the site of Vps4 binding on Vta1 is located on the solvent-exposed side of helix α8 and the binding characteristic appears to be largely hydrophilic in nature.

The dimer structure of Vta1 is required for Vps4 interaction

The fact that monomer mutants E311A and D312A failed to interact with Vps4 prompted us to examine the role of Vta1 dimer in regulating the function of Vps4. Indeed, the monomer mutants L320E and L327E also failed either to pull down Vps4 in our GST pull-down assay or to stimulate the ATPase activity of Vps4 suggesting that a stable association between Vta1 and Vps4 requires the presence of both Vps4 binding sites on Vta1 (Figure 3.4D, 3.4E). To further characterize this structural requirement, His-tagged wild-type Vta1 was co-expressed with S-tagged wild-type Vta1, Y303A, or Y310A mutants in *E. coli.* Vta1 heterodimers were isolated by tandem purification with Ni^{++}-

NTA resin and S-protein resin (Figure 3.4F). Heterodimers retained on the S-protein resin were then used to pull down Vps4^{E233Q} in the presence of ATP. Although these heterodimers behaved similarly during the process of expression and purification, only the wild-type Vta1 heterodimer could interact with Vps4. Neither WT/Y303A nor WT/Y310A heterodimer, which contains one of the two functional Vps4 binding sites, could form a stable complex with Vps4^{E233Q}. These results strongly suggested that both Vps4 binding sites on the Vta1 dimer are necessary for its stable association with Vps4.

To further examine the effect of Vta1 dimerization and Vps4 binding on the function of Vta1 in the MVB pathway, we examined the sorting of carboxypeptidase S (CPS) in yeast cells expressing wild-type *VTA1* versus mutant *vta1* alleles. Sorting of the MVB cargo GFP-CPS was analyzed by fluorescence microscopy in *vta1*Δ cells transformed with mutant forms of *vta1* (Figure 3.5). Four mutants were used in the study: two Vps4-binding deficient mutants Y303A and Y310A and two dimerization-deficient mutants L320E and L327E. Cells transformed with empty plasmid display a dramatic mis-localization of GFP-CPS to the limiting membrane of the vacuole, indicative of the MVB sorting defect observed in *vta1*Δ cells. As expected, transformation with wild type *VTA1* restores delivery of GFP-CPS into the MVB pathway as indicated by fluorescence within the vacuole lumen. However, none of the mutants is capable of complementing the MVB sorting defect observed in *vta1*Δ cells. GFP-CPS was mis-localized in cells expressing these mutants as in *vta1*Δ cells. These results highlight the importance of both Vta1 dimerization and Vps4 binding for the *in vivo* function of Vta1.

The structure of intact Vta1

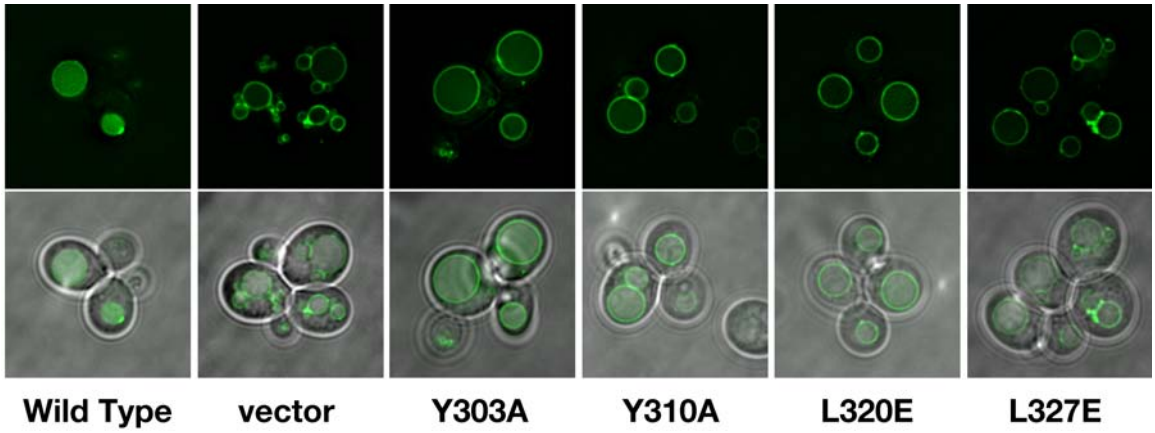

Figure 3.5 Residues involved in dimerization and Vps4 binding are required for cargo sorting in the MVB pathway.
vta1 cells (BY4742 genetic background) were transformed with both *cen*-copy plasmids expressing the indicated form of Vta1 and GFP-CPS. Live cells were visualized using fluorescence and brightfield microscopy and fluorescent images were processed using Deltavision deconvolution software.

The region between Vta1NTD and Vta1CTD (residues 168-279) was not defined crystallographically in the current study. Although this linker is present in all Vta1 proteins, there appears to be no strong sequence conservation. In addition, the length of the linker varies greatly among different Vta1 orthologs. While structure prediction for the linker suggests that it contains little regular ordered secondary structure, we sought to confirm the prediction experimentally by measuring the circular dichroism (CD) spectrum in the far UV region for the linker. Since the linker alone cannot be expressed, we obtained its spectrum indirectly by measuring the spectra for the intact and various truncation forms of Vta1. The CD spectrum of the intact Vta1 is dominated by contributions from α-helices (Figure 3.6A). The CD spectrum of the intact protein is nearly superimposable to a linear combination of the spectra of $Vta1^{1-279}$ and Vta1CTD suggesting that these isolated fragments retain their native structures as in the intact protein (Figure 3.6B). The CD spectrum for the linker can be obtained by subtracting the spectrum of Vta1NTD from that of $Vta1^{1-279}$, or, alternatively, by subtracting the spectra of Vta1NTD and Vta1CTD from that of the intact protein. These two calculated CD spectra agree with each other very well and both have a strong minimum near 195nm (Figure 3.6C). This feature is typical for random coil structures, suggesting that the linker region is mostly devoid of ordered secondary structure and likely adopts a random coil conformation.

Based on the structural information from the crystallographic and CD spectral analysis, we propose that the structure of intact Vta1 likely adopts an extremely elongated shape with Vta1CTD at the center and Vta1NTD pointing to the opposite ends, connected by the largely unstructured middle linker (Figure 3.6D). The Stokes radii of Vta1,

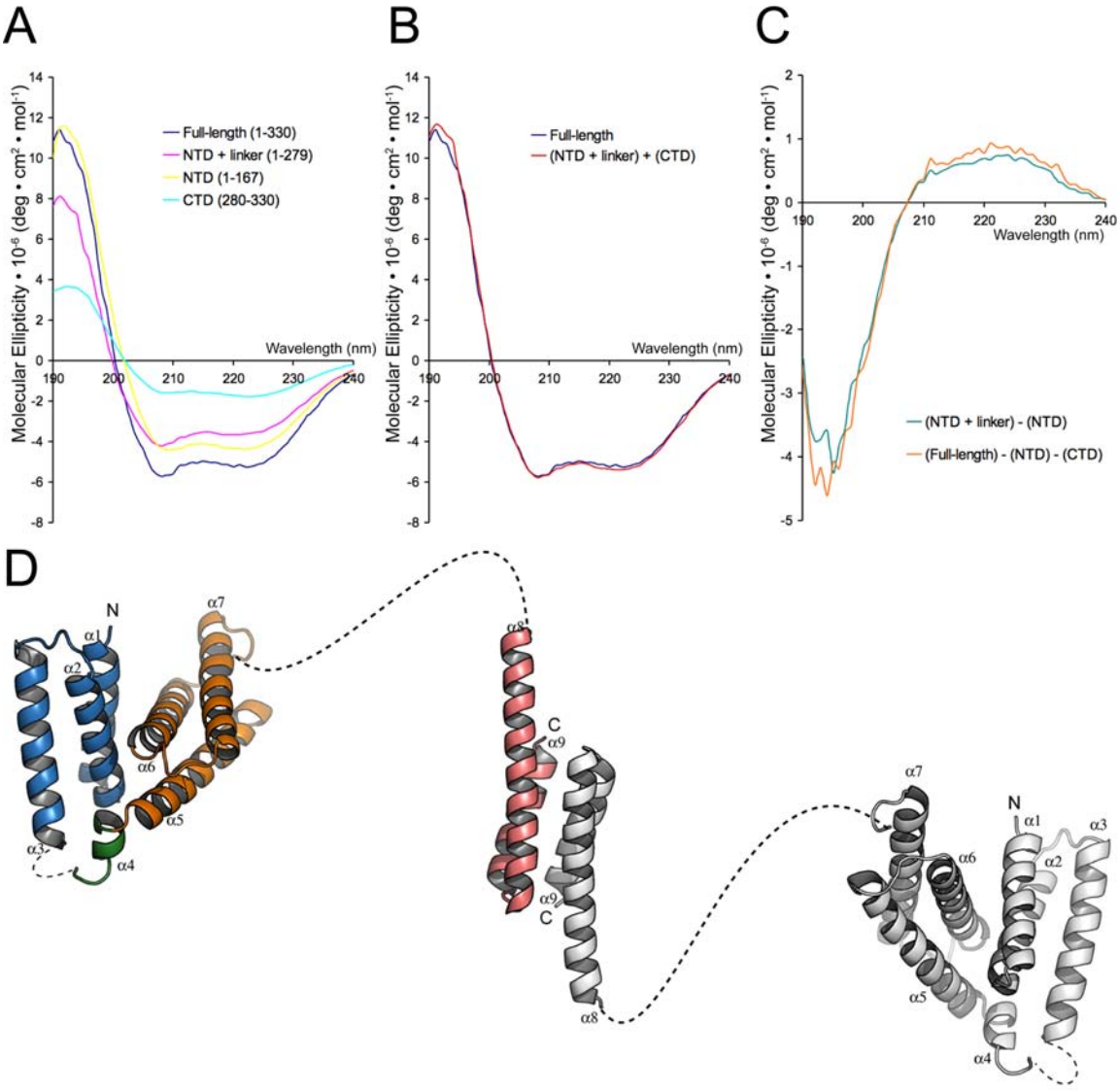

Figure 3.6 The structure of intact Vta1.
(**A**) Experimental far-UV CD spectra of Vta1, Vta1$^{1-279}$, Vta1$^{1-167}$ (Vta1NTD) and Vta1$^{280-330}$ (Vta1CTD) show α-helix-containing structures.
(**B**) The experimental CD spectrum of Vta1 is superimposable with the reconstructed CD spectrum calculated from the experimental spectra of Vta1$^{1-279}$ and Vta1$^{280-330}$.
(**C**) Calculated CD spectra of the linker region (Vta1$^{168-279}$) show random coil structure.
(**D**) A model of the full-length Vta1 dimer. One molecule is colored as in Figures 3.1A and 3.3A and the other is colored gray. The linkers between helices α3 and α4 and between helices α7 and α8 are drawn as dash lines.

Vta1CTD, and Vta1NTD are 5.9nm, 2.2nm and 1.9nm respectively, as determined by dynamic light scattering. These numbers are consistent either with the model (Vta1) or with experimentally determined structures (Vta1NTD and Vta1CTD). Interestingly, the N-terminal portion of Vta1CTD can bend to different degrees depending on its environment, strongly suggesting that Vta1 is a highly flexible molecule with the Vps60 binding N-terminal domain acting like tentacles relative to its dimeric Vps4 binding core.

DISCUSSION

Vta1 functions in the MVB pathway by interacting with at least three other class E Vps proteins, Vps4, Vps60 and Vps46/Did2. Consistent with its biological function, the structure of Vta1 is organized into three distinct regions: an N-terminal Vps60- and Did2-binding domain, a random-coiled linker region and a C-terminal Vps4 binding domain. In addition, the C-terminal domain also mediates protein homo-dimerization and the dimer structure is critical to its *in vitro* and *in vivo* function as a Vps4 regulator.

The structure of Vta1 suggests a possible mechanism of interaction between Vta1 and Vps4. Vps4 contains a unique three-stranded "β domain" structure that has been shown to mediate its interaction with Vta1 [25]. When Vps4 forms a high molecular weight ring-shaped oligomer, the β domain is situated at the periphery of the ring based on structural analogy to other AAA-ATPases whose oligomeric structures are known. Although it is still possible that the two symmetry-related Vps4 binding surfaces on Vta1CTD constitute a single Vps4 binding site, the discontinuous nature of the two surfaces would argue that they each bind to one Vps4 subunit. Given the symmetry

within Vta1, the two Vps4 subunits they bind to must also obey the same matching two-fold symmetry. This in turn suggests that the nucleotide-dependent Vps4 oligomer is a molecule with two-fold symmetries, i.e., a double-ring structure.

One could therefore envision a model where Vta1 promotes the nucleotide-dependent assembly of a double-ring structure of Vps4 by binding to one subunit of Vps4 from each ring (Figure 3.7). The activity of Vta1 would then lie in its ability to strengthen the inter-ring subunit interaction rather than the intra-ring subunit interaction, which is likely to be solely due to nucleotide binding. In fact, nucleotide-dependent oligomerization must precede the action of Vta1 as only very weak interaction is observed in the absence of nucleotide. On the other hand, while a stable Vps4 oligomer only exists in the presence of ATP, addition of Vta1 can stabilize the oligomeric structure even with ADP as the affinity between Vps4 and Vta1 increases significantly with the addition of ADP in our *in vitro* pull-down assay (Figure 3.4A). Assuming each ring of Vps4 oligomer consists of six subunits, simultaneous binding of six Vta1 molecules will significantly stabilize the structure of Vps4 oligomer.

While the biological role of Vps4-Vta1 interaction is now clearly defined, we are less certain about the function of the interaction between Vta1 and accessory ESCRT-III proteins partly due to the lack of a well-defined biochemical role for these proteins. Like other class E Vps proteins, Vps60 and Vps46/Did2 are required for proper MVB sorting and have a structural organization similar to that of the ESCRT-III subunits [8]. In an accompanying study, Vta1 membrane recruitment is demonstrated to be dependent on Did2 while Vps60 membrane recruitment is dependent on Vta1 [24]. In addition, Vps60- and Did2-binding to Vta1 is demonstrated to enhance stimulation of Vps4 in vitro. These

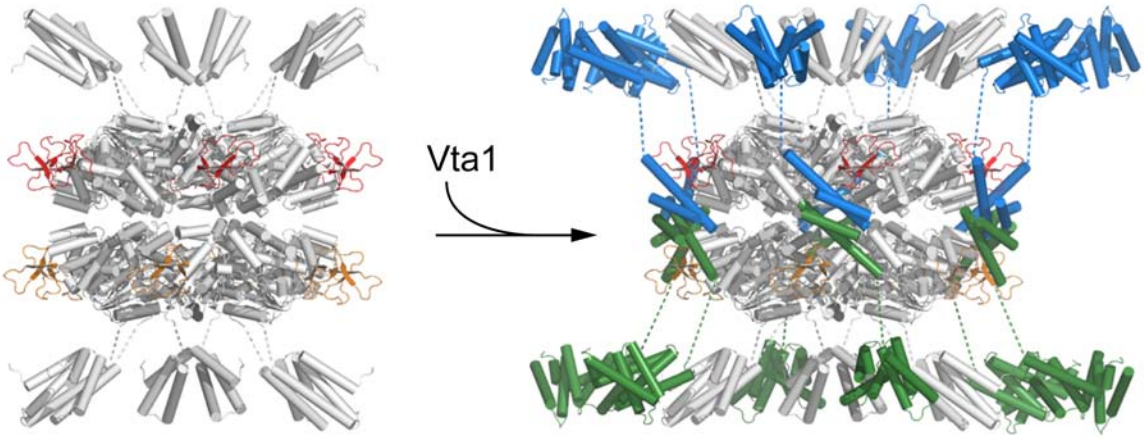

Figure 3.7 A model of Vps4-Vta1 complex.
Vps4 dodecameric ring structure (colored white) is modeled using coordinates of *S. cerevisiae* Vps4 ATPase domain (Chapter 2) based on its homology to p97 (1S3S) and FtsK (2IUU). ESCRT-III binding MIT domains (colored white, 1YXR) of Vps4 are placed at both ends of the double-ring structure. One Vta1CTD dimer (colored blue and green) is modeled between two Vta1-binding β-domains of Vps4 (one from each ring, colored red and orange) so that contacts between the known interacting structural elements from the two proteins are maximized. The long linker between Vta1CTD and Vta1NTD likely projects Vta1NTD near the MIT domain of Vps4.

results suggest that interactions between Vta1 and the accessory ESCRT-III proteins direct membrane recruitment as well as stimulation of Vps4. Our structural analysis of Vta1NTD suggests that the overall mode of interaction between Vta1 and the accessory ESCRT-III proteins likely mimics that between Vps4 and the ESCRT-III subunits and differences may lie in the critical residues involved. It would be important to illustrate these structural features in future work.

Although the middle linker region of Vta1 contains little ordered structure, it may nevertheless be functionally important. In a simple picture, the sizable linker can project the N-terminal region of Vta1 significantly beyond its dimeric C-terminal core, allowing Vta1NTD and its binding partner to interact with other proteins in the MVB pathway. For example, Vta1NTD might be close to the N-terminal domain of Vps4, thereby bringing the ESCRT-III and accessory ESCRT-III proteins together. Interestingly, we have noticed that the linker also appears to have certain effects on the affinities of Vta1 for Vps4 and the accessory ESCRT-III proteins. Both Vta1NTD and Vta1CTD show higher affinities for their respective binding partners than the full-length protein in our pull-down assays (data not shown and Figure 3.4A). These observations suggested that the linker may even function as a communicator between the two terminal domains more than just as a simple connector.

In summary, we have determined the crystal structures of the two functionally important domains of Vta1 and showed that Vta1 is an elongated molecule with a Vps4-binding dimeric core in the middle and two Did2- and Vps60-binding domains pointing in opposite direction and connected to the core by long, flexible regions. The structural information, coupled with biochemical and cell biology experiments, has provided

important insights to the molecular mechanism of Vta1 function. Emerging from this study is a model where six Vta1 molecules bind to a double-ring shaped Vps4 near its mid-section and twelve Did2- and Vps60-binding domains project to both ends of the Vps4 double-ring. In this picture, these MIT motif-containing domains will be close to the N-terminal ESCRT-III binding domain of Vps4 suggesting that the ESCRT-III like proteins might be spatially close to the ESCRT-III proteins and participate in regulating the assembly and disassembly of the ESCRT-III complex. Therefore, we predict that Vta1 plays a much more complicated role in regulating the MVB pathway than previously envisioned.

METHODS

Cloning, expression and purification

DNA fragments encoding Vta1 and Vps4 were amplified from the *Saccharomyces cerevisiae* genomic DNA. Vta1NTD was expressed in *E. coli* BL21(DE3) using a modified pET28b vector with a SUMO protein inserted between a His_6-tag and the Vta1NTD coding region. The His_6-SUMO-Vta1NTD protein was purified by Ni^{2+}-NTA affinity chromatography following standard procedures. ULP1 protease was then added to remove the His_6-SUMO tag, and the protein mixture was passed over a second Ni^{2+}-NTA column. Vta1NTD was further purified by anion exchange chromatography on a Resource-Q column (Amersham Pharmacia). Vta1CTD was expressed in BL21(DE3) using a modified pET21a vector with an N-terminal His_8-tag followed by a TEV protease cleavage site. The His_8-Vta1CTD was first purified by Ni^{2+}-NTA affinity

chromatography. Overnight TEV protease digestion cleaved the N-terminal His_8-tag, and a second Ni^{2+}-NTA step removed the tag, uncleaved protein and TEV protease. Vta1CTD was further purified using an anion exchange Source-Q column (Amersham Pharmacia). Selenomethionyl protein derivatives were expressed in *E. coli* B834(DE3) using a minimal medium where methionines were replaced with selenomethionines. Derivative proteins were purified in the same way as native proteins.

Crystallization and data collection

Native crystals of Vta1NTD were grown by the sitting drop method at 20°C. Proteins at 25 mg/ml were mixed in a 1:1 ratio with a reservoir solution of 3.5 M sodium formate in a final volume of 4 μl and equilibrated against the reservoir solution. Crystals grew to full size in several days and were transferred into 4 M sodium formate, 10% glucose before flash-frozen under liquid nitrogen. Selenomethionyl protein crystals of Vta1NTD were grown from 3.6-3.8 M sodium formate, 0.1 M HEPES (pH 7.5) and harvested in the same way. Native and selenomethinyl crystals diffracted to 2.9 Å and 3.0 Å, respectively. Diffraction data were collected at the Advanced Photon Source beam line 21-ID. Native crystals of Vta1CTD were also grown by the sitting drop method at 20°C. Proteins at 20 mg/ml were mixed in a 1:1 ratio with a reservoir solution of 30% MPD, 0.1 M Na-Acetate (pH 4.5), and 20 mM $CaCl_2$ in a final volume of 4 μl and equilibrated against the reservoir solution. Crystals were transferred into the reservoir solution before flash-frozen under liquid nitrogen. Selenomethionyl protein crystals of Vta1CTD were obtained in a similar way. Native and selenomethinyl crystals diffracted to 1.5 Å and 1.8 Å, respectively. Diffraction data were collected at the Advanced Photon Source beam line

23-ID. All data were integrated and scaled by using the program HKL2000 (HKL Research).

Structure determination and refinement

The structure of Vta1NTD was determined by the SIRAS method using a native data set and a data set collected at the peak wavelength of the selenium atom (λ = 0.9787 Å). Crystals belong to the I4 space group with a unit cell dimension of a = b = 126.17 Å, c = 70.25 Å. There are two molecules in the asymmetric unit. Six of the twelve expected selenium sites were found and cross-confirmed with SnB [26] and CNS [27]. Four additional sites were identified using anomalous difference Fourier method as implemented in SHARP [28]. Parameters for these ten sites were refined and SIRAS phases were calculated and improved by solvent flattening with SHARP. The resulting experimental map is of high quality to allow unambiguous tracing of the model. The model was built manually with O [29] and refined against the native data with CNS using 5% randomly selected reflections for cross-validation. Initial refinement was carried out with torsion angle dynamics simulated annealing using the maximum likelihood target function with the experimental phases as a prior phase distribution (MLHL) followed by rebuilding in O. At later stages of the refinement, maximum likelihood target function using amplitudes (MLF) was used and individual restrained atom B-factor was refined. Although no non-crystallographic symmetry (NCS) restraint was utilized during the refinement process, the two protomers in the asymmetric unit appear to be almost identical, with a root mean square deviation of 0.551 Å for the Cα atoms. The final

model contains residues 1-64 and 76-152 and an N-terminal alanine derived from the vector for each protomer and 11 water molecules.

The structure of Vta1CTD was determined by the MAD method using three data sets collected at the peak, the edge and a remote wavelength of the selenium atom. Crystals belong to the $P2_12_12$ space group with a unit cell dimension of a = 102.42 Å, b = 50.71 Å, c = 74.35 Å. There are six molecules in the asymmetric unit. Heavy atom search, phase calculation and refinement, and density modification were carried out with autoSHARP [28]. An initial model was automatically built using ARP/WARP [30]. The model was further refined against the native data set using CNS with intersperse manual rebuilding with O. Later rounds of refinement were performed with REFMAC5 in the CCP4 [31] suite with TLS parameters incorporated [32]. Each Vta1CTD dimer in the asymmetric unit was defined as one TLS group. The regions for 281-289 in protomer C and 280-289 in protomer F were modeled with alternative conformations with 50% occupancy for each conformation. The final structure contains residues 280-330 for chain A, 281-330 for chain B, 280-330 for chain C, 289-330 for chain D, 286-329 for chain E, and 280-330 for chain F and a total of 295 water molecules. Three protomers (A, C, and F) contain extra residues derived from the vector: Gly-Ser for A and C, and a single serine for F.

In vitro binding experiments

GST pull-down experiments were performed following standard procedures in PBS buffer supplemented with 1mM DTT and 0.1% Triton X-100. Purified proteins were incubated with either GST alone or GST-tagged proteins immobilized on glutathione

agarose beads for 40min at 4°C. The beads were then washed extensively with above buffer, and bound proteins were separated on SDS-PAGE and visualized by Coomassie staining.

The heterodimer of Vta1 were expressed using pETDuet-1 vector (Novagen) with the wild-type protein cloned in the first cassette and either wild-type or mutant proteins cloned in the second cassette. To purify the heterodimer, cells were lysed in 50mM Tris•HCl (pH 8.0), 300 mM NaCl, 15 mM imidazole, 5 mM β- mercaptoethanol, 0.1% Triton X-100 and 10 μg/ml PMSF. Cell lysate was centrifuged and the supernatant was applied to Ni^{++}-NTA resin. After extensive wash, bound proteins were eluted with the above buffer containing 500 mM imidazole. The eluted protein sample was subsequently diluted into the GST pull-down buffer (see above) and incubated with S-protein agarose (Novagen) for 1 hr at 4°C. Beads with heterodimer protein bound were harvested by centrifugation, washed extensively, and either analyzed by SDS PAGE or used for pull-down experiments as described above. Due to the similar migration positions of S-tagged Vta1 and Vps4 on SDS-PAGE, bound Vps4 proteins were detected by Western blotting with anti-Vps4 antibody (Santa Cruz, sc-21821).

Analytical ultracentrifugation

Protein samples were prepared in 25 mM Tris (pH 7.5), 100 mM NaCl, 1 mM EDTA, and 2 mM DTT. Three protein concentrations at OD_{280} of 0.7, 0.5, and 0.3 were used for each sample. All sedimentation equilibrium experiments were carried out at 4°C by using An-50 Ti rotor in a Beckman ProteomeLab XL-1 analytical ultracentrifuge (Beckman Instruments, Fullerton, CA). Data were collected at three different speeds

(32,000, 36,000, and 39,600 rpm) and represented an average of 50 scans using a scan step size of 0.001 cm. Data were analyzed using the UltraScan II program from B. Demeler (University of Texas Health Science Center, San Antonio, TX) and were converted to a plot of *Ln(absorbance)* versus *radius square*. The slope of the plot is proportional to the molecular weight of the protein. Data is plotted alongside simulations using theoretical values for molecular weight of a dimer and a monomer species, and plotted with an arbitrary Y-axis for direct comparison.

Circular dichroism (CD) spectral analysis

Far-UV CD spectra were measured with a Jasco J-810 CD spectropolarimeter at 25°C using a 1-mm cuvette. The protein of 0.3 mg/ml was in a buffer containing 20 mM KH_2PO_4 (pH 7.5). The samples were centrifuged and degassed before measurement. Spectra represent the average of five runs with buffer blanks subtracted, and the resulting spectra were normalized to molar ellipticities against the known protein concentrations with Jasco Series 810 software.

ATPase assay

The ATPase activity of Vps4 was measured using an assay based on the conversion of phosphoenolpyruvate (PEP) to pyruvate by pyruvate kinase (PK) coupled to the conversion of pyruvate to lactate by lactate dehydrogenase (LDH) [33]. Briefly, 1.25 μM Vps4 and 1.5 μM GST-Vta1 variants were first incubated in 800 μl of reaction buffer (50 mM Tris-acetate, pH7.5, 1 mM $MgCl_2$, 1 mM DTT, 3 mM phosphoenolpyruvate, 17.5 units/ml of pyruvate kinase, 12.3 units/ml lactate

dehydrogenase, 0.21 mM NADH) at room temperature. After 1.5 mM ATP was added to initiate the reaction, absorbance was monitored at 340 nm with 10 seconds interval from 300 seconds using a HP 8453E Spectroscopy system and the kinetic data were analyzed as described. Protein concentrations were measured using Bradford method.

Fluorescence Microscopy

Yeast plasmids containing mutant forms of *vta1* were generated by subcloning the mutated open reading frame out of the bacterial expression vectors into the plasmid pRS416-PnTAP with *BamHI*/*Sal*I [15]. This resulted in TAP-tagged forms of Vta1 with the desired mutation that were subsequently subcloned into pRS415 as a *Sac*1/*Xho*1 fragment. Complementation analyses were performed by transformation of the pRS415 constructs together with GFP-tagged CPS into *vta1*Δ cells (BY4742 genetic background, Open Biosystems). Fluorescence microscopy was performed on live cells using a Nikon microscope fitted with an eGFP filter set and digital camera (Coolsnap HQ, Photometrix), and images were processed using Delta Vision deconvolution software (Applied Precision Inc.).

Protein Data Bank accession number

Atomic coordinates and structure factors for yeast Vta1NTD and Vta1CTD have been deposited in the RCSB Protein Data Bank with accession code 2RKK and 2RKL, respectively.

REFERENCES

1. Katzmann, D.J., G. Odorizzi, and S.D. Emr, *Receptor downregulation and multivesicular-body sorting.* Nat Rev Mol Cell Biol, 2002. **3**(12): p. 893-905.

2. Gruenberg, J. and H. Stenmark, *The biogenesis of multivesicular endosomes.* Nat Rev Mol Cell Biol, 2004. **5**(4): p. 317-23.

3. Babst, M., *A protein's final ESCRT.* Traffic, 2005. **6**(1): p. 2-9.

4. Piper, R.C. and D.J. Katzmann, *Biogenesis and function of multivesicular bodies.* Annu Rev Cell Dev Biol, 2007. **23**: p. 519-47.

5. Morita, E. and W.I. Sundquist, *Retrovirus budding.* Annu Rev Cell Dev Biol, 2004. **20**: p. 395-425.

6. Carlton, J.G. and J. Martin-Serrano, *Parallels between cytokinesis and retroviral budding: a role for the ESCRT machinery.* Science, 2007. **316**(5833): p. 1908-12.

7. Morita, E., et al., *Human ESCRT and ALIX proteins interact with proteins of the midbody and function in cytokinesis.* EMBO J, 2007. **26**(19): p. 4215-27.

8. Williams, R.L. and S. Urbe, *The emerging shape of the ESCRT machinery.* Nat Rev Mol Cell Biol, 2007. **8**(5): p. 355-68.

9. Hurley, J.H. and S.D. Emr, *The ESCRT Complexes: Structure and Mechanism of a Membrane-Trafficking Network.* Annu Rev Biophys Biomol Struct, 2006.

10. Babst, M., et al., *Endosomal transport function in yeast requires a novel AAA-type ATPase, Vps4p.* Embo J, 1997. **16**(8): p. 1820-31.

11. Vale, R.D., *AAA proteins. Lords of the ring.* J Cell Biol, 2000. **150**(1): p. F13-9.

12. Frickey, T. and A.N. Lupas, *Phylogenetic analysis of AAA proteins.* J Struct Biol, 2004. **146**(1-2): p. 2-10.

13. Babst, M., et al., *The Vps4p AAA ATPase regulates membrane association of a Vps protein complex required for normal endosome function.* Embo J, 1998. **17**(11): p. 2982-93.

14. Xiao, J., et al., *Structural characterization of the ATPase reaction cycle of endosomal AAA protein Vps4.* J Mol Biol, 2007. **374**(3): p. 655-70.

15. Azmi, I., et al., *Recycling of ESCRTs by the AAA-ATPase Vps4 is regulated by a conserved VSL region in Vta1.* J Cell Biol, 2006. **172**(5): p. 705-17.

16. Lottridge, J.M., et al., *Vta1p and Vps46p regulate the membrane association and ATPase activity of Vps4p at the yeast multivesicular body.* Proc Natl Acad Sci U S A, 2006. **103**(16): p. 6202-7.

17. Fujita, H., et al., *Mammalian class E Vps proteins, SBP1 and mVps2/CHMP2A, interact with and regulate the function of an AAA-ATPase SKD1/Vps4B.* J Cell Sci, 2004. **117**(Pt 14): p. 2997-3009.

18. Yeo, S.C., et al., *Vps20p and Vta1p interact with Vps4p and function in multivesicular body sorting and endosomal transport in Saccharomyces cerevisiae.* J Cell Sci, 2003. **116**(Pt 19): p. 3957-70.

19. Haas, T.J., et al., *The Arabidopsis AAA ATPase SKD1 is involved in multivesicular endosome function and interacts with its positive regulator LYST-INTERACTING PROTEIN5.* Plant Cell, 2007. **19**(4): p. 1295-312.

20. Shiflett, S.L., et al., *Characterization of Vta1p, a class E Vps protein in Saccharomyces cerevisiae.* J Biol Chem, 2004. **279**(12): p. 10982-90.

21. Ward, D.M., et al., *The role of LIP5 and CHMP5 in multivesicular body formation and HIV-1 budding in mammalian cells.* J Biol Chem, 2005.

22. Scott, A., et al., *Structure and ESCRT-III protein interactions of the MIT domain of human VPS4A.* Proc Natl Acad Sci U S A, 2005. **102**(39): p. 13813-12818.

23. Takasu, H., et al., *Structural characterization of the MIT domain from human Vps4b.* Biochem Biophys Res Commun, 2005. **334**(2): p. 460-5.

24. Azmi, I.F., et al., *ESCRT-III family members stimulate Vps4 ATPase activity directly or via Vta1.* Dev Cell, 2008. **14**(1): p. 50-61.

25. Scott, A., et al., *Structural and mechanistic studies of VPS4 proteins.* Embo J, 2005. **24**(20): p. 3658-69.

26. Weeks, C.M. and R. Miller, *The design and implementation of SnB v2.0.* J Appl Cryst, 1999. **32**: p. 120-124.

27. Brunger, A.T., et al., *Crystallography & NMR system: A new software suite for macromolecular structure determination.* Acta Crystallogr D Biol Crystallogr, 1998. **54**(Pt 5): p. 905-21.

28. Vonrhein, C., et al., *Automated Structure Solution With autoSHARP.* Methods Mol Biol, 2006. **364**: p. 215-30.

29. Jones, T.A., et al., *Improved methods for building protein models in electron density maps and the location of errors in these models.* Acta Crystallogr A, 1991. **47 (Pt 2)**: p. 110-9.

30. Morris, R.J., A. Perrakis, and V.S. Lamzin, *ARP/wARP and automatic interpretation of protein electron density maps.* Methods Enzymol, 2003. **374**: p. 229-44.

31. CCP4, *(Collaborative Computational Project, Number 4) The CCP4 suite: programs for protein crystallography.* Acta Crystallogr D Biol Crystallogr, 1994. **50**(Pt 5): p. 760-3.

32. Winn, M.D., G.N. Murshudov, and M.Z. Papiz, *Macromolecular TLS refinement in REFMAC at moderate resolutions.* Methods Enzymol, 2003. **374**: p. 300-21.

33. Huang, T.G. and D.D. Hackney, *Drosophila kinesin minimal motor domain expressed in Escherichia coli. Purification and kinetic characterization.* J Biol Chem, 1994. **269**(23): p. 16493-501.

CHAPTER 4

STRUCTURAL BASIS OF IST1 FUNCTION AND IST1-DID2 INTERACTION IN THE ESCRT PATHWAY

ABSTRACT

The ESCRT machinery functions in several important eukaryotic cellular processes including formation of the internal vesicles at the multivesicular body (MVB), cytokinesis, and virus budding. AAA-ATPase Vps4 catalyzes disassembly of the ESCRT-III complex, and may regulate membrane deformation and vesicle scission as well. Ist1 was postulated to be a regulator of Vps4 but its mechanism of action remains elusive. The crystal structure of the N-terminal domain (NTD) of Ist1 reveals an ESCRT-III protein like fold. Ist1NTD also specifically interacts with Did2, and the structure of Ist1NTD in complex with a Did2 fragment shows that Ist1 interacts with the C-terminal amphipathic MIM (MIT-interacting motif) helix of Did2. The interaction site on Ist1 represents a novel non-MIT MIM-binding domain and is located in a highly conserved surface groove of Ist1. Point mutations in this region effectively abolish the interaction between Ist1 and Did2, and we have further demonstrated that Ist1-Did2 interaction is important for both yeast vacuolar sorting and mammalian cytokinesis.

INTRODUCTION

The ESCRT (Endosomal Sorting Complexes Required for Transport) machinery is an evolutionarily conserved membrane scission machine, directing membrane budding away from the cytosol. Its function has been implicated in a number of physiological and pathological processes in the eukaryotic cells, including formation of internal vesicles at the endosome, budding of enveloped viruses such as HIV (human immunodeficiency virus), and separation of the two daughter cells during cell division [1, 2]. The ESCRT machinery was initially discovered in genetic studies of the vacuolar protein sorting process in *S. cerevisiae*, where it is required for budding of intralumenal vesicles from the limiting membrane of the endosome to form the MVB (multivesicular body) structure [3]. In mammals, the MVB pathway is responsible for down-regulation of cell-surface signaling by directing activated growth hormone receptors into the lysosome where proteolytic degradation can occur [4].

Major components of the ESCRT machinery include the three ESCRT complexes (ESCRT-I, -II, and –III), the Vps27-Hse1 complex, the AAA ATPase Vps4 and associated regulators of these proteins [5, 6]. Vps27-Hse1, ESCRT-I, and ESCRT-II are involved in cargo sorting and concentration to sites of vesicle budding in the early stage; and ESCRT-III and Vps4 are responsible for membrane curvature generation and vesicle budding in the late stage. While the exact molecular mechanism by which vesiculation occurs is far from clear, it is generally believed that the ESCRT-III proteins form lattice-like oligomers on the endosomal membrane, which promotes a change in the membrane structure [7, 8]. Vps4 interacts with the ESCRT-III proteins in an ATP-dependent manner and catalyzes remodeling of the ESCRT-III lattice using the energy derived from ATP

hydrolysis [9, 10]. The action of Vps4 is required to complete the vesicle budding process and recycle the system so that protein trafficking through the MVB pathway can be sustained. Given that Vps4 catalyzes the only energy-consuming reaction in the MVB pathway, it is not surprising that the activity of Vps4 is closely regulated in the cells by a number of proteins, including Vps2, Did2, Vps60, Vta1 and Ist1 [11-14].

Vps2, Did2, Vps60 and Vta1 have all been recognized as positive regulators of Vps4. Vps2 and Did2 are ESCRT-III proteins that exert their regulatory functions through binding directly to the N-terminal MIT (microtubule interacting and transport) domain of Vps4 via a C-terminal conserved sequence motif called MIM1 (MIT interacting motif 1) [15, 16]. Vps60 also belongs to the ESCRT-III protein family but only binds indirectly to Vps4 through Vta1. Vta1 stimulates the ATPase activity of Vps4 when its C-terminal dimerization domain binds to the neighboring β-domains from the two rings of Vps4 [13]. The binding stabilizes the catalytic competent double-ring structure of Vps4. Vps60 binds to one of the two tandem MIT domains within the N-terminal domain of Vta1 and further activates Vps4 in a Vta1-dependent manner [12].

Ist1 was originally identified as an evolutionarily conserved protein that interacts with both Vps4 and Did2 [14, 17]. Binding of Ist1 to Vps4 interferes with the ATP-dependent oligomerization of Vps4 and therefore inhibits the ATPase activity [14]. Furthermore, overexpression of Ist1 in the yeast leads to a class E MVB sorting defect similar to that observed in cells depleted of Vps4, suggesting that Ist1 acts as a negative regulator of the MVB pathway [14]. Ist1 contains a C-terminal MIM1, through which it binds to Vps4. However, binding of an isolated Ist1-MIM1 peptide to Vps4 leads to stimulation rather than inhibition of the ATPase activity, suggesting that the rest of the

Ist1 structure confers inhibition [14]. Deletion of Ist1 by itself has no obvious phenotype in the yeast, but simultaneous deletion of Ist1 with either Vta1 or Vps60 gives rise to a strong class E phenotype not seen in cells devoid of either Vta1 or Vps60 [14, 17]. Interestingly, deletion of Did2 is also synthetic with Vta1 and Vps60, but not with Ist1. These results suggest that the *in vivo* function of Ist1 extends beyond its inhibitory activity towards Vps4; and that it may function together with Did2 and parallel to Vta1/Vps60 in the MVB pathway.

To provide insights into the mechanism of Its1 function, we sought to characterize the molecular structure of Ist1. Domain analysis suggests Ist1 contains an N-terminal globular domain (Ist1NTD), which it uses to bind to Did2. A linker region of variable size with little predicted secondary structure connects Ist1NTD to the C-terminal MIM1. We have further determined the crystal structure of Ist1NTD to 1.7 Å resolution. The structure reveals Ist1NTD contains a fold that is remarkably similar to that of the ESCRT-III protein CHMP3 (mammalian homolog of Vps24) despite very low level of sequence identity. Ist1NTD also specifically interacts with the MIM1 sequence within Did2 via a novel MIM1 binding site. Disruption of Ist1-Did2 interaction through mutagenesis leads to both a synthetic class E phenotype with either Vps60 or Vta1 in yeast vacuolar sorting pathway as well as a defect in abscission during mammalian cell division. These results suggest that Ist1-Did2 interaction plays an important role to the overall function of the ESCRT machinery during the late stage of membrane vesiculation.

RESULTS

The N-terminal domain of Ist1 specifically interacts with the MIM1 sequence of Did2

S. cerevisiae Ist1 has been previously shown to bind to Did2. The C-terminal region of Did2 is important for mediating this interaction [14, 17]. Indeed, GST-tagged Did2$^{176-204}$, but not GST-tagged Did2$^{104-175}$, strongly interacts with the full-length Ist1 (Figure 4.1A, 4.4C). Interestingly, deletion of the N-terminal region of Did2 significantly strengthens the interaction between the two proteins (Figure 4.1A). This is consistent with the notion that Did2 adopts an auto-inhibitory conformation at its resting state where its C-terminal region is masked [18, 19]. The increased affinity between Did2$^{176-204}$ and Ist1 also enabled us to isolate a Did2$^{176-204}$/Ist1 complex by chromatography, which was not possible when using the full-length Did2 (see Methods). Deletion of an additional 14 residues from the N-terminal end of Did2$^{176-204}$ had little effect on its affinity for Ist1 (Figure 4.1B). Therefore, the minimal Ist1-interacting sequence of Did2 appears to be Did2$^{190-204}$. This stretch of sequence has been previously characterized as a MIM1 motif due to its ability to interact with the MIT domain of Vps4 and is known to adopt a helical conformation [16].

To identify the Did2-binding site on Ist1, we subjected purified Ist1 to limited proteolysis by subtilisin. Digestion of Ist1 generated two stable fragments (Figure 4.1C) with molecular weights of 22,576 Da and 8,741 Da, respectively, as determined by mass spectrometry. We deduced that the larger fragment corresponds to the N-terminal amino acids 1-193 (Ist1NTD) and the smaller fragment corresponds to the C-terminal amino acids 226-298 (Ist1CTD). Ist1NTD, when expressed by itself, is not stable and precipitates rapidly in solution. However, when Ist1NTD and Did2$^{190-204}$ (or Did2$^{176-204}$)

Figure 4.1 The N-terminal Domain of Ist1 specifically interacts with the MIM1 motif of Did2.
(A) The C-terminal MIM1 motif of Did2 binds to Ist1. GST, GST-Did2FL, or GST-Did2$^{176-204}$ was used to pull down N-terminal His-tagged Ist1 as indicated. Proteins retained on the beads were analyzed by SDS-PAGE and visualized by anti-His immuno-blotting and Ponceau S staining.
(B) Ist1NTD specifically interacts with Did2-MIM1. His-SUMO-tagged MIM1 fragments from Did2, Vps2, Vps24, or Ist1 was co-expressed with Ist1NTD in *E. coli*. Proteins retained on the Ni^{++}-NTA beads were analyzed by SDS-PAGE and visualized by Coomassie staining.
(C) Ist1 contains two stable domains. Purified full-length Ist1 was incubated with increasing amounts of subtilisin as indicated. Digestion products were analyzed by SDS-PAGE and visualized by Coomassie staining.

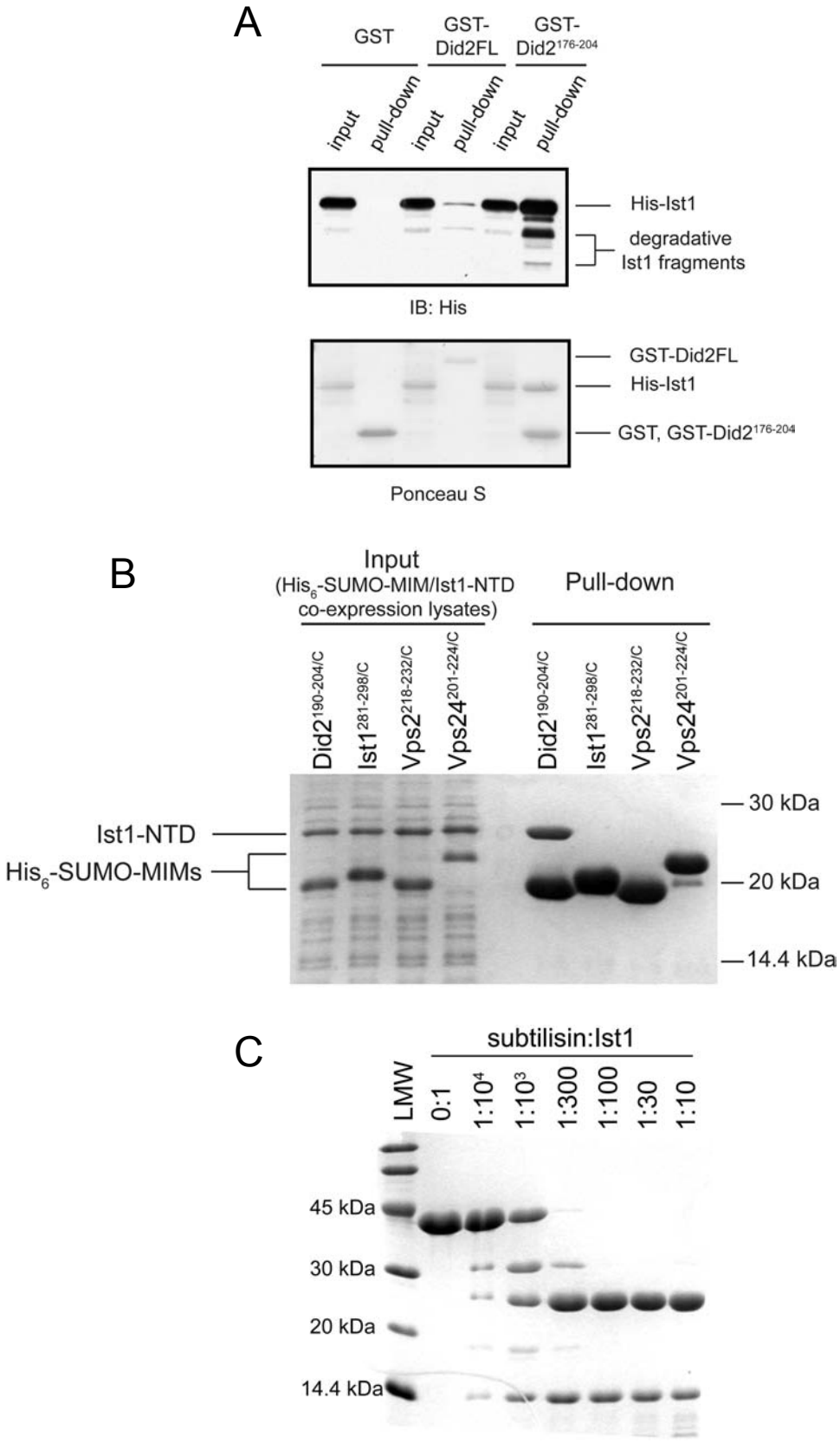
A
GST
GST-Did2FL
GST-Did2176-204
input
pull-down
input
pull-down
input
pull-down
His-Ist1
degradative Ist1 fragments
IB: His
GST-Did2FL
His-Ist1
GST, GST-Did2176-204
Ponceau S
B
Input
(His6-SUMO-MIM/Ist1-NTD co-expression lysates)
Pull-down
Did2190-204/C
Ist1281-298/C
Vps2218-232/C
Vps24201-224/C
Did2190-204/C
Ist1281-298/C
Vps2218-232/C
Vps24201-224/C
Ist1-NTD
His6-SUMO-MIMs
30 kDa
20 kDa
14.4 kDa
C
subtilisin:Ist1
LMW
0:1
1:10^4
1:10^3
1:300
1:100
1:30
1:10
45 kDa
30 kDa
20 kDa
14.4 kDa

are co-expressed in *E. coli*, they can be co-purified as a stable complex suggesting that Ist1NTD contains the Did2-binding site (See Methods and Figure 4.1B). Ist1CTD, on the other hand, does not bind to Did2.

Several other proteins, including Vps2, Vps24 and Ist1 itself, also contain homologous MIM1 sequences that can interact with the MIT domain of Vps4. To test whether these sequences can interact with Ist1, we co-expressed His-SUMO-tagged MIM1 fragments from Vps2, Vps24, and Ist1 with Ist1NTD. We used Ni^{++}-NTA affinity chromatography to examine complex formation between these respective protein pairs. Surprisingly, formation of protein complexes can only be observed between Ist1NTD and Did2-MIM1 under the assay condition (Figure 4.1B), suggesting that the interaction between Ist1NTD and Did2 is highly specific.

The crystal structure of Ist1NTD

In order to understand the structural basis of Ist1 function, we have attempted to determine the crystal structure of Ist1. Given the perceived structural flexibility within the full-length protein and the aggregation problem of Ist1NTD experienced during protein preparation, we focused our structural study on the Ist1NTD/Did2-MIM1 complex. Two crystal forms can be obtained from the purified complex. One was grown in the presence of high concentration of sodium citrate and diffracted to 3.8 Å resolution. It belongs to the space group of $P4_22$ and contains both protein fragments. The other was grown under polyethylene glycol conditions and diffracted to 1.7 Å resolution. It belongs to the space group of C2 but contains only Ist1NTD. Since the C2 crystal form diffracts significantly better than the $P4_22$ form, we first determined the structure of

Ist1NTD with a combination of multiwavelength anomalous dispersion (MAD) and single isomorphous replacement (SIR) from a native crystal, a selenomethionyl crystal, and a mercury acetate derivative crystal (Table 4.1).

Ist1NTD has an all-α fold and contains nine α-helices (α1-α9) (Figure 4.2A). Helices α1 and α2 fold into a 60 Å long helical hairpin that constitutes the core of the structure. Helix α2 takes a sharp turn at residues Arg83 and Val84, and is connected to helix α4 via a short, non-conserved helix α3 (Figure 4.2A, 4.2B). Helices α4, α5, and α6 form a three-helix bundle, which packs against the bottom half of the α1/α2 hairpin to form the core of the structure. A short helix α7 and a flexible linker extending from the core subsequently direct the rest of the sequence to the other side of the molecule, which folds into two helices α8 and α9 and packs onto the top half of the α1/α2 hairpin. There are two Ist1NTD molecules in the asymmetric unit, related by a non-crystallographic 2-fold symmetry. They are nearly superimposable with an rmsd (root mean square deviation) of 0.5 Å for the Cα atoms. The only major difference between the two molecules is located at the linker between helix α7 and α8 (residues 160-163), suggesting that this region is highly dynamic.

Ist1NTD shows remarkable structural similarity to the ESCRT-III protein CHMP3 (PDB ID: 2GD5 [20]) (Figure 4.2C). Pairwise comparison of the two structures by DaliLite [21] gives an rmsd of 2.6 Å for 103 aligned Cα atoms at 10% sequence identity. In particular, the α1/α2 helical hairpins from the two structures can be superimposed very well (Figure 4.2C). Moreover, helices α4 and α5 in Ist1NTD are structurally similar to helices α3 and α4 in CHMP3, and pack against the α1/α2 hairpin in a similar manner. Since all known ESCRT-III proteins are believed to have a similar

Table 4.1 Crystallographic Data and Refinement Statistics

	Ist1 alone					Complex
	Native	Se-peak	Se-inflection	Se-remote	Hg derivative	Native
Wavelength (Å)	0.9793	0.9793	0.9795	0.9643	1.5418	0.9793
Space group	C2	C2			C2	$P4_222$
Unit Cell	a = 144.84 Å	a = 145.63 Å			a = 145.26 Å	a = b = 165.93 Å
	b = 44.17 Å	b = 44.31 Å			b = 44.33 Å	c = 121.56 Å
	c = 66.95 Å	c = 138.34 Å			c = 136.93 Å	
	β = 110.49°	β = 112.75°			β = 112.47°	
Resolution (Å)	1.70	2.85	2.80	2.60	2.90	3.8
(last shell)	(1.73-1.70)	(2.90-2.85)	(2.85-2.80)	(2.64-2.60)	(2.95-2.90)	(3.87-3.8)
Completeness (%)	98.9	96.9	96.5	97.5	99.1	99.6
(last shell)	(95.1)	(98.9)	(87.6)	(98.9)	(99.9)	(100.0)
I/σ	34.3	26.5	26.4	30.8	10.3	16.6
(last shell)	(5.9)	(7.5)	(5.8)	(8.3)	(3.0)	(2.7)
Rmerge (%)	4.3	6.1	5.8	6.1	13.7	9.1
(last shell)	(20.4)	(17.7)	(20.7)	(23.2)	(42.5)	(65.8)
Redundancy	3.7	6.3	6.3	6.3	3.3	6.0
Unique reflections	43548	19282	19951	24749	18245	17219
Refinement statistics						
R_{work}/ R_{free} (%)	22.6/24.9					29.8/30.7
Rmsd, bonds (Å)	0.004					0.011
Rmsd, angles (°)	0.971					1.652
Mean B ($Å^2$)	23.8					147.4
Ramachandran						
core	92.9%					83.3%
allowed	7.1%					15.3%
generously allowed	0.0%					1.4%
disallowed	0.0%					0.0%
Molecules/ASU	2					4 complexes

A

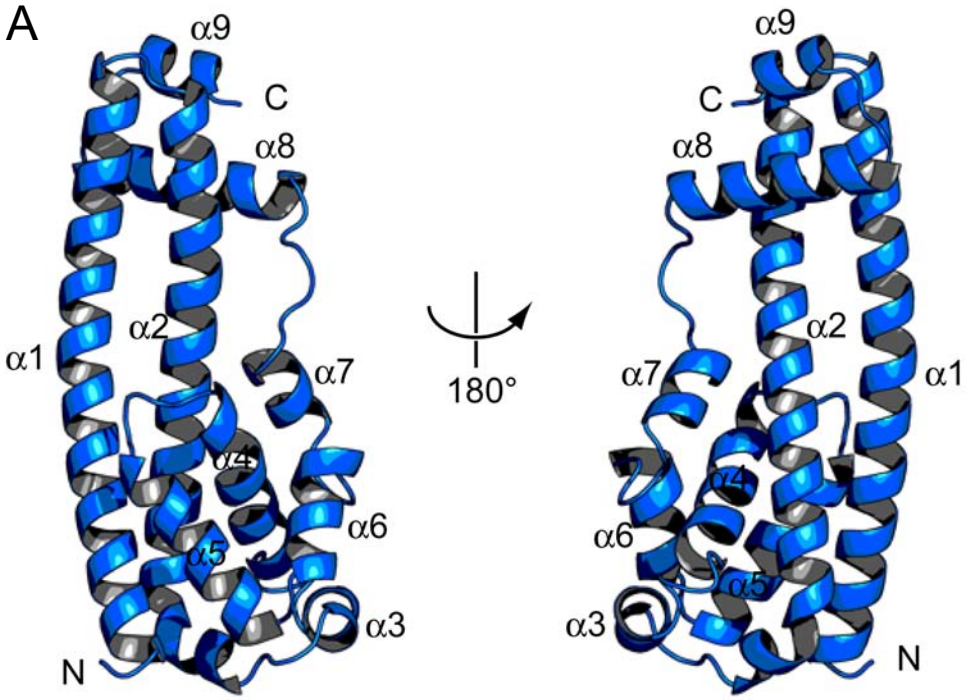

B

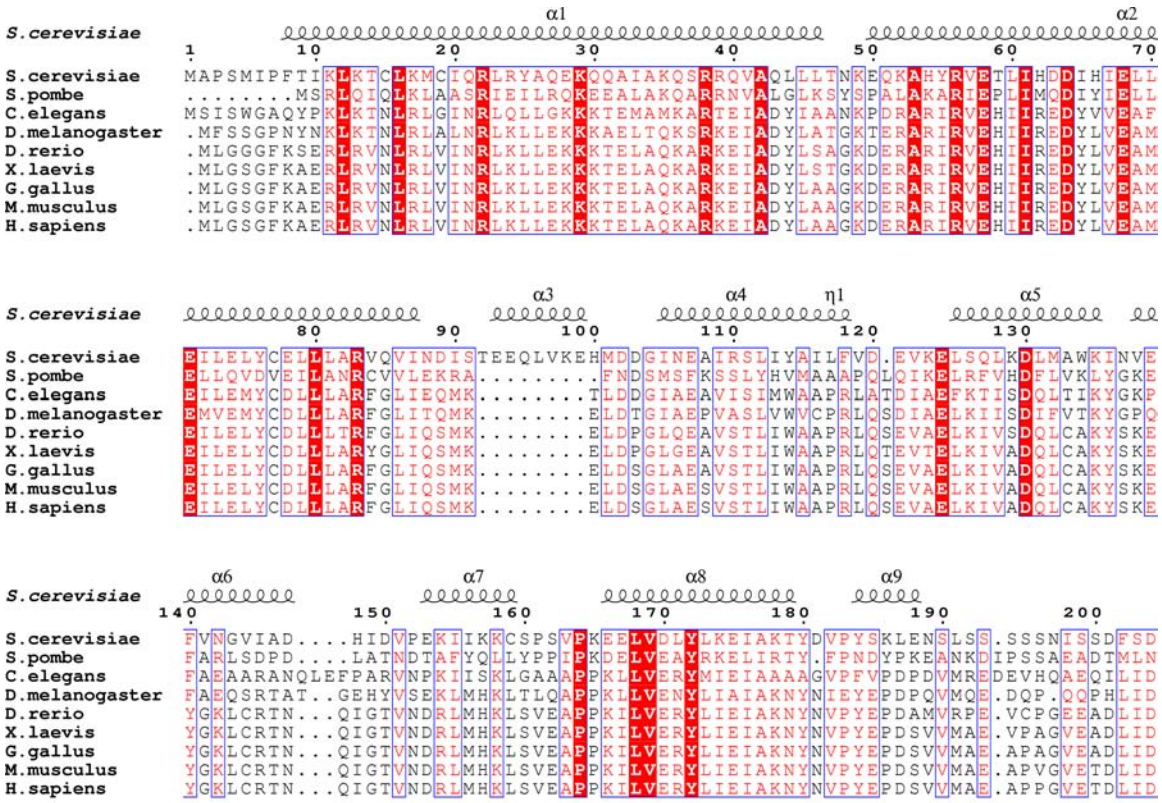

(Continued on next page)

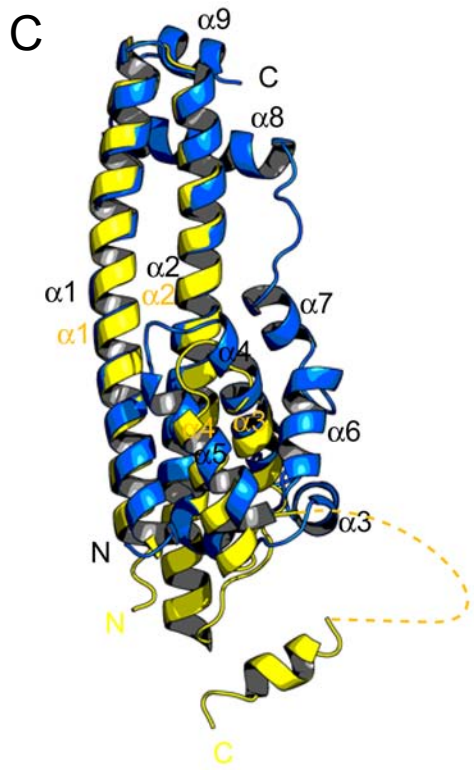

Figure 4.2 The crystal structure of Ist1NTD.
(A) Ribbon representation of Ist1NTD structure shown in two orientations. Secondary structural elements (α-helices α1-α9) and the N- and C-termini of the structure are labeled.
(B) Structure based sequence alignments of Ist1NTD. Secondary structural elements of *S. cerevisiae* Ist1NTD are also shown.
(C) Ist1NTD has an ESCRT-III like fold. Structural overlay of Ist1NTD with the ESCRT-III protein CHMP3 (PDB ID: 2GD5). Ist1NTD is colored blue and CHMP3 colored yellow. The disordered linker region between helix α4 and α5 in CHMP3 is represented as a dash line.

structure, the fold represented by helices α1-α4 in CHMP3 is likely shared by all ESCRT-III proteins therefore can be generally referred to as the ESCRT-III fold. Our observation that Ist1NTD contains an ESCRT-III fold indicates that this fold is not limited to the ESCRT-III proteins.

The ESCRT-III proteins are bi-polar molecules with a positively charged N-terminal half and a negatively charged C-terminal half [22]. During the course of MVB formation, they may form membrane-bound high-order oligomers either in the shape of helical filaments or tubular structures as revealed by recent electron microscopy (EM) studies [7, 8, 23]. Arrangement of CHMP3 in its crystal lattice displays a contiguous basic surface, formed by the N-terminal half of the molecule [20]. It is believed that this represents the membrane-binding surface for the CHMP3 polymers in the cell. In contrast, Ist1 does not exhibit a significant bi-polar sequence feature and its surface does not display any prominent positively charged patches. Full-length Ist1 is a monomer in solution, as determined by sedimentation equilibrium analytical ultracentrifugation (data not shown). Currently, there is no evidence that Ist1 forms a similar high-order oligomeric structure as the ESCRT-III proteins in *vivo*. Examination of lattice contacts in both the Ist1NTD crystal and the Ist1NTD/Did2-MIM complex crystal (Figure 4.3) shows that Ist1NTD can self-interact in a variety of ways to form oligomers/polymers, albeit different from that observed in the CHMP3 crystal lattice. Whether these oligomer or polymer assemblies represent any physiologically relevant functional state of Ist1 is uncertain.

The crystal structure of Ist1NTD in complex with Did2-MIM1

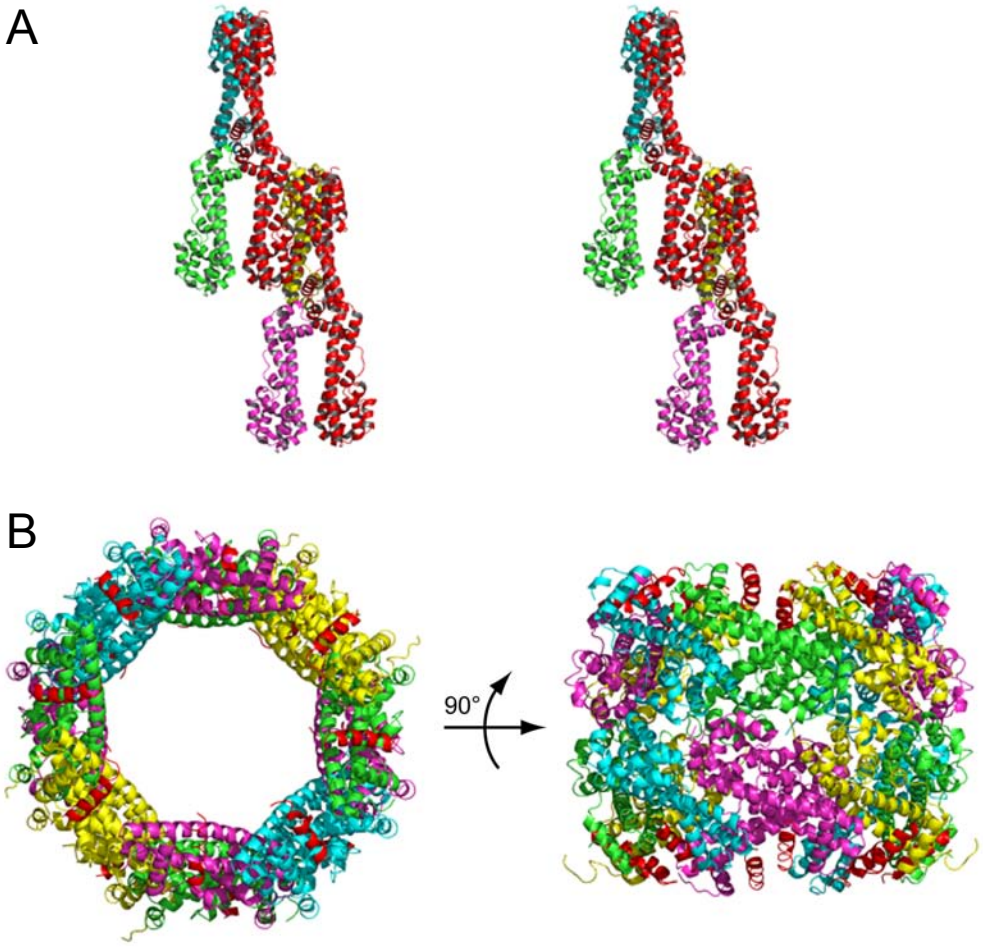

Figure 4.3 Crystal packing in Ist1NTD and Ist1NTD/Did2-MIM1 complex structures reveal Ist1NTD can potentially form polymers/oligomers.
(A) Stereo view of the polymer formed by Ist1NTD in the Ist1NTD crystal lattice. Of the two Ist1NTD molecules in the asymmetric unit, one is colored in red and the other colored in cyan, green, yellow, and magenta, respectively. Contents from four neighboring asymmetric units are shown.
(B) The Ist1NTD/Did2-MIM1 complex forms a 16-membered ring-like oligomer in the crystal lattice. The Did2-MIM1 helix is colored in red, and the four Ist1NTD molecules in the asymmetric unit are colored in cyan, green, yellow, and magenta, respectively. Sixteen Ist1NTD/Did2-MIM1 complexes from four neighboring asymmetric units form the double-stacked oligomer. Two orientations of the oligomer are shown.

The crystal structure of the Ist1NTD/Did2-MIM1(Did2$^{190-204}$) complex was determined at 3.8 Å resolution by molecular replacement using the refined Ist1NTD structure as an initial search model. A total of four Ist1NTD molecules were found in the asymmetric unit. It was immediately obvious that each Ist1NTD is bound with a Did2-MIM1 based on the electron density feature in the Fo-Fc map (Figure 4.4A). Did2-MIM1 binds to a highly conserved surface groove on Ist1NTD, formed by helix α8 and the surface of α1/α2 helical hairpin (Figure 4.4B). In particular, side chains of Arg38, Glu68, Leu168, Tyr172, and Glu175 of Ist1NTD are all pointing towards the Did2-MIM1 electron density; and therefore are likely involved in binding to the Did2-MIM1 peptide.

To examine the functional importance of these residues in contributing to Did2 binding, we introduced a series of point mutations into the full-length Ist1 and examined their effects on Ist1-Did2 interaction. Mutating Arg38 to alanine (R38A), or Glu68 to either alanine (E68A) or arginine (E68R) had no obvious effect on binding to Did2 (Figure 4.4C and data not shown); neither does mutating Leu168 or Tyr172 individually to alanine (data not shown). However, mutating Glu175 to arginine (E175R), or mutating Leu168 and Tyr172 simultaneously to alanines (L168AY172A) completely abolished the interaction between Ist1 and Did2 (Figure 4.4C), suggesting that these three conserved residues are involved in direct binding to Did2.

The resolution limit of the electron-density map made it difficult for us to register the sequence of Did2-MIM1 into the density with great confidence. However, results from the above mutagenesis and biochemical analysis put significant constraints on the potential mode of interaction between Ist1 and Did2. Given the functional importance of Glu175, it is likely that a positively charged residue of Did2-MIM1 is in close proximity

Figure 4.4 Ist1NTD interacts with Did2-MIM1 using a novel binding mechanism.
(A) Fo-Fc difference map (at 3σ) showing the location of Did2-MIM1 helix in the Ist1NTD/Did2-MIM1 structure.
(B) Did2-MIM1 binds in a highly conserved surface groove of Ist1NTD. The molecular surface of Ist1NTD is colored based on conservation scores. The most conserved residues are colored in magenta, and the least conserved colored in cyan. Residues R38, E68, L168, Y172, and E175 from Ist1NTD are potentially involved in interaction with Did2-MIM1.
(C) Conserved residues in Ist1 are important for Did2 binding. GST-tagged Did2 fragments were used to pull-down wild type or mutant Ist1 as indicated. Proteins retained on the beads were analyzed by SDS-PAGE and visualized by Coomassie staining.
(D) Ist1NTD/Did2-MIM1 complex structure. Ist1NTD is colored in blue and Did2-MIM1 colored in red. The MIM1 helix in (E) and (F) are shown in the same orientation.
(E) Vps4-MIT/CHMP1A-MIM1 complex structure (PDB ID: 2JQ9). The MIT domain of Vps4 is colored in green and CHMP1-MIM1 colored in red.
(F) Spastin-MIT/CHMP1B-MIM1 complex structure (PDB ID: 3EAB). The MIT domain of spastin is colored in cyan and CHMP1B-MIM1 colored in red.

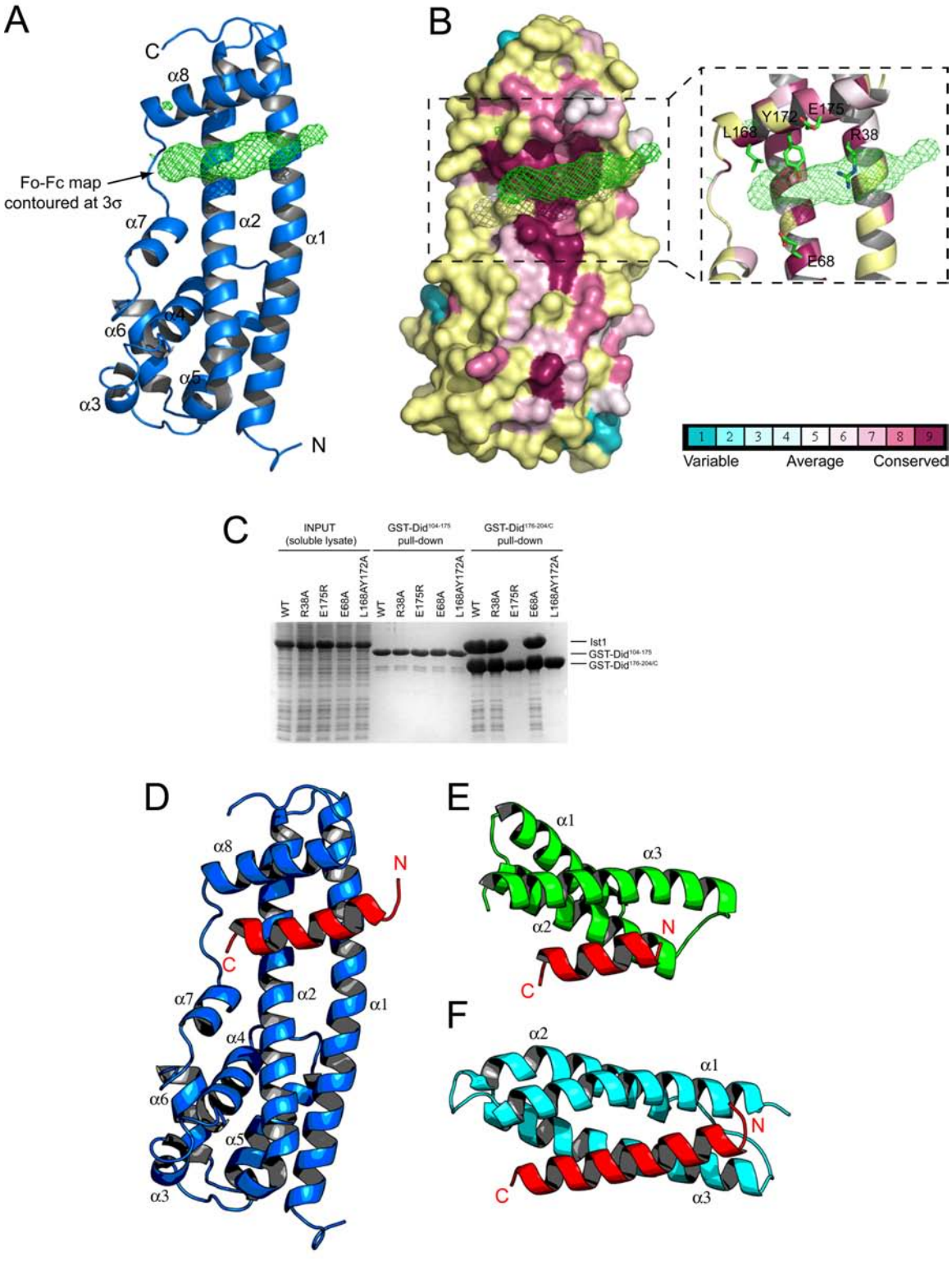
A
C
α8
Fo-Fc map
contoured at 3σ
α7
α2
α1
α4
α6
α5
α3
N
B
Y172
E175
L168
R38
E68
1
2
3
4
5
6
7
8
9
Variable
Average
Conserved
C
INPUT
(soluble lysate)
GST-Did104-175
pull-down
GST-Did176-204/C
pull-down
WT
R38A
E175R
E68A
L168AY172A
Ist1
GST-Did104-175
GST-Did176-204/C
D
α8
N
C
α7
α2
α1
α4
α6
α5
α3
E
α1
α3
α2
N
C
F
α2
α1
N
C
α3

to form a salt bridge interaction with Ist1. Moreover, this positively charged residue must be located in the mid-section of the electron density, as dictated by the position of Glu175 (Figure 4.4B). The MIM1 sequence in human CHMP1A (human Did2 ortholog) has been previously shown to form an amphipathic α-helix [16]. By modeling yeast Did2-MIM1 into a similar helix based on the sequence conservation in this region, we reasoned that the absolutely conserved Arg198 in Did2-MIM1 is most likely close to Glu175 of Ist1. This provides us a marker to fit the entire 15 residues of Did2-MIM1 into the electron density map (Figure 4.4D).

To evaluate our model, we took advantage of the fact that Ist1NTD when in complex with a longer Did2 peptide ($Did2^{176-204}$) produces isomorphous crystals. The difference map calculated with phases derived from the molecular replacement solution had a very similar electron density feature at the Did2 binding site. In particular, the density corresponding to the C-terminus of the MIM1 peptide is well defined. There are, however, extended but discontinuous density feature observed in several positions corresponding to the unstructured N-terminal region that precedes the MIM1 peptide. This indicates that the shorter peptide was modeled in the correct position and orientation. The model is also supported by further crystallographic analysis. The working and free R factors for the complex structure are 29.8% and 30.7% respectively, reasonable at the 3.8 Å resolution (Table 4.1). However, shifting the registration of Did2-MIM1 by +1 results in working and free R factors of 31.1% and 32.1% respectively; while shifting by -1 gives 30.6% and 32.9%, respectively. Moreover, there is little negative or positive difference density at either end of the modeled MIMI1 peptide. These results collectively suggest the validity of our structural model.

Did2-MIM1 displays a novel mode of binding

The structure of the MIM1 region of mammalian Did2 homolog CHMP1 has been previously characterized in complex with the MIT domains of mammalian Vps4 (CHMP1A) and spastin (CHMP1B) respectively (Figure 4.4E, 4.4F) [16, 24]. The MIT domain has a three-helix bundle structure. When in complex with Did2/CHMP1-MIM1, it can use either a groove between α2 and α3 (in Vps4) or a groove between α1 and α3 (in spastin) (Figure 4.4E, 4.4F). Three highly conserved leucine residues (corresponding to Leu195, Leu199 and Leu202 in yeast Did2) as well as a number of nearby charged residues (corresponding to Glu192, Arg198 and Arg203) of MIM1 are involved in interaction with the MIT domains in both cases. The interface in the spastin-MIM1 structure, however, is much more extensive than the one in the Vps4-MIM1 structure. Only the C-terminal three helical turns of the MIM1 helix directly contact Vps4 whereas up to six helical turns contact spastin. In addition, the MIM1 helix is much more buried in the spastin-Did2 structure than in the Vps4-Did2 structure.

The mode of interaction between Did2-MIM1 and Ist1NTD shows distinctive features unseen in the previous two cases. Unlike the MIT domain that binds to MIM1 with two parallel or anti-parallel helices, the MIM1 binding site in Ist1NTD consists of three helices with a shape resembling the letter "L" (Figure 4.4D). One helix (α8) runs anti-parallel to the MIM1 helix forming the floor in the "L" shape whereas the other two (α1 and α2) run perpendicular forming the sidewall. At total of four helical turns are involved in interaction with Ist1NTD leading to a buried interface of ~1,200 $Å^2$. In comparison, spastin-MIM1 and Vps4-MIM1 each bury ~1,900$Å^2$ and ~1,000$Å^2$,

respectively. Conserved residues that are involved in binding to the MIT domains are also seen at the interface. For example, the side chains of conserved Leu199 and Arg203 of Did2 might be involved in Van der Waals interaction with conserved Leu168 and Tyr172 of Ist1, which explains the phenotype of the L168AY172A double mutant. Arg198 of Did2 forms a likely salt bridge with Glu175 of Ist1; therefore mutating Glu175 to the positively charged arginine will strongly interfere with the interaction between the two proteins. These results suggest that the same molecular surface of Did2-MIM1 helix is involved in all three bindings despite differences in the modes of binding.

While high-resolution structural information will be ultimately required to fully elucidate the molecular basis of interaction between Ist1 and Did2, our structure model will nevertheless be valuable for designing experiments to study the molecular mechanism of Ist1 and Did2 interaction. Notably, while the Did2-bound Ist1NTD structure is largely unchanged compared to the apo-structure, the region corresponding to helix α9 in the Ist1NTD structure shows significant structural variation among the four molecules in the asymmetric unit and the helical conformation is not maintained in most of them (Figure 4.5). This suggests that Did2 binding is able to induce conformational change near the C-terminal region of Ist1, where it binds to Vps4.

Ist1-Did2 interaction is important for MVB sorting

Previous studies have suggested that Ist1 functions together with Did2 in a process parallel to the Vta1/Vps60 complex [17]. Simultaneous deletion of one component from each complex gives rise to a strong class E sorting phenotype in yeast. To examine whether a functional Ist1-Did2 complex is important in the MVB pathway,

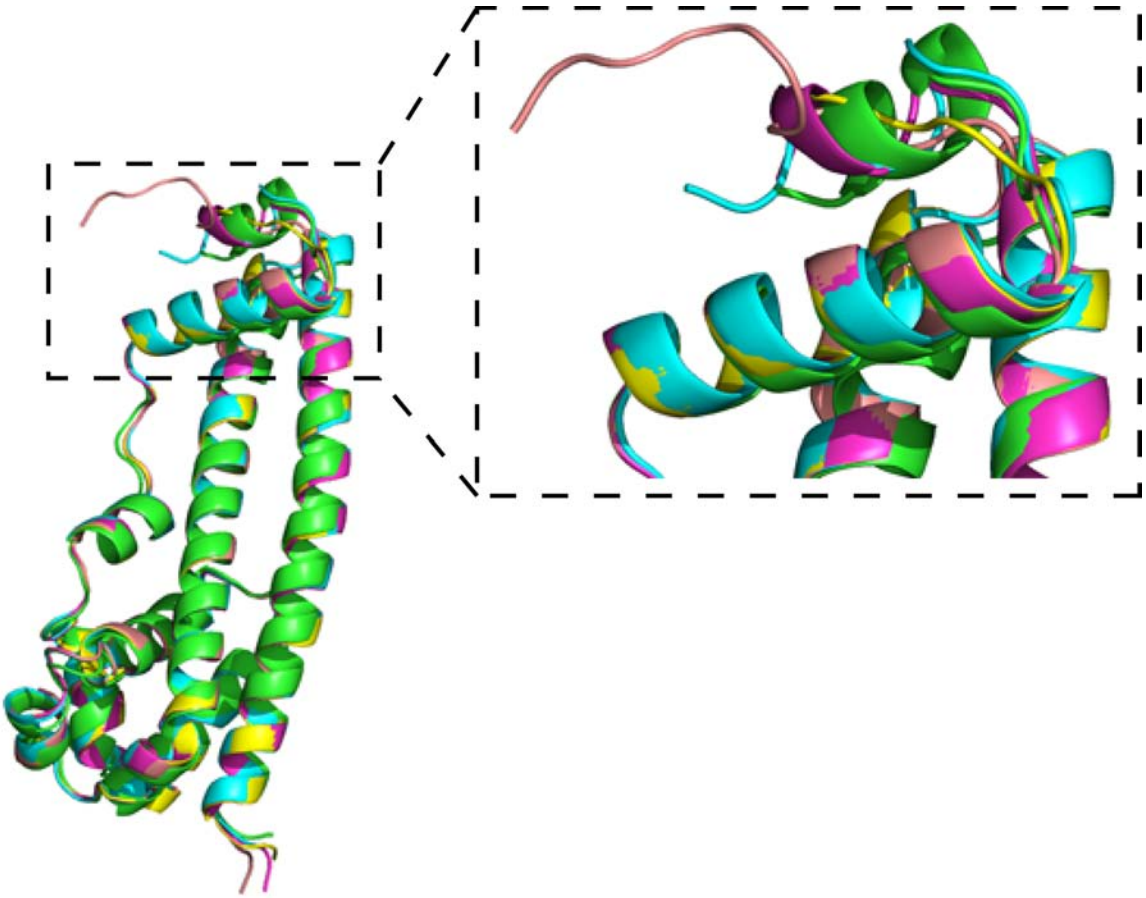

Figure 4.5 Did2 binding induces conformational change at the C-terminal region of Ist1.
The apo-structure of Ist1NTD is colored in green. The four Did2-MIM1 bound Ist1NTD molecules in the asymmetric unit of the Ist1NTD/Did2-MIM1 complex crystal are colored in cyan, yellow, magenta, and pink respectively. Note the structural variability in the region corresponding to helix α9 in the apo-structure of Ist1NTD.

we examined the sorting of yeast MVB cargo, carboxypeptidase S (CPS), in response to the disruption of Ist1-Did2 interaction. In wild type cells, the GFP-CPS fusion protein was observed exclusively in the lumen of the vacuole as a result of proper vacuolar sorting (Figure 4.6). Consistent with previous results, *ist1*Δ cells or *vta1*Δ cells has no obvious or only modest effect on GFP-CPS transport, while *ist1*Δ*vta1*Δ cells display a dramatic mis-localization of GFP-CPS to the limiting membrane of the vacuole and a special class E membrane structure (Figure 4.6). To evaluate the role of Ist1-Did2 interaction in MVB sorting, we examined the subcellular localization of GFP-CPS in *ist1*Δ*vta1*Δ yeast cells supplemented with plasmids expressing either wild type IST1 or Did2-interaction deficient *ist1* mutant. As expected, transforming wild type IST1 into *ist1*Δ*vta1*Δ cells partially restored delivery of GFP-CPS into the vacuole to a level similar to that observed in *vta1*Δ cells. However, none of the Did2-interaction defective *ist1* mutants is capable of complementing the MVB sorting defect observed in *ist1*Δ*vta1*Δ cells. These results highlight the importance of Ist1-Did2 interaction for the *in vivo* function of Ist1, suggesting that a stable Ist1-Did2 complex is required for the proper function of the ESCRT machinery in the yeast MVB pathway.

Conserved Ist1-Did2 interaction is important for efficient cytokinesis and abscission

Ist1 is evolutionarily conserved in the eukaryotic cells. BLAST search reveals a clear Ist1 homolog in higher eukaryotes, referred as “KIAA0174” in human and many other species. The function of this protein is largely uncharacterized, but the sequence homology suggests that it likely acts in a way similar to Ist1 in yeast. As the structure of the yeast Ist1-Did2 complex illustrates, the Did2 binding site of Ist1 involves one of the

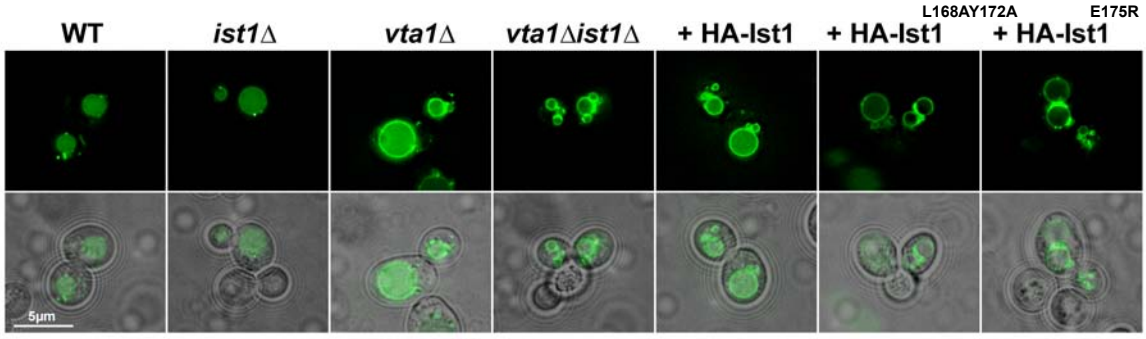

Figure 4.6 Residues involved in Did2 binding are required for cargo sorting in the MVB pathway.
The MVB cargo GFP-CPS was visualized by fluorescent and brightfield microscopy in living cells corresponding to wild type, *ist1*Δ, *vta1*Δ, *ist1*Δ*vta1*Δ, or *ist1*Δ*vta1*Δ cells expressing wild type or mutant Ist1 proteins as indicated. The absence of lumenal GFP fluorescence in *ist1*Δ*vta1*Δ cells expressing HA-Ist1$^{L168\ AY172A}$ or HA-Ist1^{E175R} indicated that the Ist1-Did2 interaction contributes to Ist1 function *in vivo*.

most conserved regions on the Ist1NTD surface (Figure 4.4B). Furthermore, residues that are important for the complex formation are absolutely conserved for the two binding partners. Mutations of the conserved residues in yeast Ist1 significantly weaken its interaction with Did2 (Figure 4.4C). To examine whether these residues are also responsible for mediating Ist1-Did2 interaction in human, we introduced corresponding mutations into the human Ist1 (hIst1) protein and tested the binding between hIst1 and one of the human Did2 homologs, CHMP1B.

As shown in Figure 4.7A, wild type hIst1, but none of the two mutants (hIst1^{E168R} and hIst1^{L161AY165A}), efficiently interacts with GST-CHMP1B. We further tested the *in vivo* interaction between these two proteins using co-immunoprecipitation (Figure 4.7B). Consistent with the pull-down experiment, wild type hIst1 formed a stable complex with CHMP1B. In contrast, neither mutant of hIst1 interacted with CHMP1B to a level that can be detected under the experimental condition, suggesting that the interaction mechanism between Ist1 and Did2 is evolutionarily conserved.

The ESCRT machinery has been recently demonstrated to be important in the abscission step during cytokinesis [25-27]. To determine whether hIst1-CHMP1 interaction also plays a role in this process, we introduced wild type and mutant hIst1 into Hela cells and examined whether the CHMP1-binding deficient mutants would comprise cytokinesis. Cells expressing wild type hIst1 showed little alteration in cell cycle progression when compared with non-transfected cells. However, expressing either hIst1^{E168R} or hIst1^{L161AY165A} mutants led to a significant accumulation of cells arrested in late phase of cytokinesis as evidenced by persisted cytoplasmic bridge structures and multi-nucleated cells (Figure 4.7C, 4.7D). Moreover, we frequently observed cells with 4

Figure 4.7 hIst1-CHMP1 interaction is important for cytokinesis.
(A) In vitro Interaction between hIst1 and CHMP1B. Cos-1 cells expressing HA-tagged hIst1 proteins were lysed and subjected to pull-down by GST or GST-CHMP1B. Proteins retained on the beads were analyzed by SDS-PAGE and anti-HA blotting.
(B) In vivo interaction between hIst1 and CHMP1B. Cos-1 cells expressing FLAG-tagged CHMP1B and HA-tagged hIst1 constructs were lysed and subjected to co-immunoprecipitation (IP) with anti-HA antibody. CHMP1B proteins associated with hIst1 were detected by anti-FLAG blotting.
(C) Disruption of hIst1-CHMP1 interaction leads to cytokinesis defects. Hela cells expressing wild type or mutant HA-hIst1 proteins were fixed and subjected to immuno-fluorescence with anti-HA (green) and anti-alpha tubulin (red). Nuclei were visualized with TORPO 3 (blue).
(D) Quantification of the cytokinesis defects shown in (C). Multi-nucleated cells (with 2 or more nuclei) or cells displaying apparent cytokinesis defect (with clear cytoplasmic bridge between the daughter cells as visualized by alpha tubulin staining) were scored. Experiments were repeated 4 times, with 100 cells counted for each sample.

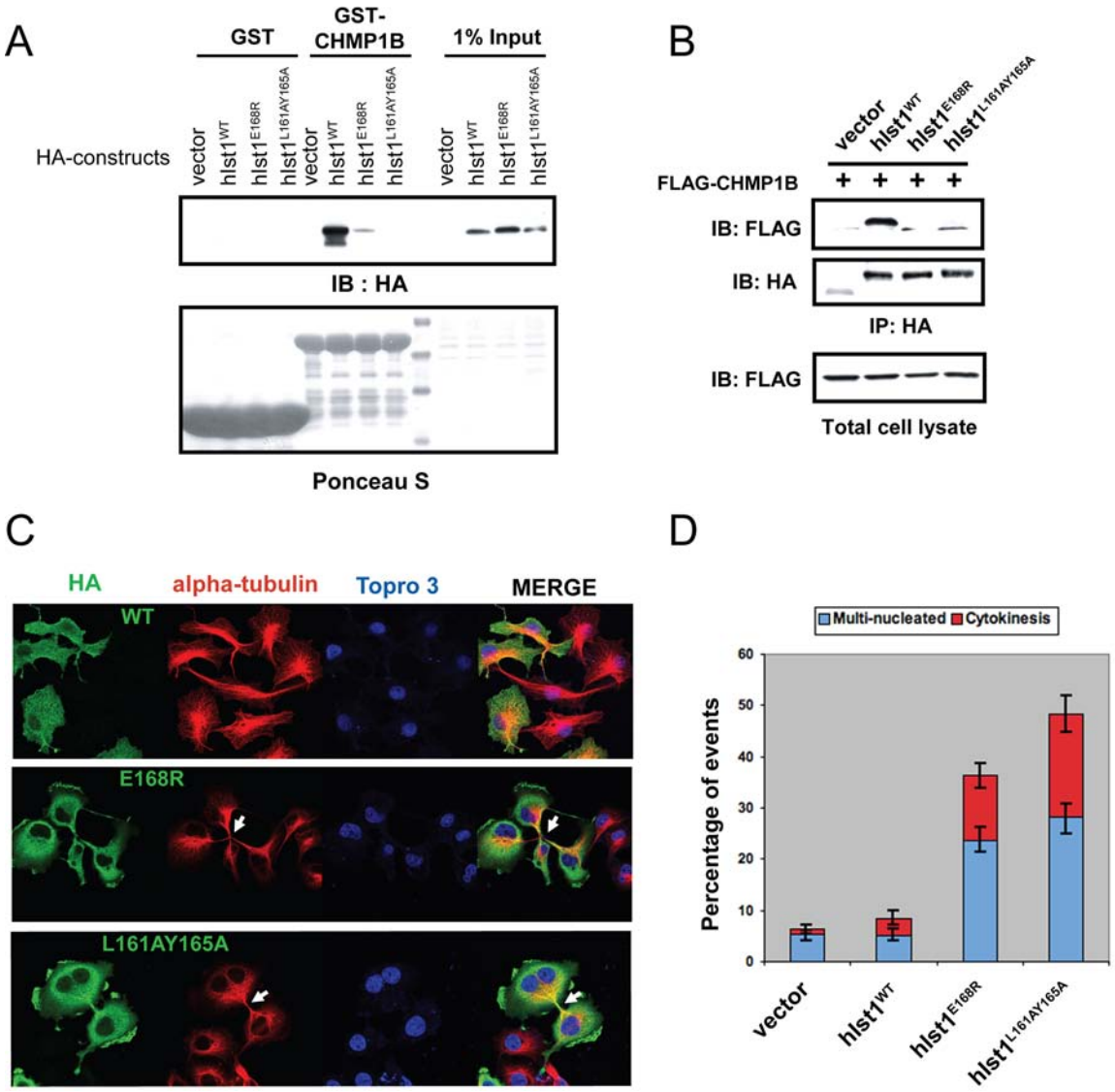
A
GST
GST-CHMP1B
1% Input
HA-constructs
vector
hIst1WT
hIst1E168R
hIst1L161AY165A
IB : HA
Ponceau S
B
vector
hIst1WT
hIst1E168R
hIst1L161AY165A
FLAG-CHMP1B
+ + + +
IB: FLAG
IB: HA
IP: HA
IB: FLAG
Total cell lysate
C
HA
alpha-tubulin
Topro 3
MERGE
WT
E168R
L161AY165A
D
Multi-nucleated
Cytokinesis
Percentage of events
0
10
20
30
40
50
60
vector
hIst1WT
hIst1E168R
hIst1L161AY165A

or more nuclei cells arrested in late cytokinesis stage and possessed cytoplasmic bridge (Figure 4.7D, arrow), indicating that these cells were able to proceed through the nuclear division (mitosis) but failed to complete their cytoplasmic division (abscission/cytokinesis). Taken together, the data suggested that loss of hIst1-CHMP1 interaction led to defects in mammalian ESCRT function, and hIst1-CHMP1 interaction is essential for cell abscission during cytokinesis.

DISCUSSION

Implications on the mechanism of Vps4 inhibition by Ist1

The fact that Ist1 contains a structural fold similar to that of the ESCRT-III proteins suggests a possible mechanism by which Ist1 acts as a negative regulator of Vps4 activity. Although the C-terminal MIM1 sequence of Ist1 constitutes the major Vps4 binding site, MIM1 alone is not sufficient for inhibition, but instead behaves as an activator of Vps4 in the *in vitro* ATPase assay [14]. Furthermore, Ist1 can interfere with the oligomerization of Vps4 and this activity also depends on Ist1NTD. Since the ESCRT-III proteins are the direct substrate of Vps4, the structural similarity between Ist1NTD and the ESCRT-III proteins suggest Ist1 might inhibit Vps4 activity by acting as a substrate mimic, competing for Vps4 binding. The reason why Ist1 is an inhibitor but other ESCRT-III proteins are substrates and/or activators might be due to the unique structural properties of Ist1. For example, the connection between the N-terminal ESCRT-III domain and the C-terminal MIM1 in Ist1 is significantly longer, which could lead to an inefficient “threading” if the ESCRT-III proteins are indeed pulled into the

central pore of Vps4 as previously proposed [28]. On the other hand, since no detectable interaction between Ist1NTD and Vps4 has been found, the inhibitory effect of Ist1NTD on Vps4 oligomerization is not likely due to a direct competition with other Vps4 subunits. Ist1NTD may interact with the pore motif of Vps4 that is responsible for remodeling the ESCRT-III complex. The interaction may disfavor the formation of the Vps4 ring structure. In this regard, many uncertainties for the inhibitory mechanism of Ist1 originate from our lack of knowledge regarding how Vps4 acts on the substrates. As such, elucidating how Ist1NTD inhibits the activity of Vps4 will help address the fundamental question on how Vps4 dissembles the ESCRT-III complex.

A new MIM-binding domain

A common feature of the protein complexes within the ESCRT machinery is that they contain domains that bind specifically to phosphoinositides, ubiquitin or specific proteins. These modular units enable the machinery to bind cargo molecules and target them to the membrane in a highly regulated fashion. The MIT domain is a novel protein-protein interaction domain identified in a number of components of the ESCRT machinery, including Vps4, Vta1, AMSH and UBPY [29]. It recognizes sequence motifs that are encoded in the ESCRT machinery, primarily within the ESCRT-III complex. These sequences are collectively called the MIMs (MIT-interacting motifs). Two types of MIM have been identified, MIM1 and MIM2. MIM1 exists in Vps2/CHMP2 and Did2/CHMP1 and is characterized by a (D/E)xxLxxRLxxL(K/R) motif (where x is any amino acid) [15, 16]. It binds to the MIT domain as an amphipathic helix. As described above, MIM1 can bind to two different surfaces on the MIT domain. MIM2 exists in

Vps20/CHMP6, Snf7/CHMP4, and archaeal ESCRT-III like proteins and is characterized by a core consensus sequence of (L/V)Px(V/L)P [30, 31]. It adopts an extended loop structure and binds between α1 and α3 on the MIT domain. Interaction between MIT and MIM has been implicated in regulating the assembly of the ESCRT-III complex on the membrane as well as targeting specific proteins to the membrane.

The crystal structure of the Ist1/Did2-MIM1 complex shows, for the first time, that MIM can interact with a structure other than the MIT domain. The increased MIM-binding structural repertoire reveals a previously unrecognized complexity within the protein-protein interaction network of the ESCRT machinery. It is interesting to note that when binding to Vps4 and Ist1, Did2 utilizes a nearly identical binding mechanism (Figure 4.8). Although we do not have the precise side chain conformation, our complex structure nevertheless clearly demonstrates that one side of the Did2-MIM1 helix is important for Ist1NTD interaction (Figure 4.8). This side involves Glu192, Leu195, Ala196, Arg198, Leu199, Leu202 and Arg203 of Did2. Similarly, the same side in CHMP1A-MIM1 helix mediates interaction with Vps4-MIT, involving corresponding residues Glu184, Leu187, Ser188, Arg190, Leu191, Leu194 and Arg195 in CHMP1A. As a result, superposing the MIM1 motifs in these two structures results in significant clash between Ist1NTD and Vps4-MIT, suggesting they cannot bind to the same Did2-MIM1 motif simultaneously. How these two interactions are coordinated in the cells is intriguing. It is unclear whether Vps4 and Ist1 bind to Did2 in a sequential and competing manner or they simultaneously bind to different Did2 molecules in a Did2 polymer.

Implication for ESCRT-III activation

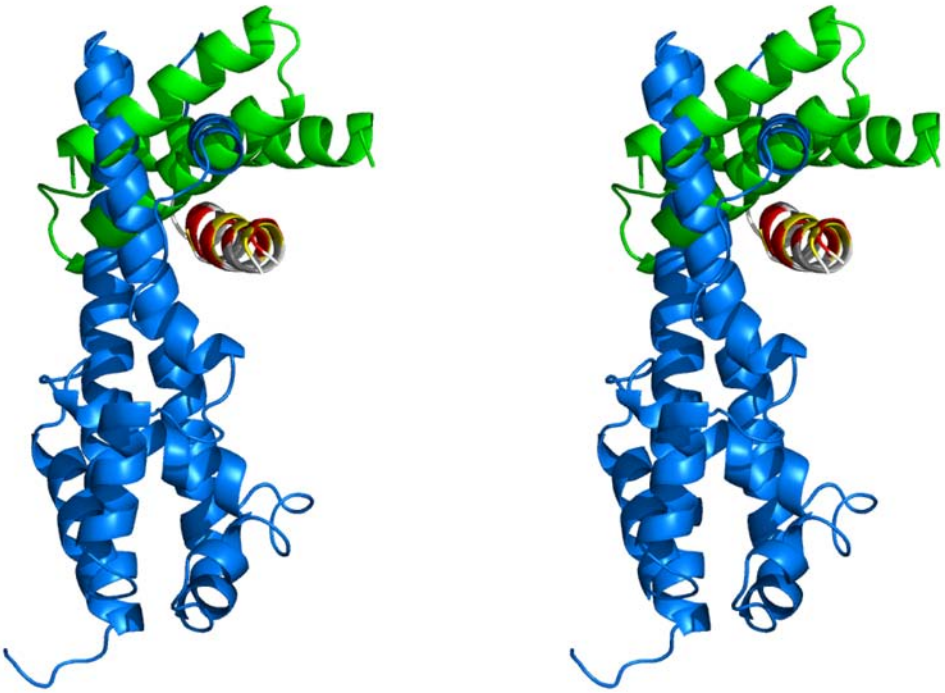

Figure 4.8 Did2 uses a similar surface to bind to Ist1NTD and Vps4-MIT. Ist1NTD/Did2-MIM1 (blue) and Vps4-MIT/CHMP1A-MIM1 (green) are aligned based on the superimposition of the MIM1s in the two complex structures (stereo image). Structural elements involved in interacting with Ist1NTD in Did2 are colored red, and those involved in interacting with Vps4-MIT in CHMP1A are colored in yellow. The rest of Did2/CHMP1A structures are colored in white.

The ESCRT-III proteins are metastable molecules that exist in two distinct conformations: a membrane-bound active form and a cytosolic inactive form. Transition between the two conformations is controlled by the C-terminal auto-inhibitory region, which binds to the N-terminal ESCRT-III fold in the inactive form to prevent the protein from oligomerization [18, 19]. The auto-inhibitory region consists of an α-helix (α5 in the CHMP3 structure) and the C-terminal MIM sequence. The CHMP3 fragment used in the structure determination lacks the MIM sequence. Thus the conformation present in the crystal structure represents an open and active form of the molecule [20]. In this form, helix α5 does not adopt a fixed position relative to the core of the structure but assumes an arbitrary conformation stabilized by lattice contact (Figure 4.2C). Moreover, most of the 26 residues-long loop that connects the ESCRT-III fold to α5 is disordered in the structure. Notably, this linker displays a high degree of sequence conservation (Figure 4.9), and therefore is very likely an important hinge region that controls the transition between the open and close conformations of the molecule.

The surprising discovery that the MIM-binding Ist1NTD contains an ESCRT-III like fold provides a possible model for the elusive, inactive or close conformation of the ESCRT-III proteins. In the Ist1NTD structure, helix α8 is linked to helix α5 (structural equivalent to helix α4 in CHMP3) by a similar length connection (30 amino acids) (Figure 4.2B). For this reason, we hypothesize that the position of helix α8 in the Ist1NTD structure might correspond to the position of helix α5 in the ESCRT-III proteins when it folds back and interacts with the ESCRT-III fold (Figure 4.10). Strikingly, in the Ist1NTD/Did2-MIM1 complex structure, the MIM1 helix binds in a site formed by Ist1NTD helix α8 (Figure 4.4D). One could envision in the inactive state of the ESCRT-

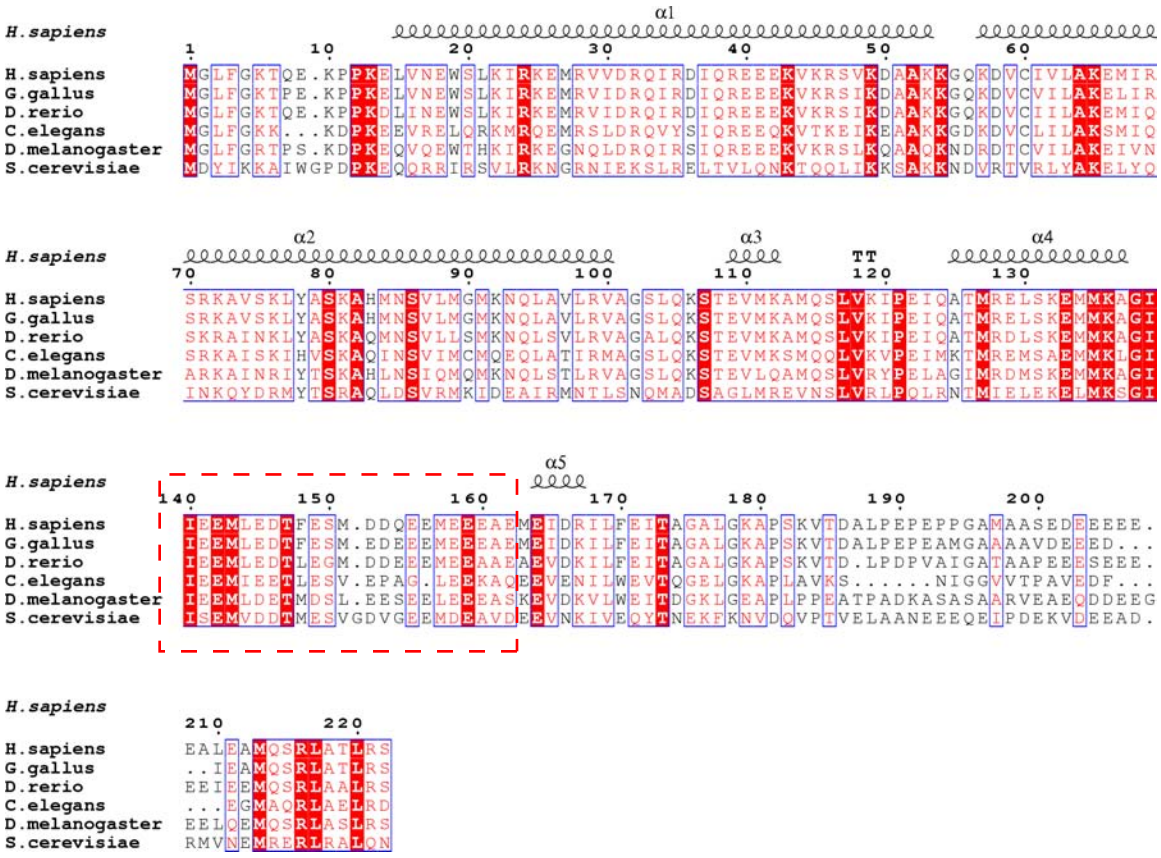

Figure 4.9 Structure based sequence alignment of the ESCRT-III protein CHMP3/Vps24.

The secondary structural elements in human CHMP3 are labeled. The conserved linker region between helix α4 and α5 is highlighted.

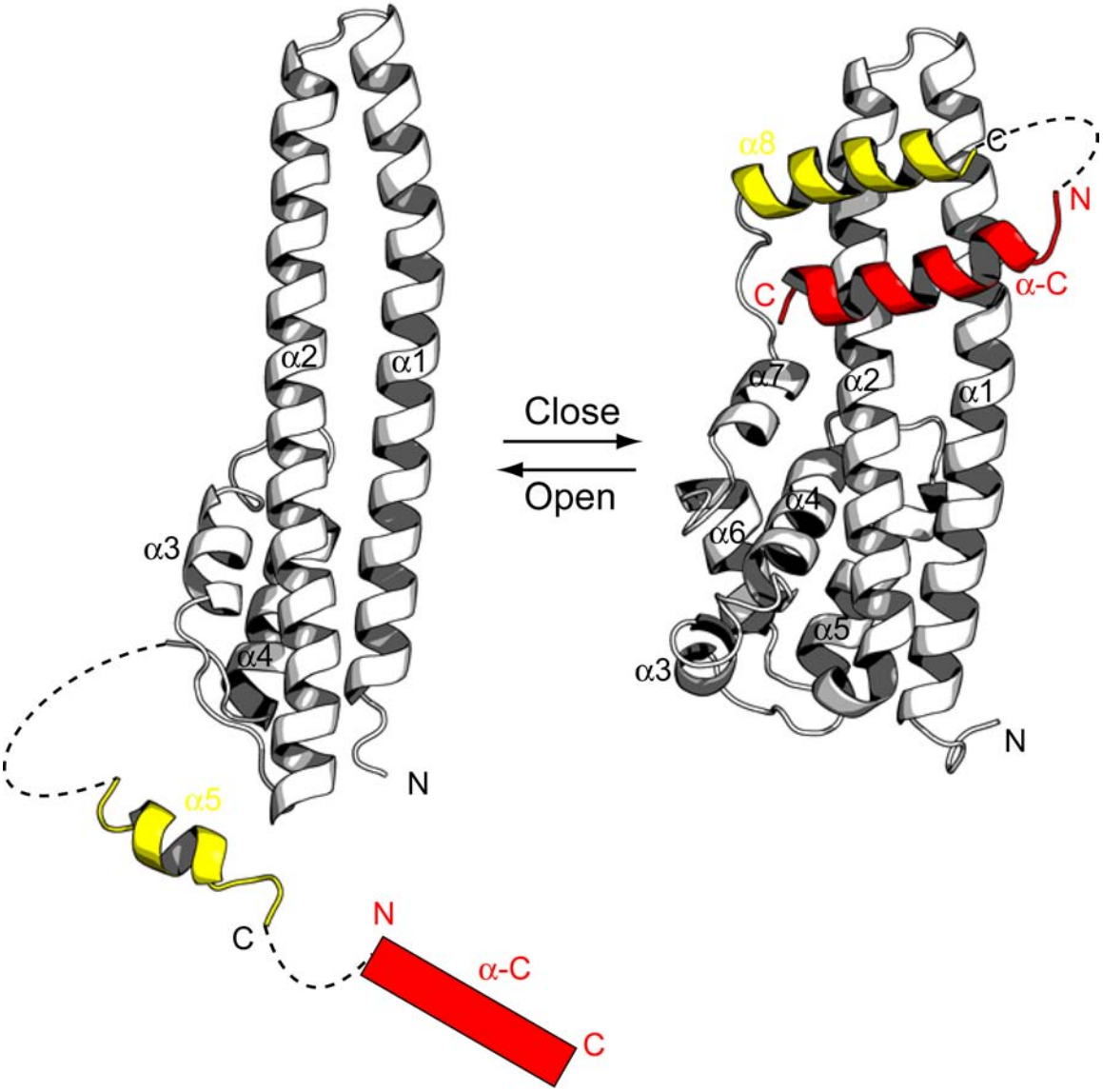

Figure 4.10 A model for the functional cycle of the ESCRT-III proteins.
The left panel shows the open conformation of the ESCRT-III proteins. Helices α1-α5 are adapted from the structure of human CHMP3. The C-terminal helix α-C is shown as a cartoon and the linker regions as a dash line. The right panel shows the speculative close conformation of the ESCRT-III proteins. Helices α1-α8 and helix α-C are adapted from the structure of the Ist1NTD/Did2-MIM1 complex.

III proteins, helix α5 and the C-terminal MIM sequence pack onto the ESCRT-III fold in a similar manner (Figure 4.10). During the course of ESCRT-III protein activation, the inherent flexibility within the conserved linker between the ESCRT-III fold and helix α5 combined with the weakening of intra-molecular interaction will lead to the exposure of both the N-terminal ESCRT-III fold and the C-terminal MIM sequence.

The role of Ist1-Did2 interaction in the cell

Our results support an important role played by Ist1-Did2 interaction in the cell. Given the weak affinity between full-length Ist1 and Did2, it is unlikely that Ist1 and Did2 will exist as a preformed complex in the cell; rather their association is tightly regulated by other binding events. Furthermore, Ist1 and Did2 interaction appears to be highly specific despite the existence of other proteins with homologous MIM1 sequences (Figure 4.1B). We have further demonstrated that Ist1-Did2 interaction has a role in both yeast vacuolar sorting and mammalian cytokinesis. However, the functional importance of the intricate interplay between Ist1, Did2, Vps4, and Vta1 remains largely elusive.

Ist1 interacts with Did2 and Vps4; and Did2 can interact with Ist1, Vta1, and Vps4. Furthermore, the MIM1 region in Did2 is involved in all binding events [12, 16]. The order and interconnection of these interactions might represent a higher level of regulation on Vps4 activity and need to be further delineated. Previous studies suggest Did2 is recruited to the membrane via the Vps2/Vps24 complex [32]. This may lead to the exposure of its MIM1 region. Depending on the physiological setting, it might either recruit Vps4-Vta1 complex in concert with the core ESCRT-III subunits to facilitate ESCRT-III dissociation, or recruit Ist1 to antagonize Vps4 activity. This is consistent

with the idea that the ESCRT-III complex has a built-in timer to control its assembly and disassembly [33], and we hypothesize the coordinated recruitment of Vps4-Vta1 and Ist1 by Did2 might contribute to this regulation process.

In summary, we have determined the crystal structures of an important functional domain of Ist1 and its complex with the Did2-MIM1 peptide. Our results reveal that Ist1NTD has an ESCRT-III like fold, and interacts with the Did2-MIM1 helix via a novel mechanism. The structural information, coupled with biochemical and cell biology experiments, has provided important insights to the molecular mechanism of Ist1 function and the biological role of Ist1-Did2 interaction. Furthermore, our results suggest that the interaction between the C-terminal amphipathic helices of the ESCRT-III proteins and their binding partners are more diversified than previously envisioned and deserve further exploration in future studies.

METHODS

Cloning, expression and purification

DNA fragments encoding yeast Ist1 and Did2 were amplified from the *Saccharomyces cerevisiae* genomic DNA. DNA fragment encoding Ist1NTD was cloned into the NcoI/XhoI site of pETDuet-1 vector (ampicillin resistant) to yield an untagged Ist1NTD protein; while Did2-MIM1 was cloned into a modified pET28a vector (kanamycin resistant), with a SUMO protein inserted between a His_6-tag and the coding region. The resulting plasmids were subsequently co-transformed into *E. coli*

BL21(DE3). For protein expression, cells were grown at 37°C in LB medium to an OD_{600} of 0.8 before induced with 0.4 mM IPTG at 20°C for 16 hours. Cells were harvested by centrifugation and frozen at -80°C. The MIM1 regions from other proteins were cloned and co-expressed with Ist1NTD using a similar strategy. DNA fragments encoding human CHMP1B and Ist1 were amplified from cDNA templates and cloned into the BamHI/XhoI site of pLenti-FLAG and pKH3 vectors, respectively.

All protein purification steps were performed at 4°C. Frozen cell pastes were re-suspended in buffer A [50 mM Tris (pH 8.0), 300 mM NaCl, 5 mM β-mercaptoethanol] supplemented with 10 μg/ml PMSF (phenylmethylsulphonyl fluoride) and disrupted by sonication. Supernatant from centrifugation was loaded on a Ni^{++}-NTA affinity column. After the column was washed extensively with buffer A, the complex was eluted with an imidazole gradient [50 mM Tris (pH 8.0), 50 mM NaCl, 250 mM imidazole, 5 mM β-mercaptoethanol]. Fractions containing the complex were collected and buffer exchanged into buffer A. His-tagged ULP1 protease was then added to remove the His_6-SUMO tag, and the resulting protein mixture was passed over a second Ni^{++}-NTA column. The complex was further purified by gel filtration chromatography on a Superdex-75 column (Amersham Pharmacia) in buffer C [25 mM Tris (pH 7.5), 300 mM NaCl, 1 mM DTT], concentrated and flash-frozen in liquid nitrogen. Selenomethionyl proteins were expressed in *E. coli* B834(DE3) using a minimal medium where methionines were replaced with selenomethionines, and purified in a similar way.

Crystallization and data collection

Native crystals of Ist1NTD were grown by the hanging drop method at 4°C. Proteins of Ist1NTD/Did2-MIM1 complex (10-15 mg/ml) were mixed with an equal volume of the reservoir solution [6-10% PEG 3000, 100 mM Na acetate (pH 5.0), 200 mM $MgCl_2$, and 100 mM glycine] in a final volume of 4 μl, and the mixture was equilibrated against the reservoir solution. Ist1NTD crystallized by itself under this condition. Crystals grew to full size in several weeks. To harvest, crystals were transferred into a cryo solution [16% PEG 3000, 20% ethylene glycol, 100 mM Na acetate (pH 5.0), 200 mM $MgCl_2$, and 100 mM glycine] in a stepwise manner before flash-frozen under liquid nitrogen. The best native crystal diffracted to 1.7 Å and has a space group of C2, with a unit cell dimension of a=144.84 Å, b=44.17 Å, c=66.95 Å, and β=110.49° (Table 4.1).

Selenomethionyl protein crystals of Ist1NTD were grown under similar conditions but initially belong to a space group of $P2_12_12_1$. These crystals decayed rapidly under synchrotron X-ray radiation. Transferring them slowly into the cryo solution by the button dialysis method at 4°C transformed them into a different C2 space group, with a unit cell dimension of a=145.63 Å, b=44.31 Å, c=138.34 Å, and β=112.75°. These crystals are more resistant to decay. Diffraction data for both the native and the selenomethionyl crystals were collected at the Advanced Photon Source beam line 21-ID-D.

For preparation of the heavy atom derivative, native Ist1NTD crystals were soaked in a solution containing 12% PEG 3000, 100 mM Na acetate (pH 5.0), 200 mM $MgCl_2$, 100 mM glycine, and 0.5 mM mercury acetate at 4°C for 2 hours. The crystals were then back-soaked and stepwise transferred into the cryo solution before flash-frozen

under liquid nitrogen. Diffraction data were collected with a Rigaku rotating anode generator and an R-AXIS IV image-plate detector system. The mercury derivative crystals belong to the larger C2 space group seen in the selenomethionyl crystals.

Ist1NTD/Did2-MIM1 complex crystals were grown by the sitting drop method at 20°C. Proteins of 10-15 mg/ml were mixed in a 1:1 ratio with the reservoir solution [1.1-1.15 M Na citrate, 100 mM Na citrate (pH5.5), and 10 mM Urea] in a final volume of 4 μl and equilibrated against the reservoir solution. Crystals grew to full size in several days and were transferred into a cryo solution (1.26 M Na citrate, 10 mM Urea, and 10% glycerol) before flash-frozen under liquid nitrogen. Diffraction data were collected at the Advanced Photon Source beam line 21-ID-D. The complex crystals belong to the space group of $P4_222$ with a unit cell dimension of a=165.92 Å, b=165.92 Å, and c=121.56 Å.

Structure determination and refinement

Diffraction data were integrated and scaled using HKL2000 (HKL Research) (Table 4.1). The structure of Ist1NTD alone was determined by a combination of multiwavelength anomalous dispersion (MAD) and single isomorphous replacement (SIR) using the data collected from the selenomethionyl crystal and the mercury derivative crystal. These two crystal forms are isomorphous and contain four molecules in their asymmetric units. For MAD, four initial Se sites (out of a maximum of twenty) were found using the program SnB [34]. Eight more Se sites were subsequently located using the anomalous difference Fourier function in SHARP [35]. Parameters of these twelve sites were then refined and used to calculate phases in SHARP. The electron density map was further improved by solvent flattening as implemented in SHARP.

Some features corresponding to secondary structural elements of a protein molecule could be seen in the resulting map; however, the poor quality of the map did not allow proper interpretation.

To improve the quality of phases, heavy atom derivative crystals were prepared. This resulted in a mercury derivative crystal isomorphous not to the native crystal but to the selenomethionyl crystal. We therefore treated the selenomethionyl data as a pseudo "native" dataset in the SIR phasing process. Hg sites were located by the isomorphous difference Fourier method implemented in CNS [36] using the MAD phases derived above. The top four sites were then used to calculate a Patterson map, and the Harker section at Y=0 of the resulting predicted Patterson map was compared with the corresponding Harker section of the experimental isomorphous difference Patterson map. The peaks from the two maps matched well, corroborating the correctness of the MAD phases as well as the four Hg sites. These four initial sites were then used to locate more sites and calculate SIR phases in SHARP. After density modification, some structural features could again be seen in the electron density map but the map was not of high enough quality for tracing. To further improve the experimental phases, the unmodified MAD phase and SIR phase were combined and further improved by solvent flattening using DM in the CCP4 suite [37, 38]. The resulting map has a significantly improved quality and displayed many side chain details. About two-thirds of one protein molecule was subsequently traced in O [39] and refined with REFMAC [40]. This partial model was then used as a search model for molecular replacement into the 1.7 Å native data set using PHASER [41]. Both molecules in the asymmetric unit were easily located and the resulting electron density map was of extremely high quality such that most of the model

was automatically built using ARP/wARP [42]. The model obtained from the auto-building process was further adjusted in O and refined with CNS, using 5% randomly selected reflections for cross-validation. Simulated annealing with torsion angle dynamics was carried out, maximum likelihood target function with amplitudes (MLF) used, and individual restrained B-factors refined. The final model contains residues 6-191 for each protomer and 452 water molecules, with a working R factor of 22.6% and a free R factor of 24.9% at 1.7 Å and excellent geometry (Table 4.1).

The structure of Ist1NTD/Did2-MIM1 complex was determined by the molecular replacement method using PHASER with the refined Ist1NTD structure as a search model. There are four complexes in the asymmetric unit. The Did2-MIM1 peptide was fitted into the electron density map with the aid of biochemical analysis (described in the Results section). The model was refined using CNS. Non-crystallographic symmetry (NCS) restraint was kept throughout the refinement process. The NCS restraint group contains Ist1NTD 8-180 and Did2-MIM 189-204 for each complex. A tight restraint was used at the beginning, with a restraint weight of 300 kcal/mole/$Å^2$, and then gradually decreased. However, a medium strength restraint was always kept, and the restraint weight used in the final rounds of refinement was 100 kcal/mole/$Å^2$. The structure was refined to a working R factor of 29.8% and a free R factor of 30.7% with good geometry. The final model contains residues 3-188 for Ist1NTD chain A (residues 3-5 modeled as alanines), 5-190 for Ist1NTD chain B (residue 5 modeled as alanine), 5-186 for Ist1NTD chain C (residue 5 modeled as alanine), 5-192 for Ist1NTD chain D (residue 5 modeled as alanine), 188-204 for Did2-MIM1 chain E and chain F (residue 188 modeled as alanines

in both), 189-204 for Did2-MIM1 chain G, and 187-204 for Did2-MIM1 chain H (residue 187-188 modeled as alanines).

Limited proteolysis

Subtilisin was used in the assay with protease to protein ratios (mass) ranging from 1:10,000 to 1:10. For a standard reaction, 1 mg/ml Ist1 was incubated with subtilisin in the reaction buffer (20 mM HEPES, pH 7.5, 200 mM NaCl, 10% glycerol). Reactions were allowed to proceed for 30 minutes on ice before terminated by protease inhibitor PMSF. Samples were boiled in SDS-loading buffer, analyzed by SDS-PAGE and visualized by Coomassie staining.

To determine the molecular mass of the resulting fragments, subtilisin was incubated with Ist1 at a 1:100 ratio and digested as described above. The reaction was stopped by PMSF, and the resulting protein mixture was fractionated on an anion exchange Resource Q column (Amersham Pharmacia). The molecular masses of Ist1NTD and Ist1CTD were measured by mass spectrometry in Michigan Proteome Consortium at the University of Michigan.

Biochemical interactions

To test the interaction between yeast Ist1 and Did2, GST pull-down experiments were performed following standard procedures. *E. coli* cell lysates were incubated with GST-tagged proteins immobilized on glutathione agarose beads in the binding buffer (PBS buffer supplemented with 1mM DTT and 0.1% Triton X-100) for 40min at 4°C. The beads were then washed with the binding buffer, and bound proteins were separated

on SDS-PAGE and visualized by Coomassie staining. For His-tag pull-down, cells were lysed in buffer A used in protein purification. Cell lysates were then centrifuged and the supernatant was mixed with Ni^{++}-NTA resin. Bound proteins were eluted with buffer B and analyzed by SDS-PAGE and visualized by Coomassie staining.

For interaction between human Ist1 and CHMP1B, GST pull-down and immuno-precipitation (IP) were carried out as described previously [43]. Briefly, Cos-1 cells grown in 10-cm dishes were lysed in buffer containing 100 mM Tris (pH 7.5), 1% Triton X-100, 10% glycerol, 150 mM NaCl, 1mM EDTA, supplemented with complete protease inhibitor tablets (Roche). For GST pull-down experiments, ~10-20 μg of fusion protein were used for each assay. For IP experiments, ~10 μl HA antibody conjugated agarose beads (Santa Cruz biotechnology) were used for each assay.

Yeast cell biology

pRS415 HA-Ist1 was generated by first amplifying the Ist1 promoter from genomic DNA along with coding sequences for an amino-terminal HA epitope and then cloning this fragment into pRS415. Ist1 coding sequences were then subcloned from the bacterial expression constructs described above (wild type or mutants) to generate pRS415 HA-Ist1, pRS415 HA-Ist1^{L168AY172A} and pRS415 HA-Ist1^{E175R} plasmids. Standard techniques were used to introduce the pRS415 HA-Ist1 constructs into *ist1*Δ*vta1*Δ yeast along with a MVB reporter construct expressing GFP-CPS. Microscopy was performed on living cells using a Nikon fluorescence microscope fitted with filters optimized for EGFP detection and a Coolsnap HQ digital camera (Photometrix). Images were analyzed using Delta Vision software (Applied Precision, Inc.).

Immuno-fluorescence and confocal microsocpy

Immuno-fluorescence experiments were carried out as described previously [44]. Hela cells grown on cover slips were fixed with 10% formalin for 10 minutes before permeablized with 0.5% Triton X-100 in Phosphate Buffered Saline (PBS, GIBCO) for 5 minutes. Additional formalin was quenched with 100 mM glycine in PBS. Cells were blocked with 1% BSA plus 1% chicken albumin in PBS and stained with rabbit anti-HA (Santa Cruz Biotechnology) at 1:500, mouse anti-alpha tubulin (clone DM1A, Sigma) at 1:500. Coverslips were mounted in Vectashield mounting media (Vector Laboratories). Confocal microscopy was performed using Olympus FluoView 500 laser scanning confocal microscope; images were taken under X60 water lens.

Figure presentation

Multiple sequence alignment was performed with ClustalW [45]. Alignment figures with secondary structures labeled were prepared using ESPript [46]. Amino acid conservation scores are calculated using the ConSurf server [47]. Structure figures were generated using Pymol (DeLano Scientific LLC). Coordinates and structure factors for structures described in the study will be deposited into the Portein Data Bank upon acceptance of the manuscript.

REFERENCES

1. Saksena, S., et al., *ESCRTing proteins in the endocytic pathway.* Trends Biochem Sci, 2007. **32**(12): p. 561-73.

2. Piper, R.C. and D.J. Katzmann, *Biogenesis and function of multivesicular bodies.* Annu Rev Cell Dev Biol, 2007. **23**: p. 519-47.

3. Babst, M., *A protein's final ESCRT.* Traffic, 2005. **6**(1): p. 2-9.

4. Katzmann, D.J., G. Odorizzi, and S.D. Emr, *Receptor downregulation and multivesicular-body sorting.* Nat Rev Mol Cell Biol, 2002. **3**(12): p. 893-905.

5. Hurley, J.H., *ESCRT complexes and the biogenesis of multivesicular bodies.* Curr Opin Cell Biol, 2008. **20**(1): p. 4-11.

6. Williams, R.L. and S. Urbe, *The emerging shape of the ESCRT machinery.* Nat Rev Mol Cell Biol, 2007. **8**(5): p. 355-68.

7. Hanson, P.I., et al., *Plasma membrane deformation by circular arrays of ESCRT-III protein filaments.* J Cell Biol, 2008. **180**(2): p. 389-402.

8. Lata, S., et al., *Helical structures of ESCRT-III are disassembled by VPS4.* Science, 2008. **321**(5894): p. 1354-7.

9. Xiao, J., et al., *Structural characterization of the ATPase reaction cycle of endosomal AAA protein Vps4.* J Mol Biol, 2007. **374**(3): p. 655-70.

10. Babst, M., et al., *The Vps4p AAA ATPase regulates membrane association of a Vps protein complex required for normal endosome function.* EMBO J, 1998. **17**(11): p. 2982-93.

11. Azmi, I., et al., *Recycling of ESCRTs by the AAA-ATPase Vps4 is regulated by a conserved VSL region in Vta1.* J Cell Biol, 2006. **172**(5): p. 705-17.

12. Azmi, I.F., et al., *ESCRT-III family members stimulate Vps4 ATPase activity directly or via Vta1.* Dev Cell, 2008. **14**(1): p. 50-61.

13. Xiao, J., et al., *Structural basis of Vta1 function in the multivesicular body sorting pathway.* Dev Cell, 2008. **14**(1): p. 37-49.

14. Dimaano, C., et al., *Ist1 regulates Vps4 localization and assembly.* Mol Biol Cell, 2008. **19**(2): p. 465-74.

15. Obita, T., et al., *Structural basis for selective recognition of ESCRT-III by the AAA ATPase Vps4.* Nature, 2007. **449**(7163): p. 735-9.

16. Stuchell-Brereton, M.D., et al., *ESCRT-III recognition by VPS4 ATPases.* Nature, 2007. **449**(7163): p. 740-4.

17. Rue, S.M., et al., *Novel Ist1-Did2 complex functions at a late step in multivesicular body sorting.* Mol Biol Cell, 2008. **19**(2): p. 475-84.

18. Zamborlini, A., et al., *Release of autoinhibition converts ESCRT-III components into potent inhibitors of HIV-1 budding.* Proc Natl Acad Sci U S A, 2006. **103**(50): p. 19140-5.

19. Shim, S., L.A. Kimpler, and P.I. Hanson, *Structure/function analysis of four core ESCRT-III proteins reveals common regulatory role for extreme C-terminal domain.* Traffic, 2007. **8**(8): p. 1068-79.

20. Muziol, T., et al., *Structural basis for budding by the ESCRT-III factor CHMP3.* Dev Cell, 2006. **10**(6): p. 821-30.

21. Holm, L., et al., *Searching protein structure databases with DaliLite v.3.* Bioinformatics, 2008.

22. Babst, M., et al., *Escrt-III: an endosome-associated heterooligomeric protein complex required for mvb sorting.* Dev Cell, 2002. **3**(2): p. 271-82.

23. Ghazi-Tabatabai, S., et al., *Structure and disassembly of filaments formed by the ESCRT-III subunit Vps24.* Structure, 2008. **16**(9): p. 1345-56.

24. Yang, D., et al., *Structural basis for midbody targeting of spastin by the ESCRT-III protein CHMP1B.* Nat Struct Mol Biol, 2008.

25. Spitzer, C., et al., *The Arabidopsis elch mutant reveals functions of an ESCRT component in cytokinesis.* Development, 2006. **133**(23): p. 4679-89.

26. Carlton, J.G. and J. Martin-Serrano, *Parallels between cytokinesis and retroviral budding: a role for the ESCRT machinery.* Science, 2007. **316**(5833): p. 1908-12.

27. Morita, E., et al., *Human ESCRT and ALIX proteins interact with proteins of the midbody and function in cytokinesis.* EMBO J, 2007. **26**(19): p. 4215-27.

28. Scott, A., et al., *Structural and mechanistic studies of VPS4 proteins.* EMBO J, 2005. **24**(20): p. 3658-69.

29. Hurley, J.H. and D. Yang, *MIT domainia.* Dev Cell, 2008. **14**(1): p. 6-8.

30. Kieffer, C., et al., *Two distinct modes of ESCRT-III recognition are required for VPS4 functions in lysosomal protein targeting and HIV-1 budding.* Dev Cell, 2008. **15**(1): p. 62-73.

31. Samson, R.Y., et al., *A Role for the ESCRT System in Cell Division in Archaea.* Science, 2008.

32. Nickerson, D.P., M. West, and G. Odorizzi, *Did2 coordinates Vps4-mediated dissociation of ESCRT-III from endosomes.* J Cell Biol, 2006. **175**(5): p. 715-20.

33. Teis, D., S. Saksena, and S.D. Emr, *Ordered Assembly of the ESCRT-III Complex on Endosomes Is Required to Sequester Cargo during MVB Formation.* Dev Cell, 2008. **15**(4): p. 578-89.

34. Weeks, C.M. and R. Miller, *Optimizing Shake-and-Bake for proteins.* Acta Crystallogr D Biol Crystallogr, 1999. **55**(Pt 2): p. 492-500.

35. Vonrhein, C., et al., *Automated structure solution with autoSHARP*. Methods Mol Biol, 2007. **364**: p. 215-30.

36. Brunger, A.T., *Version 1.2 of the Crystallography and NMR system.* Nat Protoc, 2007. **2**(11): p. 2728-33.

37. Cowtan, K.D. and K.Y. Zhang, *Density modification for macromolecular phase improvement.* Prog Biophys Mol Biol, 1999. **72**(3): p. 245-70.

38. *The CCP4 suite: programs for protein crystallography.* Acta Crystallogr D Biol Crystallogr, 1994. **50**(Pt 5): p. 760-3.

39. Jones, T.A., et al., *Improved methods for building protein models in electron density maps and the location of errors in these models.* Acta Crystallogr A, 1991. **47 (Pt 2)**: p. 110-9.

40. Murshudov, G.N., et al., *Efficient anisotropic refinement of macromolecular structures using FFT.* Acta Crystallogr D Biol Crystallogr, 1999. **55**(Pt 1): p. 247-55.

41. McCoy, A.J., et al., *Phaser crystallographic software.* J Appl Cryst, 2007. **40**(Pt 4): p. 658-674.

42. Morris, R.J., A. Perrakis, and V.S. Lamzin, *ARP/wARP and automatic interpretation of protein electron density maps.* Methods Enzymol, 2003. **374**: p. 229-44.

43. Chen, X.W., et al., *Activation of RalA is required for insulin-stimulated Glut4 trafficking to the plasma membrane via the exocyst and the motor protein Myo1c.* Dev Cell, 2007. **13**(3): p. 391-404.

44. Chen, X.W., et al., *RalA-exocyst-dependent recycling endosome trafficking is required for the completion of cytokinesis.* J Biol Chem, 2006. **281**(50): p. 38609-16.

45. Larkin, M.A., et al., *Clustal W and Clustal X version 2.0.* Bioinformatics, 2007. **23**(21): p. 2947-8.

46. Gouet, P., et al., *ESPript: analysis of multiple sequence alignments in PostScript.* Bioinformatics, 1999. **15**(4): p. 305-8.

47. Landau, M., et al., *ConSurf 2005: the projection of evolutionary conservation scores of residues on protein structures.* Nucleic Acids Res, 2005. **33**(Web Server issue): p. W299-302.

CHAPTER 5

CONCLUSIONS AND PERSPECTIVES

The ESCRT machinery was originally characterized in the multivesicular body pathway in eukaryotic cells. Recent studies demonstrated its broad involvement in other related membrane fission processes, including enveloped virus budding and cell division. Delineating the molecular mechanism of the ESCRT machinery will help to develop new approaches for the prevention and treatment of a number of human diseases ranging from cancer, viral infection to neurodegeneration. The ESCRT machinery includes the ESCRT complexes and the AAA ATPase Vps4, with the latter serving as the only energy donor during the entire MVB functional cycle. Although the phenotype of perturbing Vps4 activity includes the massive accumulation of the ESCRT complex on the membrane, the primary function of Vps4 could be to drive membrane deformation and constriction with ESCRT dissociation just being an end product associated with this function. Elucidating the mechanism of function and regulation of Vps4 will be important for us to understand and potentially harness the MVB related processes.

Vps4 is a member of the AAA ATPase family, the general functional theme of which is to remodel protein or protein complexes through the ATP binding and hydrolysis powered internal molecular motion. Therefore, characterizing the conformational change of Vps4 during its ATPase reaction cycle will be a key to

understand its function. Chapter 2 of this thesis describes my initial efforts toward this goal. I have determined the crystal structures of *S. cerevisiae* Vps4 in both the nucleotide-free form and the ADP-bound form. By examining their differences, I have presented a structural view of the domain motion of Vps4 induced by the change in its nucleotide status. Furthermore, I have demonstrated that Vps4 interacts with the substrate ESCRT-III proteins in a nucleotide-dependent manner, which suggests a mechanism for the coordination between ATP hydrolysis and substrate binding/release by Vps4.

The function of Vps4 is closely regulated in the cells by a network of proteins, including Vta1, Did2, Vps60, and Ist1. Studies in Chapter 3 and Chapter 4 aimed at understanding the intricate molecular interactions that support the functional interplay between Vps4 and these proteins. Chapter 3 focuses on the structural basis of Vta1 function. Vta1 is a co-factor of Vps4. It binds and stabilizes the active form of Vps4. In fact, accumulating evidence suggest the functional assembly that disassembles the ESCRT-III complex *in vivo* is a Vps4-Vta1 complex, rather than Vps4 alone. In addition to binding to Vps4, Vta1 also interacts with accessory ESCRT-III proteins Did2 and Vps60. To gain insights into the functional mechanism of Vta1, I have determined the crystal structures of the Did2- and Vps60-binding N-terminal domain and the Vps4-binding C-terminal domain of *S. cerevisiae* Vta1 and elucidated their respective binding sites. Importantly, I found that the C-terminal domain also mediates Vta1 dimerization; and both subunits in a Vta1 dimer are required for its function as a Vps4 regulator. I also revealed the N-terminal domain of Vta1 contains two MIT-like motifs that resemble the ESCRT-III binding domain of Vps4. Therefore, the MIT-like motif are a generic ESCRT-III recognition motif and likely evolves from a common origin. Based on these results, I

proposed the following regulation mechanism of Vta1: the C-terminal domain of Vta1 uses its dimerization property to stabilize the ATP-dependent double ring assembly of Vps4 by strengthening the cross-ring interaction; while the MIT motif containing N-terminal domain of Vta1 provides an additional level of contact between the Vps4 disassembly machinery and the membrane-bound ESCRT-III polymer.

Chapter 4 is devoted to another regulatory protein of Vps4, Ist1. Ist1 was postulated to be an inhibitor of Vps4. It was shown to suppress the ATPase activity and interfere with the function of Vps4 *in vivo*. This property of Ist1 depends on its N-terminal predicted DUF292 domain. To understand the mechanism of Ist1 function, I have determined the crystal structure of this important domain (Ist1NTD). Strikingly, my results demonstrate it contains an ESCRT-III protein like fold. Furthermore, the structure of Ist1NTD might reflect an inactive state for the ESCRT-III proteins. Based on this result, I speculate that Ist1 might inhibit Vps4 activity by functioning as a substrate mimic. Ist1NTD also specifically interacts with Did2, and I have further determined the crystal structure of this domain in complex with a Did2 fragment. I found Ist1 interacts with the C-terminal amphipathic MIM (MIT-interacting motif) helix of Did2. The interaction site on Ist1, however, represents a novel non-MIT MIM-binding motif and is located in a highly conserved surface groove. Single point mutation in this region can effectively abolish the interaction between Ist1 and Did2. Given the biological importance of Ist1-Did2 complex in modulating Vps4 activity *in vivo*, my results provide novel insights for understanding the molecular mechanism of their function. Also, my results suggest the interactions between the ESCRT-III proteins and their binding partners are more complicated than previously envisioned and deserve further study.

While these results give us a better understanding for the function and regulation mechanism of Vps4, many questions still remain to be answered, particularly with regard to how Vps4 acts on the substrates and how Vps4 and its different regulators are temporally and spatially organized in the cells. For example, the ATP-dependent oligomeric structure of Vps4 has yet to be characterized at an atomic resolution. As such, proposals on the action mechanism of Vps4 rely largely on homologous modeling of Vps4 to other known AAA ATPase oligomeric structures. However, it is not known to what extent these models reflect the real active assembly of Vps4; and in fact, few AAA ATPase actually form double-ring structure. Also in analogy to other AAA proteins, it is hypothesized that the ESCRT-III proteins are drawn into the central pore of Vps4 oligomer to get unfolded. Direct proof supporting this model, however, has yet to be acquired.

With all the structural and biochemical information accumulated, it is possible that experiments can now be designed to test the above hypothesis. The MIM motifs of the ESCRT-III proteins are the signals recognized by Vps4. It will be interesting to test whether these motifs can be placed onto other proteins, to render fusion proteins as pseudo substrates of Vps4. If they do, these fusion proteins can be employed to investigate whether Vps4 can unfold a domain that precedes the recognition tag. A range of proteins with different thermal stabilities can be tested to evaluate the strength of Vps4 unfolding activity. Similar method has been employed previously for the study of the ClpXP degradation machinery [1]. Mutation analysis can also be performed to evaluate the role of the central pore residing in the Vps4 oligomer, and cross-linking experiments and even fluorescence resonance energy transfer (FRET) technique can be used to test the

substrate-threading hypothesis. Another possibility is to engineer a Vps4 variant whose substrate-binding MIT domain is replaced by the MIT domains from katanin or spastin, and then test whether this Vps4 variant acquires microtubule-severing activity. A similar type of idea has been used previously to convert the molecular chaperone ClpB into a ClpP associated protein as part of a degrading machine [2].

To further delineate the mechanics used by the double-ring assembly of Vps4, it will be necessary to generate hetero-oligomers of Vps4. In light of a previous study on ClpX [3], it might be possible to engineer genes encoding six covalently linked Vps4 subunits. By carefully designing the length of the linkers between different Vps4 subunits, a biologically active Vps4 ring might be generated. An entire Vps4 assembly can then be obtained by two of such pseudo hexamers. These two pseudo hexamers can be further tagged differently, such that a hetero-double-ring can be purified. This will give us a lot of opportunities to manipulate each individual subunit in the Vps4 oligomer. For example, we can selectively make one or multiple subunits as ATP-binding/hydrolysis deficient mutants or substrate-binding deficient mutants. These reagents will be tremendously useful in deciphering the function of the Vps4 double-ring structure and the contribution of individual subunits within the oligomer.

Vps4 can bind to different substrate proteins using distinct modes of interactions. The ESCRT-III proteins that interact with Vps4 contain either a C-terminal MIM1 helix or an internal MIM2 motif. Although the individual binding modes have been characterized at atomic levels, how they are coordinated *in vivo* remains largely unknown. Similar situation also applies to the interactions between Vps4 and its regulator proteins. For example, Did2 can bind to Vps4, Vta1, and Ist1 and the same region in Did2

is involved in each binding. The order and interconnection of these binding events might represent a higher level of regulation on Vps4 activity and needs to be further delineated in future studies.

Much of our frustration in understanding the function and regulation of Vps4 lies in our lack of understanding of its substrate: the ESCRT-III complex. Despite much effort, how the ESCRT-III complex is assembled and organized *in vivo* remains largely a mystery. As a first step to unravel this enigma, a recent publication revealed the order of the assembly process for the core ESCRT-III complex [4]. However, many details remain to be uncovered. Interestingly, three recent studies show the ESCRT-III proteins can form helical or tubular structures *in vitro* [5-7]. Though inspiring, they differ from each other significantly in detail. More importantly, the physiological implications of these studies are uncertain. The ESCRT-III complex is known to only form on the membrane [8]. For this reason, it might be ultimately important to study them in an environment mimicking the membrane condition. In this regard, it will also be necessary to elucidate the interaction mechanism between the ESCRT-III proteins and lipid molecules.

In the end, the ultimate question will be how Vps4 cooperates with the ESCRT-III proteins to generate membrane curvature and eventually lead to scission and/or vesiculation. The membrane deformation process is unlikely to be a random spontaneous reaction thus energy input will be required. Therefore, the action of Vps4 is very likely to be directly coupled to this process. Further studies on the functional repertoire by Vps4, Vps4 regulators and the ESCRT-III complex will be enlightening in this regard; and the results presented in this thesis may provide clues and useful reagents to address this question.

REFERENCES

1. Kim, Y.I., et al., *Dynamics of substrate denaturation and translocation by the ClpXP degradation machine.* Mol Cell, 2000. **5**(4): p. 639-48.

2. Weibezahn, J., et al., *Thermotolerance requires refolding of aggregated proteins by substrate translocation through the central pore of ClpB.* Cell, 2004. **119**(5): p. 653-65.

3. Martin, A., T.A. Baker, and R.T. Sauer, *Rebuilt AAA + motors reveal operating principles for ATP-fuelled machines.* Nature, 2005. **437**(7062): p. 1115-20.

4. Teis, D., S. Saksena, and S.D. Emr, *Ordered Assembly of the ESCRT-III Complex on Endosomes Is Required to Sequester Cargo during MVB Formation.* Dev Cell, 2008. **15**(4): p. 578-89.

5. Hanson, P.I., et al., *Plasma membrane deformation by circular arrays of ESCRT-III protein filaments.* J Cell Biol, 2008. **180**(2): p. 389-402.

6. Lata, S., et al., *Helical structures of ESCRT-III are disassembled by VPS4.* Science, 2008. **321**(5894): p. 1354-7.

7. Ghazi-Tabatabai, S., et al., *Structure and disassembly of filaments formed by the ESCRT-III subunit Vps24.* Structure, 2008. **16**(9): p. 1345-56.

8. Babst, M., et al., *Escrt-III: an endosome-associated heterooligomeric protein complex required for mvb sorting.* Dev Cell, 2002. **3**(2): p. 271-82.